Quantification of Synergy in Mixtures of Glycosyl Hydrolases on Cellulosic Biomass

A Dissertation

Presented to the Faculty of the Graduate School

of Cornell University

in Partial Fulfillment of the Requirements for the Degree of

Doctor of Philosophy

by

Marie K. Donnelly

August 2013

QUANTIFICATION OF SYNERGY IN MIXTURES OF GLYCOSYL HYDROLASES ON CELLULOSIC BIOMASS

Marie K. Donnelly, Ph.D.

Cornell University 2013

Cellulases are an important class of cell-wall degrading enzymes that are being deployed for biochemical conversion of cellulose to fermentable sugars. Individual cellulases hydrolyze cellulose relatively slowly; however, mixtures of cellulases and other plant cell wall degrading enzymes act synergistically to amplify hydrolysis. A major question affecting cellulase binding and synergistic behavior is to what extent does cellulose morphological structure influence cellulase accessibility to cellulose polymers and how does this accessibility change with different cellulases?

In nature, cellulose is contained within a complex matrix of polymers that comprise the plant cell wall. Organisms that rely on cellulose use a cocktail of enzymes to access the cellulose within the plant cell wall matrix quickly and efficiently. Identifying novel enzymes from the organisms that can be incorporated into synergistic mixtures will allow for greater diversity in biomass feedstocks and greater efficiency in conversion. To this end, a high through-put method was developed to screen plant pathogenic fungi for cellulolytic ability. Within a small sample, some isolates had crude activities comparable to that of *Trichoderma reesei*, particularly at lower temperatures and on more complicated biomass substrates.

Cellulase binding and synergistic behaviors on simple and complex cellulose structures can be studied using advanced imaging techniques with high temporal and spatial resolution. A method for observing *Thermobifida fusca* cellulases Cel5A and Cel6B binding on immobilized cellulose using fluorescence microscopy techniques was established. This method allows for simultaneous imaging of

binding on cellulose fiber and mat structures at a range of temperatures to encourage or discourage hydrolysis. Having established this method, equimolar mixtures of Cel5A and Cel6B were applied to the cellulose substrates and binding was observed. The binding data's temporal resolution obtained by this method allows for the calculation of degree of synergistic binding throughout the time course on both cellulose fibers and mats. Hydrolytic activity enhances the DSB early in the time course for fibers and throughout the time course for mats, indicating a significant effect of cellulose structure and accessibility on cellulase binding in a synergistic mixture.

BIOGRAPHICAL SKETCH

Marie Donnelly was born in Stoneham, Massachusetts in July 1984. In 1992, she moved to Pleasanton, California with her family. She attended the University of California, Riverside and graduated in 2006 with a degree in Environmental Engineering. Marie began her Ph.D. program at Cornell University in August of 2006 in the field of Biological and Environmental Engineering with Larry Walker as her advisor. She currently lives in Berkeley, California with her husband, cat, and dog.

“It's still magic even if you know how it's done.”

— Terry Pratchett*, A Hat Full of Sky*

“If you trust in yourself. . .and believe in your dreams. . .and follow your star. . . you'll still get beaten by people who spent their time working hard and learning things and weren't so lazy.”

— Terry Pratchett, *The Wee Free Men*

For Trevor

ACKNOWLEDGEMENTS

I would like to acknowledge the people who have worked with me, guided me, or otherwise supported me during my time as a graduate student at Cornell.

First and foremost, I would like to thank my advisor, Larry Walker, for his support and guidance as I learned what it meant to be a researcher. Thank you for believing in my abilities, even when I was in doubt and for giving me the chance to prove you right. I believe I owe you a bottle of Champagne.

I would also like to thank David Wilson, Harold Craighead, and Donna Gibson for being a part of my committee and supporting my research goals. David was always a source of important cellulase information and insights, as well as ideas to pursue to further my research goals. Harold and his research group hosted me in their lab space to make use of their microscope and knowledge of microscopes, which was vital to the development of Chapters 4 and 5 of this dissertation. Donna gave me the opportunity to work with her student, Brian King, on screening plant pathogenic fungi for novel cellulases and provided valuable insights and support to Chapter 3. Additionally, I would like to acknowledge Gary Bergstrom, who provided the collection that was screened for Chapter 3. The interdisciplinary nature of research at Cornell is a fantastic environment to develop as a researcher in and I am lucky to count these people among my influences.

I want to thank my parents for all their support, from sparking and stoking my interest in science, to encouraging me to challenge myself in school, to sending me to college on the other side of the state and then to graduate school on the other side of the country. I also want to thank my sisters for believing in me all the way.

The members of the Walker lab group have been another source of support and encouragement for me while I worked on my dissertation. I would like to specifically acknowledge Jose Moran-Mirabal for introducing me to microscopy and biophysical methods, and teaching me how to use them in pursuit of my research goals. I would also like to acknowledge Stephane Corgie for advice and mentoring in various lab techniques and protocols, for many interesting research conversations, for being the other person in the BRL office most days, for introducing me to the Big Red Barn, and for making always making the days interesting and pleasantly weird. Many other people have been a part of the Walker lab during my time in it, and my experience would not have been the same without them, from Aaron Saathof, Sarah Munro, Navaneetha Santhanam, Linelle Fontenelle, Ed Evans, and Deborah Sills, to Jeremy Luterbacher, Hnin Aung, and Dong Yang. Finally, I would like to acknowledge Ben Heavner, who started with Larry and the group at the same time I did, and immediately became a good friend and constant source of support.

My time at Cornell would not have been the same without the friends I have made outside the lab. First, the 4:30 crew, Ryan, Tony, Matt Kennedy, Matt Gaubatz, Ashish, and even Dennis. I would not have had near as much fun in my second and third years without you guys, nor met nearly as many people. Also, I would not have had bowling, and the bowling was important. I am proud to have been part of E. Bowling Virus, five time champions of various IM bowling leagues.

It's hard to begin to acknowledge how important Sarah Perdue, Jenny Nelson, and Julia Crane are to my time at Cornell. Girls' Night was the thing to look forward to, to make Mondays better and to snuggle Victor. We killed it in the women's bowling league. We traveled to Philadelphia to cheer on the Brewers, and to Auburn to cheer on the DoubleDays. There is no other group of women that I would

rather watch terrible TV or movies with. Or spend Thanksgiving with, or Easter, or any other holiday requiring a large meal. There's no other group I'd rather dress up for Halloween with, drink wine, and hand out candy (or pencils) to the children of Fall Creek with. Thanks for learning to cross country ski with me, and for going to hockey games, both at Lynah and at Cass Park or the Rink. Thank you for being the best friends anyone could ask for, I'm so happy to know you.

Finally, I want to acknowledge Trevor. He has truly been in the trenches with me, from prepping for my A exam to finally finishing this dissertation. I am so lucky to have a partner who supports me and my goals fully and without hesitation. Thank you.

TABLE OF CONTENTS

List of Figures

List of Tables

CHAPTER 1: INTRODUCTION

Efficient and economic conversion of plant cell-wall materials into fermentable sugars is the principal technical challenge to utilizing lignocellulosic biomass for industrial biotechnology (Usdoe 2003; Usdoe 2006; Fales et al. 2007; Himmel et al. 2007; Jørgensen et al. 2007; Coyle 2010). The biological conversion of lignocellulosic biomass to fermentable sugars is called cellulose hydrolysis and is chiefly accomplished by a class of enzymes called cellulases (Bayer et al. 1998; Lynd et al. 2002; Zhang and Lynd 2004; Zhang et al. 2006; Meyer et al. 2009; Wilson 2009). At the most fundamental scale, cellulose hydrolysis occurs when cellulases bind to cellulose polymers and hydrolyze the β-1,4 linkages between glucose monomers (Ghosh and Singh 1993; Bayer et al. 1998; Wilson 2009). However, gaining access to polymers requires that cellulases diffuse and bind to complex three dimensional structures such as cellulose microfibers, mats, and particles. In addition, cellulases exhibit different binding characteristics depending on their reactive domains (Coughlan 1985; Walker and Wilson 1991; Warren 1996; Wilson and Irwin 1999; Cantarel et al. 2009).

In nature, biomass is a very complicated substrate for cellulose hydrolysis (Rose 2003; Berlin et al. 2005; Berlin et al. 2007; Schmer et al. 2008). The plant cell wall is made up of cellulose polymers, complexed with hemicellulose, lignin, and other polymers that give the plant cell wall its structure and resistance to disease (Tomme et al. 1995; Cosgrove 2005; Gilbert 2010). Organisms that rely on cellulose for their carbon source employ a suite of cellulases and other plant cell wall degrading enzymes to break down the plant cell wall and hydrolyze the cellulose polymer to its glucose monomers and understanding how these enzymes and cellulases work together will be key to biomass hydrolysis in the service of a larger bioeconomy (Rosgaard et al. 2006). It is well documented that individual cellulases hydrolyze cellulose relatively slowly, but mixtures of cellulases and other plant cell wall degrading

enzymes have been observed to act synergistically to enhance rates and extents of hydrolysis. In a classical synergism model, the actions of endocellulases on the cellulose polymer create new chain ends on which exocellulases can bind. The actions of the exocellulases on the ends of the polymer chains expose additional chains below the surface for endocellulases to act on. Elucidating the molecular mechanisms that give rise to synergistic behavior is an important research goal.

A major question is to what degree does cellulose morphological structure influence cellulase accessibility to cellulose polymers and how does this accessibility change with different cellulases? The adsorption of cellulases onto the cellulose polymer is a key step in the hydrolysis reaction and due to the dynamic nature of cellulose hydrolysis, the adsorbed concentrations of cellulases will change as the reaction proceeds. Understanding the mechanism of this dynamic binding will begin to elucidate the synergistic interactions that yield enhanced hydrolysis of lignocellulosic biomass. The objective of the research presented in this dissertation is to explore the role of cellulose accessibility and morphological structure in cellulase binding and synergistic behaviors.

The plant cell wall is the major barrier that pathogens must surmount for successful invasion of plant tissue and overcoming its structural integrity essential to utilizing biomass for industrial biotechnology (Mendgen et al. 1996; Annis and Goodwin 1997; Esquerre-Tugaye et al. 2000; Tonukari 2003; Aro et al. 2005; Toth and Birch 2005). Many conventional cellulase activity assays rely on the use of purified cellulose substrates to measure hydrolysis, but these idealized substrates are not reflective of the accessibility of the cellulose in the plant cell wall (Berlin et al. 2005). To this end, a high throughput screening method was developed to screen a collection of fungal plant pathogens for cellulolytic abilities on real biomass. In designing the assay, the effects and interactions of fungal species, growth media,

and assay temperature on hydrolysis rates of different polysaccharide substrates were examined in order to develop a standardized methodology for evaluating a large number of isolates (King et al. 2009). The crude fungal extracts contained the full complement of plant cell wall degrading enzymes necessary for accessing and hydrolyzing the cellulose contained within the matrix of plant cell wall polymers. The high throughput screening method developed showed the importance of using complex cellulose substrates in prospecting for novel cellulolytic enzymes.

Even when not contained within a plant cell wall, cellulose is composed of simple and complex morphological structures. Pretreated biomass materials that will be used for industrial biotechnology have been largely stripped of the polymer matrix that comprises the plant cell wall, but these materials still present accessibility issues for cellulase binding and activity (Zhu et al. 2011; Luterbacher et al. 2013; Luterbacher et al. 2013; Yang et al. 2013). It is possible to study the influence of cellulose morphological structures on cellulase transport and binding mechanisms through the use of advanced imaging techniques and biochemically well characterized fluorescently labeled cellulases. Cellulases can be labeled with small organic dyes of various colors in a way that will minimize the effect on native activity, and cellulose can be immobilized on a solid substrate for stability in long term imaging, yielding good spatial and temporal data for binding curves. Chapter 4 presents the method for observing cellulase binding on simple and complex cellulose structures using fluorescence microscopy. A spectrum of reaction temperatures was employed to observe binding at various levels of hydrolytic activity. In this method, bacterial microcrystalline cellulose is immobilized on a glass substrate in such a way that both single BMCC fibers and dense mat structures can be imaged simultaneously. Cellulose density is a major factor influencing the rate and extent of cellulase binding and the method presented in Chapter 4 allows us to tease out the differences in cellulase binding on simple and complex cellulose structures.

Having established the method for using fluorescence imaging to observe cellulase binding, we can begin to answer the question, to what extent does cellulase synergism affect binding and accessibility on simple and complex cellulose substrates? Synergistic behavior has been observed in mixtures of endocellulases and exocellulases, leading to enhanced rates and extents of binding and hydrolysis activity (Beldman et al. 1988; Bothwell et al. 1993; Irwin et al. 1993; Nidetzky et al. 1994; Henrissat et al. 2002; Jeoh et al. 2002; Watson et al. 2002; Santhanam and Walker 2008; Wilson 2008). An endocellulase and an exocellulase, each labeled with a different fluorescent tag were applied to the immobilized cellulose substrates described in Chapter 4. The binding time course was observed both with and without the influence of hydrolytic activity by regulating the temperature of the binding reactions. While Jeoh et al observed the concentration of bound cellulase throughout a 16 hour hydrolysis reaction, they were limited in their temporal resolution to a scale of hours (Jeoh et al. 2006). The method presented in Chapter 4 obtains bound cellulase data every 15 seconds to every 2.5 minutes, giving us a more complete picture of cellulase binding and synergistic behaviors very early in the time course. In calculating the degree of synergistic binding throughout the time course, we can begin to understand the dynamic nature of cellulase binding on simple and complex cellulose structures and the influence of cellulose structure and complexity on hydrolysis.

Cellulases

Cellulases represent several types of enzymes that hydrolyze cellulose and are part of a larger group of enzymes known as glycoside hydrolases. Glycoside hydrolases comprise a large group of enzymes which catalyze the hydrolysis of glycosidic bonds between two carbohydrates, as shown in Figure 1 (Withers and Williams 2010).

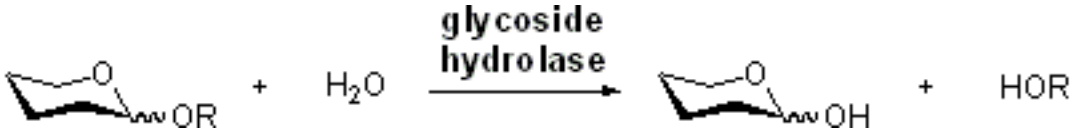

Figure 1: Diagram of hydrolysis of a glycosidic bond between two carbohydrates from Withers and Williams 2010.

In the case of cellulases, the glycosidic bond is a β-1,4 linkage between glucose monomers within a cellulose polymer. Glycoside hydrolases in general and cellulases in particular can be classified in several different ways, depending upon the most useful context.

The Enzyme Commission (EC) number uses a numerical scheme to categorize enzymes based on the reactions they catalyze (Webb 1992). Each EC number is four numbers separated by periods, progressively representing finer levels of classification. Glycoside hydrolases are denoted as EC 3.2.1.-, for the class of enzymes that hydrolyze the glycosidic bond between two or more carbohydrates, or a carbohydrate and some other moiety (Cantarel et al. 2009). Glycoside hydrolases are also classified by reaction mechanism, most commonly as either retaining or inverting (Davies and Henrissat 1995). These

reaction mechanisms were first described by Koshland (Koshland 1953). The inverting mechanism is a one-step, single-displacement reaction, occurring via an acid/base reaction assisted by two amino acid side chains. These side chains are generally glutamic acid or aspartic acid and are usually located 6 – 11 Å apart (Mccarter and Withers 1994). The inverting mechanism for a beta-glucosidic bond is shown in Figure 2 (Withers and Williams 2010)

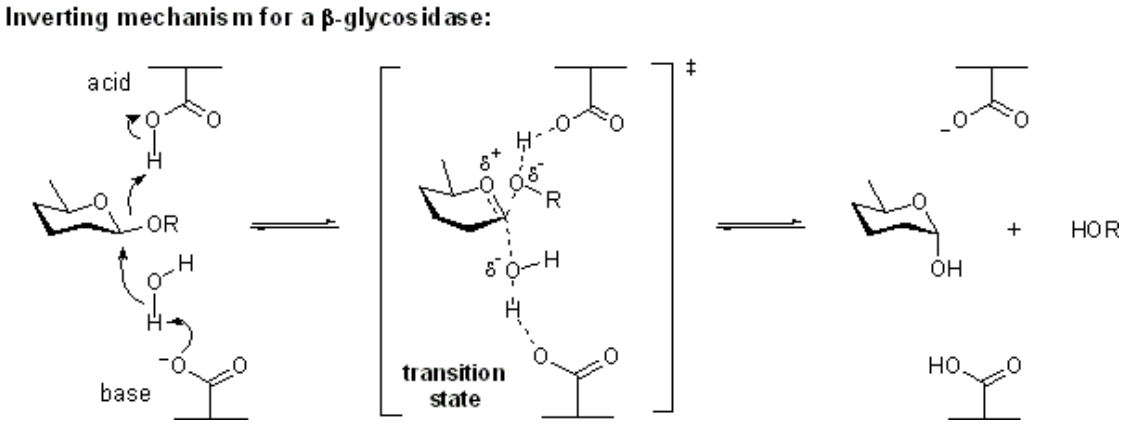

Figure 2: Diagram of the inverting mechanism for hydrolysis of a β-glucosidic bond by a glycoside hydrolase from Withers and Williams 2010.

The retaining mechanism is a two-step, double-displacement reaction, making use of acid/base and nucleophilic assistance from two amino acid side chains, generally glutamate or aspartate, located 5.5 Å apart (Koshland 1953). The retaining mechanism for a β-glucosidic bond is shown in Figure 3 below (Withers and Williams 2010).

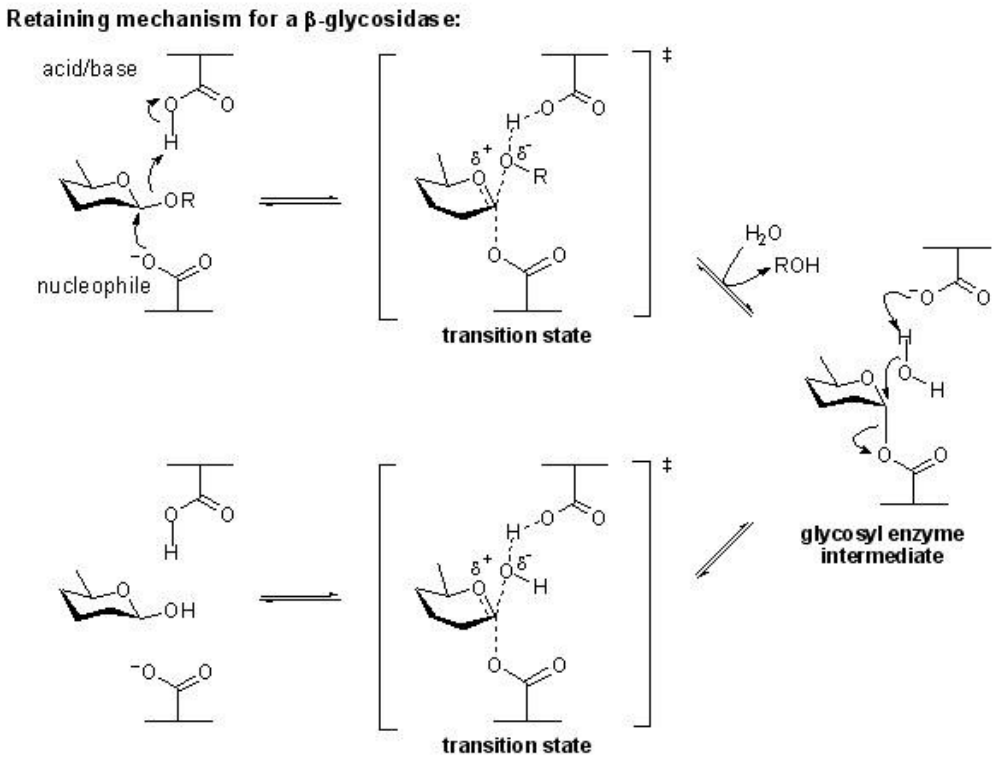

Figure 3: Diagram of the retaining mechanism for hydrolysis of a β-glucosidic bond by a glycoside hydrolase from Withers and Williams 2010.

Glycoside hydrolases can also be classified according to sequence information. This classification scheme was proposed in 1991 by Bernard Henrissat based on the comparison of the amino acid sequences of 301 glycoside hydrolases and related enzymes (Henrissat 1991). This initial classification identified 35 families with significantly similar amino acid sequences and having no significant similarity with other families (Henrissat 1991). There are currently over 100 identified families listed in the glycoside hydrolases section of the Carbohydrate-active enzyme (CAZy) database (**http://www.cazy.org/**) , maintained by Bernard Henrissat and his team (Cantarel et al. 2009). Significant similarity in amino acid sequence is a good indication of folding similarities and one can assume that members of the same family have similar folding characteristics. Sequence data can also be connected back to the mechanistic

classification, since most glycoside hydrolases act by an acid catalysis mechanism characterized by the participation of two amino acid residues in a single-displacement or double-displacement reaction resulting in the inversion or retention respectively of the configuration of the anomeric carbon of the hydrolyzed glycoside (Koshland 1953; Henrissat 1991). Active site residues can be located on the enzyme structure by locating the appropriate amino acid residues in the sequence.

Finally, and perhaps most relevantly to this research, glycoside hydrolases can be classified according to how they act on a substrate and where on that substrate they cleave the glycosidic bond. *Endo* acting enzymes attach at random locations along a carbohydrate polymer and cleave bonds from the middle of the chain, resulting in smaller chains of carbohydrates (Walker and Wilson 1991). Processive *endo* acting enzymes randomly attach to cellulose polymers and release sugars as they move along the microfibril (Coughlan 1985; Warren 1996; Wilson and Irwin 1999). *Exo* acting enzymes bind to the ends of cellulose polymers and process along the chain, releasing cellobiose. Exo-acting enzymes can attack on either the reducing and non-reducing ends of cellulose chains (Coughlan 1985; Walker and Wilson 1991; Cantarel et al. 2009). In cellulase synergism, it is assumed that the actions of endocellulases create more available sites for exocellulases to act, thereby increasing the overall activity of the mixture to an extent that is greater than the sum of the activities of the individual enzymes. Cellobiose is the major product of exocellulases, and is inhibitory to their activity (Duff and Murray 1996; Wen et al. 2004). Many cellulase systems employ β-glucosidase to hydrolyze cellobiose and other oligosaccharides produced by cellulases to glucose, reducing end product inhibition and increasing total fermentable sugar yield (Wilson 2008).

Cellulases are identified by EC numbers 3.2.1.4 if they are endo-acting or 3.2.1.91 if they are exo-acting. There are twelve identified families with endo-activity and four families with exo-activity (Cazy). All four families with exo-activity also have endo-activity, as shown in Table 1.

Table 1: Cellulolytic mode of action, reaction mechanism, and catalytic amino acid residues for glycoside hydrolase families showing cellulase activity.

GH family	*Cellulose acting: Endo/Exo*	*Mechanism: Inverting/Retaining*	*Catalytic nucleophile/base*	*Catalytic acid*
5	endo, non-reducing end exo	retaining	Glu	Glu
6	endo, non-reducing end exo	inverting	Asp	Asp
7	endo, reducing end exo	retaining	Glu	Glu
8	endo only	inverting	Asp	Glu
9	endo, non-reducing end exo	inverting	Asp	Glu
12	endo only	retaining	Glu	Glu
44	endo only	retaining	Glu	Glu
45	endo only	inverting	Asp	Asp
48	endo, non-reducing end exo, reducing end exo	inverting	unknown	Glu
51	endo only	retaining	Glu	Glu
74	endo only	inverting	Asp	Asp

Cellulases of all types are generally composed of two domains, the carbohydrate binding module (CBM) and the catalytic domain (CD) connected by a flexible linker region (Gilkes et al. 1988; Tomme et al. 1988). CBM's are continuous amino acid sequences within a carbohydrate active enzyme, like a glycoside hydrolases, with a discrete fold having the ability to bind carbohydrates (Gilkes et al. 1988; Tomme et al. 1988). The CBM binds the enzyme to the cellulose, allowing the CD to come into proximity with the cellulose polymer and hydrolyze the bonds (Boraston et al. 2004). Similar to the glycoside hydrolases categorized by the CAZY database, CBMs can currently be classified into 59 families

based on structure (Cantarel et al. 2009). CBM's were first proposed as early as the late 1940s, and were initially characterized as cellulose binding domains (CBD) based on the initial discovery of domains that bound cellulose (Shoseyov et al. 2006). Many carbohydrate active enzymes, however, have binding domains specific to carbohydrate polymers other than cellulose. CBMs contain between 30 and 200 amino acids and exist as a single, double, or triple domain in one protein (Shoseyov et al. 2006). Structural data indicates that CBMs from different families are structurally similar and the carbohydrate binding capacity may come from several aromatic residues making up a hydrophobic surface (Shoseyov et al. 2006). Many bacterial cellulases possess Family 2 CBMs, while Family 1 CBMs are almost exclusively found in fungi (Boraston et al. 2004). Binding to the cellulose polymer is an important step in the overall hydrolytic reaction. Several factors influence binding, including enzyme concentration, size, cellulose morphology and available surface area (Bothwell et al. 1997; Jung et al. 2003).

Cellulose Chemical and Physical Structure

Cellulose is the most abundant biosynthetic polymer on earth, produced by predominantly by algae and plants, but also by some bacteria, marine invertebrates, and fungi (Tomme et al. 1995; Jarvis 2003; Saxena and Brown 2005). It is a polymer of β-1,4-linked glucose units, with a degree of polymerization ranging from approximately 100 to more than 10,000 units. A single molecule of cellulose is simple, but the complex enzyme systems required for its degradation arise from the range of physical forms of cellulose produced by organisms for various purposes (Tomme et al. 1995). As a result of this, a thorough description of a cellulose substrate must include size, shape, porosity, surface area, any association with non-cellulose components, molecular conformation and crystallinity. Cellulose chains pack together to form cellulose microfibrils, which are linear crystals, characterized by the arrangement of the individual cellulose chains in a unit cell with respect to each other (Jarvis 2003;

Saxena and Brown 2005). Microfibrils in most plants have a lateral dimension of 3 nm, while microfibrils in algae can be 20 nm thick or larger (Tomme et al. 1995).

Crystallinity

Cellulose crystallinity is a factor in determining a cellulose substrate's susceptibility to cellulase hydrolysis (Ladisch et al. 1983; Coughlan 1985; Walker et al. 1993). Native cellulose predominantly occurs as crystalline cellulose, called cellulose I. The polymer chains in cellulose I are arranged parallel to each other along the long axis of the microfibril (Tomme et al. 1995; Saxena and Brown 2005). Cellulose I is further characterized as either cellulose I_α or I_β, occurring in differing amounts from cellulose found in nature (Atalla and Vanderhart 1984; Saxena and Brown 2005). The I_α and I_β fractions for various cellulose substrates as estimated from NMR spectra and modeling by Lennholm et al. are shown in Table 2 (Lennholm et al. 1994). Ambiguity in the interpretation of crystallographic data for these cellulose samples can be attributed to the fact that the samples are not pure, they contained both types of cellulose I, making it difficult to distinguish between the two in the study (Lennholm et al. 1994; O'sullivan 1997).

Table 2: Values of crystallinity and amounts of cellulose I_α and I_β studied on various cellulose substrates by NMR.

Cellulose Sample	I_α	I_β	*Total Crystallinity*
Cellulose from Valonia ventricosa	0.47	0.44	0.91
BMCC	0.36	0.39	0.75
Cotton	0.25	0.41	0.66
Fibrous cellulose powder (Whatman CF-11)	0.22-0.25	0.46-0.49	0.71
Oxygen prebleached hardwood pulp	0.17	0.26	0.43
Softwood craft pulp	0.21	0.33	0.54

(Lennholm et al. 1994)

Cellulose I_α and I_β differ by their crystal packing, molecular conformation and hydrogen bonding, but have many common features. In both forms, the cellulose chains approximate a flat ribbon and lie parallel, bound edge to edge by hydrogen bonds. Sheets of these chains are stacked one on top of another with a stagger along the microfibril, that differs between cellulose Iα and I_β (Jarvis 2003). Cellulose microfibrils can contain both types of cellulose I and the physical properties of the cellulose fibers is dependent on the ratio of the two (Saxena and Brown 2005). Cellulose Iα is the predominate form of cellulose in the cell wall produced by bacteria, such as *Acetobacter* and some algae, such as *Laminaria, Cladophora* and *Valonia* species; while cellulose Iβ predominates in the cell walls of plants. Algal cellulose has both Iα and Iβ alternating along the length of the microfibril (Tomme et al. 1995). The diversity of cellulose structures may account for the cocktail of enzymes that microorganisms use to degrade cellulose in nature.

Crystalline cellulose can also occur as cellulose II, produced naturally by a few organisms, or by converting cellulose I via alkali treatment to cellulose II (Tomme et al. 1995; Saxena and Brown 2005). Cellulose chains in cellulose II are anti-parallel and have an additional hydrogen bond per glucose residue, making cellulose II a very thermodynamically stable form. Cellulose can exist in other possible lattice forms, denoted as cellulose III_I, III_{II}, IV_I or IV_{II}, which are characterized by the arrangement of the

cellulose chain sheets and the organization of the hydrogen bonds between these sheets (Tomme et al. 1995).

For the purposes of cellulose hydrolysis, cellulose is most often considered as either crystalline or amorphous, with native cellulose occurring as a combination of the two. Amorphous cellulose, where the hydrogen bonding interactions are perturbed, may result from imperfections in the chain packing or mechanical damage to the chain itself (Tomme et al. 1995). The percentage of total cellulose that is crystalline in a given material is called the crystallinity index (Walker et al. 1993).

Table 3: Values of the crystallinity index for model cellulose and lignocellulosic substrates.

Substrate[1]	*Crystallinity Index*	*Specific Surface Area (m^2/g)*	*Reference*
Avicel	0.5-0.6	2-20	(Zhang and Lynd 2004)
BMCC	0.76-0.95	200	(Zhang and Lynd 2004)
Sigmacell	0.87	1.84	(Walker et al. 1993; Carrasco et al. 1994)
PASC	0-0.04	240	(Zhang and Lynd 2004)
Cotton	0.81-0.95	na	(Zhang and Lynd 2004)
Filter paper	0.45	na	(Zhang and Lynd 2004)
Wood pulp	0.5-0.7	61-55	(Carrasco et al. 1994; Zhang and Lynd 2004)
Switchgrass	0.46	na	(Chang and Holtzapple 2000)
Bagasse	0.5	na	(Chang and Holtzapple 2000)

[1] BMCC is bacterial microcrystalline cellulose; PASC is phosphoric acid swollen cellulose

Cellulose produced by *Acetobacter* species is highly crystalline, as is cellulose in cotton, while cellulose swollen in phosphoric acid is generally amorphous cellulose (Tomme et al. 1995). Model substrates derived from bleached commercial wood pulps, including Avicel and filter paper are considered blends of amorphous and crystalline cellulose (Zhang and Lynd 2004). Typical values for the crystallinity index of cellulose substrates are shown in Table 3. Differences in values may result from the substrate source, the method of preparation, and the method used to analyze the crystallinity (Zhang

and Lynd 2004). Cellulose hydrolysis rates by fungal cellulases are generally 3-30 times faster for amorphous cellulose compared to crystalline cellulose (Lynd et al. 2002). The initial degree of crystallinity of cellulose is an important factor in determining the rate of a hydrolysis reaction (Hall et al. 2010). Variations in the degree of crystallinity of lignocellulosic substrates may be another reason that cellulolytic organisms employ so many cellulases with different modes of action to degrade a single polymer.

Accessible Surface Area

Another important feature to consider in cellulose hydrolysis is the surface area available for cellulase adsorption. Cellulose is a heterogeneous and porous material that features both external and internal surfaces (Walker et al. 1993). The values of the specific surface area for some model cellulose substrates are shown in Table 3. The external surface area is determined by the size and shape of the cellulose structure. Single cellulose fibrils have the greatest amount of surface area while larger cellulose structures, such as mats and particles, have much lower surface area. The internal surface area depends on the capillary structure of the cellulose fibrils and the size of the enzyme or penetrating reactant that could be active on the internal surface (Walker et al. 1993). The relative importance of crystallinity compared to surface area is difficult to assess in cellulase binding. Several pretreatments that are meant to reduce the degree of crystallinity also increase surface area, obscuring the effects of both crystallinity and surface area on cellulase binding (Zhang and Lynd 2004).

Cellulose Model Substrates

Purified cellulose substrates are used to analyze cellulase activity in a laboratory setting. There are limits to the efficacy of these substrates, because they are generally modified from the native form

in order to be good for biochemical studies (Tomme et al. 1995; Saxena and Brown 2005). Cellulose substrates for analyzing the hydrolytic ability of a cellulase include Avicel, filter paper, and cotton among others because they are considered good representatives of crystalline cellulose and are easy to find (Tomme et al. 1995). The products of the various cellulases on these substrates can be translated into activities measurements by using different substrates to elucidate modes of attack (Ghose 1987). The standard filter paper activity assay is a good measure of total cellulase activity since filter paper is a nearly pure cellulose substrate and is readily available, with an established and accepted assay method (Ghose 1987; Coward-Kelly et al. 2003; Xiao et al. 2004; Zhang et al. 2006). Microcrystalline cellulose, such as Avicel, can be used to measure exocellulase activity because it has a low degree of polymerization and relatively low accessibility (Wood and Bhat 1988; Zhang et al. 2006). Soluble cellulose substrates such as carboxymethyl cellulose (CMC) can be used to measure endocellulase activity, because CMC has a high degree of polymerization and is readily accessible for endocellulolytic cleavage, but methylation may block processive enzyme action (Ghose 1987; Wood and Bhat 1988; Irwin et al. 1998; Xiao et al. 2005; Zhang et al. 2006).

Native Plant Cell Wall Chemistry

In contrast to pure cellulose, however, the plant cell wall is a heterogeneous matrix of polysaccharides with diverse composition and linkages, as well as aromatic compounds found in lignin. The cellulose encountered by cellulolytic microorganisms is complexed within the plant cell wall, embedded in an amorphous matrix of other polysaccharides and polymers. Due to the small size of cellulose microfibrils in the plant cell wall, 3-5 nm, the proportion of chains on the surface of the microfibril is a large part of the total cellulose, ranging from 33% in birch wood, to 47% in birch pulp, 67% in spruce pulp and 75% in cotton (Atalla and Vanderhart 1984; Wickholm et al. 2001; Cosgrove

2005). These chains are most closely associated with the various other matrix components (Atalla et al. 1993; Cosgrove 2005). These complexed chains are the substrate the cellulolytic organism encounters (Tomme et al. 1995). The plant cell wall is primarily composed of the polysaccharides cellulose, hemicellulose, and pectin, with secondary walls containing lignin, a heterogeneous aromatic polymer (Gilbert 2010). These components give the plant its mechanical strength and protection from disease, but the exact composition of the plant cell wall varies with species, age of the plant and environmental conditions.

Table 4: Plant cell wall polysaccharides with their structures and functions within the plant cell wall.

Polysaccharide		*Structure*	*Function*
Cellulose		unbranched β -1,4 -$_D$-glucan, partially crystalline	Mechanically strong, scaffold material
Hemicelluloses	xyloglucan	β -1,4 -$_D$-glucan, xylose branches on 3 of 4 glucose residues	Binds to surface of cellulose, branching prevents crystallinity, matrix polysaccharide
	arabinoxylan	β -1,4 -$_D$-xylan, arabinose branches	
	mannan	β -1,4 -$_D$-mannan	
	glucomanan	β -1,4 -$_D$-glucan and β -1,4 -$_D$-mannan randomly dispersed	
Pectins	homogalacturonan	Polygalacturonic acid backbone	Binds to surface of cellulose, promote flexibility, matrix polysaccharide
	rhamnogalacturan I	Alternating disaccharide [(α-1,4)-$_D$-galacturonic acid → (α-1,2)-$_L$-rhamnose], branched	
	rhamnogalacturonan II	13 different sugars, 20 different linkages	

References: (Cosgrove 2005; Gilbert 2010)

Hemicellulose is composed of heterogeneous polysaccharides of monomeric residues, including glucose, galactose, mannose, xylose, arabinose, and glucuronic acid, among others that can form hydrogen bonds with cellulose chains (Somerville et al. 2004). The most common hemicelluloses are

xyloglucan, arabinoxylan, mannan and glucomannam. The backbones of hemicelluloses polysaccharides are decorated with a variety of sugars and acetyl groups (Cosgrove 2005; Gilbert 2010). The exact composition of hemicelluloses in a plant varies by species and environmental conditions. Pectins are a complex and heterogeneous group of polysaccharides consists of distinctive domains, which are believed to be covalently linked together and promote flexibility in the plant cell wall (Cosgrove 2005). Lignin is a polymer of phenyl propane units and the most abundant non-polysaccharide component in lignocelluloses. Lignin gives the cell wall its mechanical strength and protects the plant from microbial and chemical degradation, making it a principle obstacle in making cellulose accessible to enzymatic degradation.

Hydrolysis of plant biomass is much more complex than for pure cellulose (Rose 2003; Berlin et al. 2005; Berlin et al. 2007; Schmer et al. 2008). Commercial enzyme preparations comprising various *T. reesei* enzymes such as endoglucanases, cellobiohydrolases and β-glucosidases are often limited in their activity on lignocellulosic substrates, and activities determined on filter paper, Avicel, and CMC do not necessarily correlate with activities on biomass (Berlin et al. 2005; Chundawat et al. 2008). Complete hydrolysis requires relatively large quantities and diversity of the enzyme product and often must incorporate additional enzymes with different catalytic behaviors in order to better degrade lignocellulosic biomass (Rosgaard et al. 2006). A comparison of enzyme activities of 14 commercial products on filter paper, cellobiose, AZCL-dyed xylan and grass and wheat bran fractions found large differences in performance dependent on the substrate (Kabel et al. 2006). Due to the heterogeneous composition of plant biomass, the enzymatic components needed for hydrolysis do not fall neatly into any catalytic activity category. Efficient degradation requires endocellulase and exocellulase activities as well as activity associated with β-glucosidase, xylanase, esterase, and additional CWDEs (Berlin et al.

2007; Selig et al. 2008). Measuring enzymatic activity on both simple substrates and complex biomass substrates such as those that would be fed into a biomass conversion plant may provide more information regarding the activity profiles of enzyme mixtures than only looking at one or a few substrates.

Hydrolysis of Native Plant Cell Walls by Synergism in Cellulases and Accessory Enzymes

Organisms that utilize cellulose and produce cellulases in nature often do so with a full complement of other plant cell wall degrading enzymes. Various species of fungi are an example. The profile of cellulolytic enzymes produced varies widely by species. While these species may have the genes to produce certain enzymes, their production must be activated by environmental conditions (Duff et al. 1987; King et al. 2009). *Trichoderma reesei* is the major industrial source for cellulases and hemicellulases. However, genome sequencing and analysis have revealed that it contains the smallest number of plant cell wall degrading enzymes when compared to those found in 13 other fungal genomes (Martinez et al. 2008; King et al. 2009). For example, the phytopathogens *Magnaporthe grisea* and *Fusarium graminearum* contain many more cellulases, hemicellulases, pectinases, carbohydrate binding modules, carbohydrate esterases, and polysaccharide lyases than *T. reesei* does (Martinez et al. 2008). Some phytopathogens, such as *Giberella zeae*, produce complete systems for biomass hydrolysis including endocellulases, exocellulases, β-glucosidases, hemicellulases, and ferulic acid esterases (Phalip et al. 2005; Paper et al. 2007; King et al. 2009). In addition to having a greater total number of cell wall degrading enzymes predicted from genomic analysis, *G. zeae* also possesses enzymes from several families of glycosyl hydrolases (GH 16, 51, 53, 93) that are not represented in the *T. reesei* genome (Phalip et al. 2005; Paper et al. 2007; Martinez et al. 2008).

The plant cell wall is the major barrier that pathogens must surmount for successful invasion of plant tissue (Mendgen et al. 1996; Annis and Goodwin 1997; Esquerre-Tugaye et al. 2000; Tonukari 2003; Aro et al. 2005; Toth and Birch 2005). Because the living plant can mount defenses, plant pathogens need to rapidly penetrate the plant cell wall in order to survive and reproduce (Esquerre-Tugaye et al. 2000). Thus, plant pathogens must employ a range of cellulases and accessory enzymes to quickly infiltrate into the cell and overcome the plant's defenses (Walton 1994; Annis and Goodwin 1997; Tonukari 2003).

Lignocellulosic biomass is diverse in composition and in nature the degradation of biomass is slow due to the presence of lignin and non-cellulose polysaccharides in the cell wall matrix (Berlin et al. 2005; Berlin et al. 2007). Generally, lignocellulosic biomass must be modified by some sort of pretreatment before being presented for enzymatic hydrolysis. Pretreatments can remove the hemicellulose fraction or the lignin fraction, or in some cases, just modify the cell wall to make it more accessible to saccharification (Gao et al. 2010). Different pretreated biomasses will likely require tailored enzyme cocktails to most effectively hydrolyze the available polysaccharides (Rosgaard et al. 2006; Berlin et al. 2007). Accessory enzymes such as xylanase and pectinases enhance cellulose hydrolysis in lignocellulosic biomass by removing non-cellulosic polysaccharides that coat the cellulose fibers (Berlin et al. 2007).

Berlin et al. have evaluated cocktails of several fungal cellulases and accessory enzymes to optimize the accessibility and hydrolysis of cellulose in pretreated softwoods and corn stover (Berlin et al. 2005; Berlin et al. 2007). They have also investigated the inhibitory effects of lignin in the softwood preparation (Berlin et al. 2006). Lignin reduces the accessibility of cellulose to cellulases and adsorbs

cellulases for non-productive binding. In their 2005 study, Berlin et al. screened the hydrolytic abilities of three commercial *T. reesei* cellulase preparation and four preparations they obtained through random mutagenesis and selection of *Trichoderma* and *Penicillium* strains in the laboratory on pretreated softwoods and various model cellulose substrates. They found little correlation between a preparation's activity on the model substrates with the activity on the pretreated wood, but did find significant correlation between activity on softwood and endogenous β-glucosidase levels (Berlin et al. 2005). The authors also found good correlation between the hydrolytic abilities of the preparations on softwoods and the endogenous levels of xylanase activity, which indicates a significant contribution from xylanases to the effectiveness of a cellulase preparation on lignocellulosic biomass. Berlin et al. point to this result as evidence that xylanases are a good target for improvement in reducing the costs of cellulase preparations. Building on this result in 2007, Berlin et al. developed a high-throughput microassay to assess and identify an optimal mixture of cellulases and appropriate supplements to hydrolyze cellulose in pretreated corn stover (Berlin et al. 2007). The mixture identified had approximately a twofold reduction in total protein required to reach a specified hydrolysis target. Rapid analysis of experimental and commercial cellulase preparations like the method in Berlin et al. can contribute to the reduction of costs for industrial enzymes and for prospecting for novel cellulase and plant cell wall degrading enzymes in nature.

In addition to the method developed by Berlin et al. described above, much work has been done to develop high through-put technologies for characterizing enzymes and biomass for hydrolysis. The conventional International Union for Pure and Applied Chemistry (IUPAC) filter paper assay (FPA) method for measuring hydrolytic activity has been automated by Decker et al. (2003) to reduce operator error and adapted to use small reaction volumes by Xiao et al. (2004) (Decker et al. 2003; Xiao et al.

2004; Xiao et al. 2005). A high-throughput methodology for measuring the digestibility of lignocellulosic biomass has been developed by Chundawat et al. (2008) using crystalline cellulose (Avicel) and ammonia fiber expansion (AFEX) pretreated-corn stover as substrates and a bio-enzymatic assay to determine fermentable sugars (Chundawat et al. 2008). King et al. adapted the methods developed by Xiao et al. (2004, 2005) using 3,5-dinitrosalicylic acid (DNS) to use biomass substrates to measure the crude native hydrolytic abilities of fungal plant pathogens (King et al. 2009). The authors developed a standardized method for quantitative high throughput characterization of prospective microbial sources for enzymes capable of hydrolyzing plant cell wall polysaccharides. Typical biomass substrates were included in the analysis due to the incongruity between a cellulase preparation's activity on a model cellulose substrate and its activity on a biomass substrate, as previously noted by Berlin et al. and others. In designing the assay, the effects and interactions of fungal species, growth media, and assay temperature on hydrolysis rates of different polysaccharide substrates were examined in order to develop a standardized methodology for evaluating a large number of isolates. From a small initial screen of the native crude enzyme profile of four plant pathogens, including a strain of *T. reesei*, a few isolates were determined to have comparable or superior activity on biomass substrates than the crude *T. reesei* preparation. These strains are worthy of further investigation and the method has since been applied to a larger collection of possible cellulase source microbes.

Gao et al. set about rationally designing an enzyme cocktail of cellulases and hemicellulases specific for ammonia fiber expansion (AFEX) pretreated biomass (Gao et al. 2010). They used a combination of six enzymes, including endocellulases, endoxylanases, exocellulases, β-glucosidases and β-xylosidases at three different total protein loadings inclusive of all six enzymes (Gao et al. 2010). They found that the optimal enzyme ratios for maximum hydrolysis were very dependent on the total enzyme

loading. Incorporating the hemicellulases into the synergistic mixture significantly contributed to the overall glucose yield, probably due to the increased accessibility to cellulose as the hemicellulose was broken down. Statistical plots of their data reveal that the relative ratio of enzymes becomes less important at higher total protein loading, provided there is at least a minimal amount of each component in their mixture (Gao et al. 2010). This is an interesting result, showing not only the value of accessory enzymes in a synergistic mixture, but also that effective hydrolysis can be achieved with lower total protein loading if the appropriate ratios of synergistic components are used. Reducing the amount of enzyme required reduces the costs associated with the overall process.

Meyer et al. used a similar method to begin developing a minimal enzyme cocktail for biomass processing (Meyer et al. 2009). The minimal enzyme cocktail concept addresses the need to find the minimum number of enzymes required, the minimum protein loading, and the optimum combination of these components to maximize the hydrolysis of cellulose and hetero-xylans in biomass. This concept requires the investigation of two major hypotheses: first, that native, multi-component crude cellulolytic and/or xylan degrading enzyme cocktails are not necessarily optimal for degradation of pretreated materials; and second, that it is possible to replace these crude native enzyme cocktails with more efficient designed cocktails. (Meyer et al. 2009). Meyer et al. use the suite of cell wall degrading enzymes produced by *Trichoderma reesei* as an example of a native, multi-enzyme system. *T. reesei* secretes two exocellulases, five different endocellulases, some β-glucosidase activity, some endoxylanase activity and at least one β-xylosidase enzyme (Rosgaard et al. 2007; Meyer et al. 2009). The exocellulases are produced in the greatest quantity relative to the other proteins in the cocktail, at approximately 50-80% of the total, followed by the endocellulases at approximately 6-20% of the total (Rosgaard et al. 2007). These ratios are sufficient for synergistic mixtures on BMCC (Jeoh et al. 2002). In

the time since *T. reesei* was first isolated, various mutants have increased the overall production of protein, but have not altered the profile of proteins produced by the microorganism, making it a favorite for cellulase production in industry. However, these activities are traditionally determined on purified cellulose substrates, and not necessarily on pretreated biomass, making it difficult to predict how the native cellulase cocktail will perform on more complicated substrates. Pretreatment may produce inhibitors to both hydrolysis and fermentation, and the sensitivity of enzyme components to these compounds may not be apparent from activity assays on produced cellulose substrates. Meyer et al. tested varying ratios of the four main cellulolytic activities present in native *T. reesei* secretions to find one that is optimal for the degradation of cellulose in pre-treated straw. They also examined arabinoxylan degradation and synergistic mixtures between *T. reesei* cellulases and plant cell wall degrading enzymes from other microorganisms. Additionally, Meyer et al. investigated what effect different pretreatments would have on the ratios of enzymes required (Meyer et al. 2009). The results showed that an altered profile of the four cellulases from *T. reesei* was more effective at hydrolyzing pretreated materials than the native profile. Additionally, a synergistic mixture between *T. reesei* cellulases and arabioxylan degrading enzymes from other microorganisms was more effective at degrading pretreated straw than the *T. reesei* native profile, and they confirmed that differently pretreated substrates require different profiles of cell wall degrading enzymes for optimal hydrolysis.

The results from the Berlin, Meyer and Gao studies demonstrate the need for thoughtfully designed enzyme cocktails composed of cellulolytic and accessory enzymes for the efficient hydrolysis of lignocellulosic biomass. These studies complement our own native enzyme profile study, King et al., investigating the efficiency of secreted proteins from virulent fungal plant pathogen at degrading plant cell wall materials (King et al. 2009).

Cellulase-Cellulose Interaction

The cellulase-cellulose interaction is a heterogeneous reaction, involving several steps to liberate smaller oligosaccharides from the polymer. These steps include:

1. Adsorption of cellulases onto the cellulose substrate
2. Location of a cleavable bond
3. Formation of an enzyme-substrate complex
4. Hydrolysis of the bond
5. Desorption of the cellulase from the cellulose

(Bansal et al. 2009). There has been much research devoted to understanding the mechanism by which cellulases bind to cellulose and to what extent binding influences the rate and extent of hydrolysis (Bothwell, 1997; others). Early work by Mandels et al. at the United States Army Research and Development Laboratory in Natick, Massachusetts demonstrated saturating binding behavior (Mandels et al. 1971; Bothwell et al. 1997).

The binding of cellulases to cellulose and the formation of the cellulose-cellulase complex is a critical step in the hydrolytic reaction (Jung et al. 2003). In an intact cellulase, the CBM is thought to bind to the cellulose polymer first, bringing the CD into close proximity to the cellulose in order for the reaction to occur. The simplest model of a cellulase has one CBM and one CD, though there are instances in which cellulases or other plant cell wall degrading enzymes have multiple CBM's (Boraston et al. 2004). This is perhaps a reflection of the complex nature of cellulose within the plant cell wall matrix.

In order to better understand the mechanism by which cellulases bind cellulose for hydrolysis, it is important to start with a simplified system. Cellulose substrates, as discussed, vary widely by source and exhibit different sizes, shapes, crystallinty, and pore structure, among other characteristics (Tomme, 1995). Bothwell et al. compared the binding of several intact cellulases from *T. fusca* and *T. reesei* and the CBM from the *T. fusca* exocellulase on both BMCC and Avicel (Bothwell et al. 1997). The *T. fusca* cellulases all possess Family 2 CBMs and the *T. reesei* cellulase has a Family 1 CBM. Maximum binding levels for all cellulases were 9-30 times higher on BMCC than on Avicel and association constants for individual cellulases were dependent on the substrate. The morphologies of BMCC and Avicel are very different from one another, even though both are considered crystalline cellulose substrates. It has been experimentally shown that BMCC has a much greater surface area per mass than Avicel, which is consistent with the results that Bothwell et al. found (Bothwell et al. 1997). On both substrates, the maximum observed adsorption decreased with increasing molecular weight of the enzyme. Based on these two observations and the assumption that the maximum bound fraction of enzyme is proportional to the available surface area of cellulose, Bothwell et al. were able to establish some general trends for cellulase binding on cellulose. First, both substrates show a decrease in accessibility with increasing cellulase molecular weight. Second, the decrease is greater on Avicel than on BMCC for cellulases smaller than 60kDa. BMCC provides more accessible pore structure, limiting the observed differences in binding with size, while Avicel has a much more restrictive structure (Bothwell et al. 1997).

Cellulase Binding and Kinetic Models

Experimental data from cellulose hydrolysis by cellulases can highlight aspects of the reaction mechanism, and potential obstacles to industrial use of cellulases in biotechnology, but these observations cannot necessarily be scaled up to a process level design. To this end, mathematical

modeling is an important tool in understanding cellulase-cellulose interactions at the molecular level and what the implications of this reaction are for reactor-scale design (Bansal et al. 2009). Modeling efforts began in the 1970s with Michaelis-Menten based approaches by Suga et al. and others (Suga et al. 1975). Generally, models for cellulase-cellulose interaction can be broken down into three categories: empirically based models, Michaelis-Menten based, and adsorption based. Additional models exist for soluble substrates and two models have been developed using jamming and fractal kinetics (Xu and Ding 2007; Bansal et al. 2009).

Michaelis-Menten Based Kinetics

Suga et al., Okazaki and Moo-Young, Gusakov et al., and Nidetzky et al. are all examples of modeling work based on the Michaelis-Menten framework (Okazaki and Moo-Young 1978; Gusakov et al. 1985; Nidetzky et al. 1994). The model assumes the reaction between cellulases and cellulose follows the common Michaelis-Menten scheme:

$$S + E \underset{k_2}{\overset{k_1}{\leftrightarrow}} SE \xrightarrow{k_3} E + P \qquad 1$$

Where S is the concentration of substrate, E is the concentration of enzyme, ES is the enzyme-substrate complex, P is the product and k_n is the kinetic constant for each reaction.

Suga et al. and Okazaki and Moo-Young used analytical methods to determine kinetic parameters for cellulase hydrolysis, both in single component mixtures and in synergistic mixtures. The specifics of their models will be discussed as they pertain to modeling synergistic mixtures in the next section. Gusakov et al. developed a two phase substrate model, reflecting both the amorphous and crystalline phases of the cellulose based on the following principles: (1) the products of the hydrolysis

are $_D$-glucose and cellobiose only; (2) $_D$-Glucose and cellobiose are produced directly from cellulose by different enzymes and independently of each other, cellobiose can be hydrolysed to $_D$-glucose by cellobiose; (3) cellulases are competitively inhibited by relevant products; (4) during hydrolysis, the cellobiose-producing enzymes are inactivated, while the $_D$-glucose-producing enzymes retain their activity; (5) cellulose consists of amorphous and crystalline regions; and (6) the amorphous moiety of cellulose is hydrolysed at a higher rate than the crystalline moiety. The model is composed of the following system of equations:

$$\frac{dS_{am}}{dt} = -v_1 - v_3$$

$$\frac{dS_{cr}}{dt} = -v_2 - v_4$$

$$\frac{dG_2}{dt} = v_1 + v_2 - v_5 \qquad 2$$

$$\frac{dG}{dt} = v_3 + v_4 + v_5$$

Where S_{am} is the concentration of amorphous substrate, S_{cr} is the concentration of crystalline substrate, G_2 is cellobiose, G is glucose and:

$$v_1 = \frac{V_1 S_{am} e^{-k_{in}t}}{K_{m,1}\left(1 + G_2/K_{i,1} + S_{cr}/K_{m,2}\right) + S_{am}} \qquad 3$$

is the rate of cellobiose formation from amorphous cellulose,

$$v_2 = \frac{V_2 S_{cr} e^{-k_{in} t}}{K_{m,2}\left(1 + G_2/K_{i,2} + S_{cr}/K_{m,1}\right) + S_{cr}} \quad (4)$$

is the rate of cellobiose formation from crystalline cellulose,

$$v_3 = \frac{V_3 S_{am}}{K_{m,3}\left(1 + G/K_{i,3} + S_{cr}/K_{m,4}\right) + S_{am}} \quad (5)$$

is the rate of glucose formation from amorphous cellulose,

$$v_4 = \frac{V_4 S_{cr}}{K_{m,4}\left(1 + G/K_{i,4} + S_{am}/K_{m,3}\right) + S_{cr}} \quad (6)$$

is the rate of glucose formation from crystalline cellulose, and

$$v_5 = \frac{V_5 G_2}{K_{m,5}\left(1 + G/K_{i,5}\right) + G_2} \quad (7)$$

is the rate of glucose formation from cellobiose (Gusakov et al. 1985). V_i represents the maximum rate of reaction, $K_{m,i}$, is a Michaelis constant and $K_{i,i}$ is the constant of inhibition. The system of equations (2) was solved by numerical integration on a computer and the results fit well for a batch reactor at 70-80% conversion. The model enables the prediction of the extent of cellulose hydrolysis and the hydrolysate composition at any moment of the reaction (Gusakov et al. 1985). The time course aspect of the model is important, as cellulose hydrolysis by cellulases is a dynamic system with rates of hydrolysis changing with time. This model was meant to highlight the relative effect of each factor affecting the hydrolysis, to better design the reaction system for a batch reactor.

Langmuir Kinetics

Adsorption kinetics is another example of a modeling framework for cellulase-cellulose interactions. Bothwell et al. used Langmuir kinetics to model the binding behavior for the cellulases on the cellulose substrates. The Langmuir adsorption model was developed to consider the amount of an ideal gas adsorbed on an idealized surface as a function of partial pressure or concentration at a fixed temperature. The gas is presumed to bind on distinct binding sites contained on the surface. The basic assumptions hold well for simplified cellulase binding kinetics. The assumptions are as follows:

1. The system is at equilibrium, that is, the rate of adsorption equals the rate of desorption
2. The surface with the binding sites is perfectly flat, with no imperfections
3. All binding sites are equivalent
4. Each site can hold at most one unit of the adsorbate
5. There are no interactions between adsorbate units on adjacent sites.

The reaction mechanism governing Langmuir kinetics is as follows:

$$A_f + S \rightarrow A_{ads} \quad 8$$

Where A_f is a some ideal gas in a free solution, S is the idealized surface and A_{ads} is the adsorbed complex. The simplest model of Langmuir adsorption assumes that adsorption and desorption are elementary processes where the rate of adsorption, r_{ad}, and the rate of desorption, r_d are given by the following expressions:

$$r_{ad} = k_{ad} A_f S \quad 9$$

$$r_d = k_d A_{ads} \quad 10$$

Where k_{ad} and k_d are the kinetic parameters for adsorption and desorption respectively. Since the system is assumed to be at equilibrium, with the rate of adsorption equal to the rate of desorption, equations 9 and 10 can be set equal to each other and rearranged to give:

$$\frac{A_{ads}}{A_f S} = \frac{k_{ad}}{k_d} = K_{eq}^A \quad 11$$

Where K_{eq}^A is some kinetic parameter incorporating both the parameters for adsorption and desorption. The concentration of all sites on the surface S_0 is given by the sum of the free sites and the occupied sites:

$$S_0 = S + A_{ads} \quad 12$$

By substituting this back into equation 11 we obtain:

$$S_0 = \frac{A_{ads}}{K_{eq}^A A_f} + A_{ads} = \frac{1 + K_{eq}^A A_f}{K_{eq}^A A_f} \quad 13$$

By defining the fraction of surface sites occupied by A as θ_A:

$$\theta_A = \frac{A_{ads}}{S_0} \quad 14$$

And combining that definition with the previous equation yields the Langmuir adsorption isotherm:

$$\theta_A = \frac{K_{eq}^A A_f}{1 + K_{eq}^A A_f} \quad 15$$

For cellulose hydrolysis, the model predicts the amount of bound species and two binding parameters, the association binding constant and the maximum binding level of the enzyme (Bothwell

and Walker 1995). While some assumptions hold and the model tends to fit empirical data, there are some concerns. The cellulose surface is almost guaranteed not to be flat, particularly if the cellulose is embedded in a matrix including hemicellulose and lignin, as in the plant cell wall. Additionally, some binding sites may be in amorphous or more easily accessible regions on the cellulose while others may be more crystalline, making these sites inequivalent (Jung 2002). Despite this, Langmuir is a popular model for cellulase binding because it is a simple mechanistic model to compare kinetic properties of cellulase-cellulose systems (Bothwell and Walker 1995).

Estimating Langmuir Parameters

Bothwell et al. described a Langmuir binding isotherm for cellulase hydrolysis that predicts the amount of bound species, E_b, as a function of the free species concentration and two binding parameters, the association binding constant, K_a, and the maximum binding level of the enzyme, $E_{b,m}$.

$$E_b = \frac{E_{b,m} K_a E_f}{1 + K_a E_f} \tag{16}$$

Where E_f is the free enzyme concentration.

The kinetic parameters are estimated by fitting the theoretical curve to a set of experimental data. The Langmuir model can be linearized to estimate the kinetic parameters, K_a and $E_{b,m}$, using the Lineweaver-Burk, the Hanes-Woolf, or the Eadie-Hofstee linearizations, shown in Table 5. (Bothwell and Walker 1995).

Table 5: Linearizations of Langmuir adsorption isotherm.

Linearization	*Langmuir Isotherm*

Untransformed	$$E_b = \frac{E_{b,m} K_a E_f}{1 + K_a E_f}$$
Lineweaver-Burk	$$\frac{1}{E_b} = \frac{1}{E_{b,m}} + \frac{1}{E_{b,m} K_a}\left(\frac{1}{E_f}\right)$$
Hanes-Woolf	$$\frac{E_f}{E_b} = \frac{1}{E_{b,m}} + \frac{1}{E_{b,m} K_a}\left(E_f\right)$$
Eadie-Hofstee	$$E_b = E_{b,m} - \frac{1}{K_a}\left(\frac{E_b}{E_f}\right)$$

The transformed data are plotted and the parameters can be estimated either graphically or by linear least squares. The Eadie-Hofstee linearization transformation has resulted in non-linear plots for several investigators, however (Woodward et al. 1988; Gilkes et al. 1992; Bothwell and Walker 1995). The non-linear behavior can be attributed to enzyme interactions and/or multiple binding sites, since cellulases have two functional domains that react with cellulose (Bothwell and Walker 1995). The accuracy for the linearizations in predicting the kinetic parameters is affected by experimental error, specifically the inversion of the variables in the Lineweaver-Burk and Hanes-Woolf linearizations causes the smallest values of the dependent variable, E_b, to be unduly accentuated in determining the placement of the fitted line (Bothwell and Walker 1995). In the Hanes-Woolf and the Eadie-Hofstee, the independent and the dependent variables, E_f and E_b, respectively, appear on both sides of the equation, creating a correlation effect and introducing error on both the abscissa and the ordinate.

Bothwell et al. also investigated nonlinear forms of the Langmuir equation, specifically: the traditional Langmuir form, equation 16; an E_b vs E_t form, shown in equation 18; and an E_f vs E_t form,

shown in equation 19. The latter two models were derived using the following cellulase mass balance and substituting it into the traditional Langmuir form:

$$E_t = E_f + E_b S \tag{17}$$

$$E_b = \frac{K_a E_{b,m} + K_a E_t + 1 - \sqrt{\left(K_a E_{b,m} S + K_a E_{b,m} S + 1\right)^2 - 4K_a^2 S E_{b,m} E_t}}{2K_a S} \tag{18}$$

$$E_f = \frac{-\left(K_a E_{b,m} S - K_a E_t + 1\right) + \sqrt{\left(K_a E_{b,m} S - K_a E_t + 1\right)^2 - 4K_a E_t}}{2K_a} \tag{19}$$

Equations 18 and 19 are the solutions to the quadratic equation resulting from the substitution of equation 17 into the traditional Langmuir form (16). Both equations 18 and 19 have E_t as their independent variable, and E_t is a known, controlled input, which eliminates the need to convert E_f to E_t and allows for a direct prediction of E_b from the resulting graph. Also, since E_t is known, it can be assumed that no errors are associated with the independent variable (Bothwell and Walker 1995).

The Bothwell study compared the linear and nonlinear models and various parameter estimation techniques to find the model that best fit a set of experimental data. The three linearization techniques were coupled with the general least squares technique to estimate the kinetic constants. The results showed significant variation among the kinetic parameters, with $E_{b,m}$ varying by a factor of 1.5 and K_a by a factor of 3.6 between the highest and lowest predicted values. When the predicted values were put back into the Langmuir form and the model plotted with the data, the curves were not a good fit. The best fitting data was that obtained by the Hanes-Woolf linearization. Four methods were used to estimate the binding constants from the nonlinear models: Gauss, Box-Kanemasa, Levenburg-Marquadt

and Complex box. Of the four, the Complex Box always converged on a global minimum independently of the initial parameter guesses and the Levenburg-Marquardt always converged on a solution, so long as the initial parameter guesses were in the vicinity of the true values. The nonlinear models all had a better fit to the experimental data (Bothwell and Walker 1995).

Table 6: Values of the Langmuir kinetic parameters from literature

Cellulase	*Cellulose Substrate*	$E_{b,m}$ *(umol* g^{-1}*)*	K_a *(l umol-*^{1}*)*	*Reference*
T. fusca Cel6B	Avicel	0.4	0.2	Bothwell et al. 1997, at 50°C
T. fusca Cel6B	BMCC	11.4	0.1	
T. fusca Cel5A	Avicel	0.67	0.22	
T. fusca Cel5A	BMCC	12	0.13	
T. fusca Cel9A	Avicel	0.34	0.077	
T. fusca Cel9A	BMCC	9.7	0.044	
T. fusca CBM	Avicel	1.77	0.182	
T. fusca CBM	BMCC	16.5	0.124	
T. reesei CBHI	Avicel	0.48	0.09	
T. reesei CBHI	BMCC	4.6	0.28	
T. reesei CBHI	Avicel	1.1	0.28	Stalhberg et al. 1991, at 25°C
T. reesei CBHI	BMCC	4.2	0.43	Srisodsuk et al. 1993, at 4°C
T. reesei CBHI	Avicel	0.29	na	Tomme et al. 1988, at 20°C
T. reesei CBHI	Avicel	0.1	na	Woodward et al. 1988, at 23°C

Additional adsorption models for cellulase-cellulose interaction include Converse and Optekar, Gan et al., Zhang and Lynd, and Moran-Mirabal et al (Converse and Optekar 1993; Zhang and Lynd 2006; Moran-Mirabal et al. 2008).

Jung et al. expanded upon the idea of the Langmuir adsorption isotherm for higher concentrations of cellulase and to account for the pore structure and interstice spaces observed in BMCC. Experimental data was fit to an equation that contained three submodels representing three

different regions of binding: 1) Langmuir binding (region I), 2) interstice penetration (region II), and 3) interstice saturation (region III). The three submodels are shown in equations (20)-(22) below:

$$g_1(x_t, \beta_1) = \frac{\beta_{01} x}{1 + \beta_{11} x} \quad 0 \leq x \leq \alpha_1 \tag{20}$$

$$g_2(x_t, \beta_2) = \beta_{02} + \beta_{12} x \quad \alpha_1 \leq x \leq \alpha_2 \tag{21}$$

$$g_3(x_t, \beta_3) = \beta_{03} \quad \alpha_2 \leq x \leq b \tag{22}$$

Where α_1 represents the transition from Langmuir binding to interstice penetration, α_2 represents the transition from interstice penetration to interstice saturation. β_{01} and β_{11} related to the Langmuir parameters, β_{11} is the equilibrium binding constant K_a and β_{01} is the product of the equilibrium constant K_a and the maximum amount of adsorbed enzyme on the freely accessible surface, $E_{e,m}$. β_{12} is the ratio of interstice to free enzyme and β_{03} is the total maximum binding level, $E_{t,m}$, observed for region I, the $E_{e,m}$, and inside the interstices, $E_{i,m}$, such that $E_{t,m} = E_{e,m} + E_{i,m}$. The combined model for interstice saturation is shown in equation (23) below:

$$f_3(x) = \min\left(\max\left(\frac{\beta_{01} x}{1 + \beta_{11} x}, \beta_{02} + \beta_{12} x\right), \beta_{03}\right) \tag{23}$$

Where $f_3(x)$ is the bound concentration of enzyme and χ is is the free concentration of enzyme. The model adequately simulates cellulase saturation on the freely accessible surface and cellulase penetration into the constrained interstice space.

Assessing the Binding Dynamics

Jung et al examined the binding behavior of intact *T. fusca* cellulases Cel5A, Cel6B and Cel48A, their corresponding CDs, and their CBMs at 5°C. The CBM dominates binding behavior of intact cellulases, but the CD is an important component to consider in analyzing how the two domains influence binding on cellulose substrates and subsequent hydrolysis (Jung et al. 2003). At 5°C, the intact cellulases bind irreversibly to BMCC due to the irreversible binding of their CDs. Intact cellulases were found to penetrate the interstice surface and bind there, but the maximum amount of bound cellulase in the interstice depended on the dimensions of the enzyme, suggesting the importance of molecular size as a parameter of interstice binding capacity (Jung et al. 2003). CBMs were found to be able to freely access the interstice surfaces, likely due to their smaller size, resulting in much higher values for $E_{b,m}$. Jung et al. explained how limited accessibility to the interstice surfaces of BMCC could impact reversibility. Enzymes bound to constrained surfaces were trapped, and therefore seemed to be bound irreversibly.

While there is an extensive body of literature for cellulase-cellulose modeling, there are some inherent limitations for each category and there is a need for more robust models. Empirical models help quantifying the effects of various substrate and enzyme properties on hydrolysis, but are not applicable outside of the experimental conditions under which they were developed. Michaelis-Menten based models fit experimental data well, but are based on mass action laws for homogeneous reactions that cannot be directly applied to the heterogeneous cellulase-cellulose reaction. The Langmuir adsorption isotherm also fits experimental data well, but suffers from underlying assumptions about the system that may not apply to the actual reaction (Zhang and Lynd 2004; Bansal et al. 2009). In all cases, a more robust model must consider more enzyme and substrate properties in order to gain a more fundamental understanding of the relevant variables, such as concentration, degree of polymerization,

accessibility, adsorption capacity, cellulase composition, adsorbed cellulase concentration and synergism (Bansal et al. 2009). Such a model is also necessary to identify the rate-limiting factors as well. Though there are limits to the mathematical frameworks of the models previously described, they are still an important tool in understanding the mechanism of cellulase-cellulose hydrolysis.

Measuring the concentration of bound cellulase to obtain an experimental data set that can be fit to a model has been performed both by direct and indirect methods. The concentration of cellulases in a supernatant solution is measured and the bound fraction is determined based on the difference between the known total enzyme input and the measured enzyme in free solution. The indirect methods use cellulase activity assays to determine the concentration of free enzyme. Substrates such as filter paper and CMC can be used to determine the concentrations of exocellulases and endocellulases (Walker et al. 1993; Santhanam and Walker 2008). These assays, however, are not very specific, as exocellulases also have some small activity on CMC. Direct methods of measuring the concentration of cellulases in a solution include enzyme linked immunosorbent assays (ELISA), radiolabeling, fast protein liquid chromatography (FPLC) and capillary electrophoresis (Santhanam and Walker 2008). These methods, while directly measuring the amount of protein, have their limitations in estimating the concentration of bound cellulase on cellulose. Immunoassays are extremely specific and require antibodies exclusive to the enzyme of interest. Generating these antibodies is a time consuming process. The radiolabeling techniques are limited to the availability of different radio isotopes for labeling proteins, which is not such a problem for single component systems, but limits the study of enzymes in mixtures. Proteins may interact with the capillary surface in capillary electrophoresis at low pH, making measurements difficult (Santhanam and Walker 2008). Even if these limitations were overcome, these

are all still measurements of the free enzyme in a system when the bound concentration is the desired value.

Fluorescently labeled cellulases coupled to an appropriate detection system can be used to directly measure the concentration of cellulase bound to a cellulose surface, both in single component systems and in mixtures of cellulases (Jeoh et al. 2002; Moran-Mirabal et al. 2008; Santhanam and Walker 2008; Moran-Mirabal et al. 2009). The intensity of the fluorescent signal corresponds to the concentration of bound cellulase. Using fluorescence to detect bound cellulases has greater sensitivity and the many fluorescent tags and dyes available make it possible to simultaneously measure multiple types of cellulases acting synergistically in a solution. Knowing the concentration of bound cellulase makes the dependent variable in the Langmuir models a known quantity, eliminating the error associated with estimating the quantity from a measure of the free enzyme. Jeoh et al., Santhanam and Walker, and Moran-Mirabal et al. have demonstrated the possibility of measuring the concentration of cellulases on cellulose using a fluorescent imaging system (Jeoh et al. 2002; Jeoh et al. 2006; Moran-Mirabal et al. 2008; Santhanam and Walker 2008). Jeoh et al. used a spectrophotometer to measure fluorescent signal and made individual time point measurements in triplicate to determine the bound concentration of cellulose in spin tubes (Jeoh et al. 2002; Jeoh et al. 2006). Santhanam and Walker used a micro-plate reader for small volume reactions in a high-throughput set-up to measure bound cellulase concentration on BMCC (Santhanam and Walker 2008). Both of these methods provided good data at distinct time points, but were lacking a continuous temporal dimension. Moran-Mirabal et al. adapted the fluorescent enzyme system for larger volume reactions on BMCC on an immobilized glass substrate, which could be mounted on a microscope and observed continuously, or at distinct time points with sufficiently short intervals to discern changes in binding rate during the rapid initial phase, the leveling

off phase, and finally the saturation phase (Moran-Mirabal et al. 2008; Moran-Mirabal et al. 2009). Moran-Mirabal et al. demonstrated the feasibility of using this reaction system with single component cellulase reactions, but with appropriate filters and objective, it can be extended to mixtures of cellulases as well. This temporal resolution will allow us to track changes in the dynamic binding rates of cellulases in a synergistic mixture.

Synergism

Individual cellulases exhibit low activities on cellulose substrates. A cocktail of cellulases with different modes of catalysis will effectively hydrolyze cellulose substrates, both pure and in lignocellulosic biomass better than would be expected of each component working individually (Irwin et al. 1993; Walker et al. 1993; Santhanam and Walker 2008). This enhanced activity is called synergism and is measured as the degree of synergistic effect (DSE), given by the following equation 24.

$$DSE = \frac{X_{mix}}{\sum_{i=1}^{2} X_i} \quad 24$$

Where X_{mix} is the activity of a synergistic mixture and X_i is the activity of the individual enzymes in that mixture. The DSE is the ratio of the activity of a cellulase mixture to the sum of the activities of the individual components of the mixture (Jeoh et al. 2002; Santhanam and Walker 2008). The synergistic interaction of multiple cellulases has been observed to effectively hydrolyze cellulose, and synergistic mixtures of cellulases with accessory enzymes have been observed to more effectively degrade the plant cell wall components that comprise lignocellulosic biomass.

Table 7: Degree of synergistic effect for mixtures of cellulases on different celluloses at 50°C.

Cellulase Mixture	*Cellulose*	*Cellulase molar ratio*	*DSE*	*Reference*
T. reesei				

Endo/Exo	Avicel 105	1	1.2	Woodward et al. 1988
Endo/Exo	Avicel 105	1.25	1.5	Woodward et al. 1988
T. fusca				
Cel5A/Cel6B	BMCC	1	1.9	Jeoh et al. 2002
Cel5A/Cel9A	BMCC	1	1.18	Jeoh et al. 2002
Cel6B/Cel9A	BMCC	1	1.87	Jeoh et al. 2002
Cel5A+Cel6B+Cel9A	BMCC	0.1 + 0.75 + 0.15	3.3	Santhanam and Walker 2008

In nature, cellulose degrading organisms, such as plant pathogenic fungi, produce a cocktail of enzymes, including cellulases with varying modes of action and accessory enzymes for biomass hydrolysis (Phalip et al. 2005; Paper et al. 2007; King et al. 2009; King et al. 2011). Though there has been much experimental work to describe synergism and its effect on cellulose hydrolysis, modeling attempts have been somewhat limited by the complicated nature of the mixtures and the reaction itself. Modeling synergistic kinetics will require separate mathematical expressions for each cellulase component and must include the change in available binding sites on the substrate as a variable (Bansal et al. 2009). It is even more difficult to model cellulase kinetics on lignocellulosic biomass due to the heterogeneous nature of the substrate itself. A model for lignocellulosic degradation must include mathematical expressions for each cellulase, any accessory enzymes, new binding sites created by cellulase activity and new binding sites and surfaces liberated by the actions of hemicellulases and other plant cell wall degrading enzymes.

Jeoh et al. observed cellulase binding on BMCC using mixtures of *T. fusca* cellulases Cel5A, Cel6B and Cel9A, representing a classical endocellulase, an exocellulase and a processive endocellulase respectively, at 5 and 50°C (Jeoh et al. 2002). It was hypothesized that the effects of synergism are

related to cellulase binding in mixtures. At 5°C, binding levels of cellulases in mixtures were only 22-70% of observed binding levels of single components and the degree of synergistic effect (DSE) observed was <1, indicating anti-synergistic behavior. Cellulases exhibit very little activity at temperatures < 40°C, so this lower extent of binding is due to competition for a limited number of available binding sites (Jeoh et al. 2002; Jung et al. 2003). At 50°C, binding levels in mixtures were observed to be 40-126% higher than binding levels for single components, with at DSE >1. The higher binding is due to an increase in the number of available binding sites, created by the greater extent of hydrolysis observed (Jeoh et al. 2002). Furthermore, Jeoh described the effect of varying the loading molar ratio of cellulases in binary mixtures on synergism, using the cellulases described above. The DSE was found to be sensitive to the molar loading ratio, and that a combination of an exocellulase with either an endocellulase or a processive endocellulase enhanced synergism in both hydrolysis and binding (Jeoh et al. 2006). Limited synergism was observed in the combination of the endocellulase with the processive endocellulase. These observations support the idea that the activity of endocellulases increases the number of available binding sites for exocellulases in a mixture. Binary synergistic mixtures are also influenced by cellulose recalcitrance, with less synergistic effect observed on more recalcitrant substrates (Jeoh et al. 2006). The availability of cellulase binding sites increases with increased hydrolysis activity, but easily hydrolysable fractions are generally degraded first, leaving a more recalcitrant substrate for the enzymes to act on. In a time course experiment of sufficient length, cellulases in a mixture could be observed binding on the easily hydrolysable fraction, followed by desorption of enzymes from hydrolysed materials and the binding to the more recalcitrant fraction. Whether the endocellulases or exocellulases bind more on the recalcitrant fraction, or if the concentration of bound enzymes changes from endos bound to a greater extent to exos bound more, is an interesting question.

Jeoh et al. attempted to answer this question with binding time course data for BMCC and pre-hydrolyzed BMCC (PHBMCC), representing the easily hydrolysable and the more recalcitrant fractions of cellulose (Jeoh et al. 2006). Samples of either BMCC or PHBMCC were incubated with binary mixtures of *T. fusca* cellulases Cel5A, Cel6B and Cel9A for up to 16 hours and the extent of hydrolysis and concentration of bound enzymes were measured to calculated DSE and the degree of synergistic binding (DSB). DSB is defined as follows:

$$DSB = \frac{E_{b,mix}}{\sum_{i=1}^{2}\left(E_{b,single}\right)_i} \qquad 25$$

Where $E_{b,mix}$ is the concentration of bound enzyme in the mixture and $E_{b,single}$ is the concentration of bound cellulase in a single component reaction. Observing the DSB throughout a time course provided some insight on whether one or both cellulases in a mixture exhibited increased binding due to synergism and when that enhanced binding occurred. On BMCC, all three binary mixtures showed rapid initial binding in the first two hours, after which time the bound concentrations leveled off or decreased. In all three mixtures, at least one of the cellulases in the mixture exhibited a DSB ≥ 1. On the PHBMCC, the temporal binding trends showed more variation, with little evidence of enhanced binding effects. Rapid binding in the first two hours was observed again, but not to the extent observed on the BMCC. Interestingly, the only binary mixture to show any synergistic binding was a mixture of 70% Cel6B and 30% Cel9A. The enhanced binding is only apparent towards the end of the experiment, after 10 hours, when the bound concentration of both enzymes begins increasing again after having leveled off from some initial rate. This result shows the importance of good temporal data, as end point data would not have shown the second increase in binding after the leveling off period. This study showed enhanced activity from the same binary mixture at 16 hours on PHBMCC, but the other binary mixtures did not.

Cellulase binding on cellulose is a dynamic system, which is apparent in the 50°C reactions Jeoh et al. observed. Jeoh et al. concluded that synergism decreases as the cellulose substrate becomes more recalcitrant, but the results they observed with Cel9A in the binary mixture on the more recalcitrant cellulose suggest that there may have been endo-endo synergism (Jeoh et al. 2006).

Continuing work in the Walker lab, Santhanam and Walker developed a high-throughput assay to measure binding and synergism in ternary mixtures of cellulases on BMCC (Santhanam and Walker 2008). The ternary mixtures investigated were composed of *T. fusca* cellulases Cel5A, Cel6B and Cel9A, an endocellulases, exocellulase and a processive endocellulases respectively. The results showed the highest DSE with all three cellulases in the mixture and confirmed that the exocellulase should be at least 75% of the enzyme loaded to achieve optimal hydrolysis. Interestingly, when the maximum extent of hydrolysis was observed, exocellulases were 90% of the measured bound enzymes. Exceeding this level of exocellulase binding, however, did not correspondingly increase the observed hydrolysis. Despite being at higher ratios in the loaded mixture, the bound fractions of Cel5A and Cel9A were relatively low, confirming the previous work of Jeoh et al. showing that only 10% or so of the loaded mixture should be Cel5A (Jeoh 2002, confirm this). What is interesting about these ternary mixtures is that they are closer to what is observed in nature, having exocellulase activity, classical endocellulases activity and processive endocellulases activity. As mentioned, Jeoh et al. observed little synergism effect between the *T. fusca* endocellulases and processive endocellulases, yet the organism produces both (Jeoh et al. 2006).

Modeling of Synergistic Interactions

Modeling synergistic mixtures will require individual mathematic expressions for each enzyme component and some expression to account for the creation of new binding sites by enzymatic action (Bansal et al. 2009). Adsorbed concentrations of cellulases in a mixture are susceptible to change as substrate conversion progresses, making it important to study these variations and the implications for synergism.

Michaelis-Menten Based Synergistic Models

Many models for synergistic behavior rely on a Michaelis-Menten type kinetic framework, despite the limitations it has for cellulase-cellulose interactions. One of the earliest attempts to model synergistic behavior between an endocellulase and an exocellulase was presented by Suga et al. in 1975 based on Michaelis-Menten kinetics. From this basis, the authors derived the following model for the action of endocellulases on polysaccharide chains of length i:

$$\frac{dC_i}{dt} = -k_1 C_E (i-1) C_i + k_2 (C_{ES})_i + 2k_3 \sum_{j=i+1}^{\infty} \{(C_{ES})_j/(j+1)\} \quad 26$$

Where $(C_{ES})_i$ is the concentration of the enzyme-glycosidic bond complex on the chain length i fragments. For the change in enzyme-glycosidic bond complex, the following equation applies:

$$\frac{d(C_{ES})_i}{dt} = k_1 C_E (i-1) C_i - (k_2 + k_3)(C_{ES})_i \quad 27$$

For the change in free enzyme:

$$C_E = C_{E_t} - \sum_{i=2}^{\infty} (C_{ES})_i \quad 28$$

Using a quasi-steady state assumption, the left side of equation 27 can be neglected and the remainder combined with equation 28 to yield:

$$k_1\left\{C_{E_t}-\sum_{i=2}^{\infty}(C_{ES})_i\right\}(i-1)C_i-(k_2+k_3)(C_{ES})_i=0 \qquad 29$$

By summing over i and rearranging from equation 29 the following equations are obtained:

$$\sum_{i=2}^{\infty}(C_{ES})_i=\frac{\sum_{i=2}^{\infty}(i-1)C_i\,C_{E_t}}{\sum_{i=2}^{\infty}(i-1)C_i+\frac{k_2+k_3}{k_1}} \qquad 30$$

And

$$C_E=\frac{\frac{k_2+k_3}{k_1}C_{E_t}}{\sum_{i=2}^{\infty}(i-1)C_i+\frac{k_2+k_3}{k_1}} \qquad 31$$

From equation 30 the following equation is obtained:

$$(C_{ES})_i=\frac{(i-1)C_iC_{E_t}}{\sum_{i=2}^{\infty}(i-1)C_i+\frac{k_2+k_3}{k_1}} \qquad 32$$

Substituting equations 31 and 32 in to 26 yields the following equation for endocellulase activity:

$$\frac{dC_i}{dt}=\frac{-k_3C_{E_t}(i-1)C_i}{K_m+\sum_{i=2}^{\infty}(i-1)C_i}+2\frac{k_3C_{E_t}\sum_{j=i+1}^{\infty}C_i}{K_m+\sum_{i=2}^{\infty}(i-1)C_i} \qquad 33$$

When only an exocellulase is present, the rate of change of C_i is given by:

$$\frac{dC_i}{dt} = \frac{-k'_3 C_{E'_t} C_i}{K'_m + \sum_{i=2}^{\infty} C_i} + \frac{k'_3 C_{E'_t} C_{i+1}}{k'_m + \sum_{i=2}^{\infty} C_i} \quad (34)$$

Combining the two equations above for the degradation resulting from a combination of endo and exocellulases yields the following:

$$\frac{dC_i}{dt} = \frac{-k_3 C_{E_t} (i-1) C_i}{K_m + \sum_{i=2}^{\infty} (i-1) C_i} + 2\frac{k_3 C_{E_t} \sum_{j=i+1}^{\infty} C_i}{K_m + \sum_{i=2}^{\infty} (i-1) C_i} + \frac{-k'_3 C_{E'_t} C_i}{K'_m + \sum_{i=2}^{\infty} C_i} + \frac{k'_3 C_{E'_t} C_{i+1}}{K'_m + \sum_{i=2}^{\infty} C_i} \quad (35)$$

Where i = (2, 3, … ∞). For i = 1:

$$\frac{dC_1}{dt} = 2\frac{k_3 C_{E_t} \sum_{j=2}^{\infty} C_i}{K_m + \sum_{i=2}^{\infty} (i-1) C_i} + 2\frac{-k'_3 C_{E'_t} C_2}{K'_m + \sum_{i=2}^{\infty} C_i} \quad (36)$$

The authors developed a kinetic rate law for a soluble biopolymer. The model showed enhanced production of monomers and reduction of chain length when an exocellulase was combined with an endocellulase over the theoretical activity of the individual components (Suga et al. 1975). Experimentally, the products of endo-exo synergism are likely to be smaller oligosaccharides, like cellobiose, rather than monomers of glucose, thus requiring the use of β-glucosidase to fully hydrolyze the products of endo-exo synergism. The model is limited in its usefulness, as cellulose is generally in an insoluble form for industrial purposes, with a high degree of polymerization. Suga et al.'s model is further limited because it takes no account of substrate inhibition and product inhibition in the kinetic calculations.

The synergistic modeling work of Okazaki and Moo-Young, based on Michaelis-Menten type kinetics for concurrent random and endwise substrate attack, builds on Suga's model to include product

inhibition and the use of β-glucosidase (Okazaki and Moo-Young 1978). This model is also appropriate for insoluble substrates with DP ≥ 3, like cellulose. Endocellulase activity is denoted E_1, exocellulase activity is E_2 and the β-glucosidase is denoted as E_3 in the model. The following system of equations describes the activities of E_1 with noncompetitive inhibition:

$$E_1 + C_i \underset{k'_{S1}}{\overset{k_{S1}}{\leftrightarrow}} (E_1C_i) \xrightarrow{k_1} E_1 + C_i' + C_i''$$

$$E_1 + C_1 \underset{k'_{G1}}{\overset{k_{G1}}{\leftrightarrow}} (E_1C_1)$$

$$E_1 + C_2 \underset{k'_{C1}}{\overset{k_{C1}}{\leftrightarrow}} (E_1C_2)$$

$$(E_1C_i) + C_1 \underset{k'_{G1}}{\overset{k_{G1}}{\leftrightarrow}} (E_1C_iC_1) \qquad 37$$

$$(E_1C_1) + C_i \underset{k'_{S1}}{\overset{k_{S1}}{\leftrightarrow}} (E_1C_iC_1)$$

$$(E_1C_i) + C_2 \underset{k'_{C1}}{\overset{k_{C1}}{\leftrightarrow}} (E_1C_iC_2)$$

$$(E_1C_2) + C_i \underset{k'_{S1}}{\overset{k_{S1}}{\leftrightarrow}} (E_1C_iC_2)$$

Where k_1, k_{S1}, k'_{S1}, k_{G1}, k'_{G1}, k_{C1}, k'_{C1} are rate constants for E_1 independent of DP_i; (E_1C_i), (E_1,C_1), (E_1C_2), ($E_1C_iC_1$), ($E_1C_iC_2$) are the enzyme-substrate and/or end-product complexes; C_i' and C_i'' are the hydrolyzed

cellulose segments. From these equations through manipulation similar to Suga et al. the following equation for the rate of change of concentration of cellulose of DP_i with E_1 can be obtained:

$$\frac{dC_i}{dt} = \frac{k_1 E_1 \left(2\sum_{j=i+1}^{\infty} C_j - (i-1)C_i\right)}{\left(K_{M1} + \sum_{i=3}^{\infty}\{(i-1)C_i\}\right)(1 + C_1/K_{G1} + C_2/K_{C1})} \quad 38$$

Where i ≥ 3 and $K_{M1} = \frac{k'_{S1}+k_1}{k_{S1}}$, $K_{G1} = \frac{k'_{G1}}{k_{G1}}$, $K_{C1} = \frac{k'_{C1}}{k_{C1}}$.

For E_2 with no inhibition by end-products and cellulose molecules with $DP_i \geq 3$:

$$E_2 + C_i \overset{K_{S2}}{\longleftrightarrow} (E_2 C_i) \overset{k_2}{\rightarrow} E_2 + C_{i-2} + C_2 \quad 39$$

When E_2 is inhibited noncompetitively by cellobiose and glucose, the rate of change of the concentration of cellulose for $DP_i \geq 3$ is given by:

$$\frac{dC_i}{dt} = \frac{k_2 E_2 (C_{i+2} - C_i)}{\left(K_{M2} + \sum_{i=3}^{\infty} C_i\right)(1 + C_1/K_{G2} + C_2/K_{C2})} \quad 40$$

Where K_{M2} is the Michaelis-Menten constant of E_2 and K_{G2}, K_{C2} are dissociation constants between E_2 and C_1 or C_2.

For the hydrolysis of cellulose by a combination of E_1, E_2, and E_3 with non-competitive inhibitions the following equation applies:

$$\frac{dC_i}{dt} = \frac{E_{A1}\left(2\sum_{j=i+1}^{\infty} C_j - (i-1)C_i\right)}{\left(K_{M1} + \sum_{i=3}^{\infty}\{(i-1)C_i\}\right)(1 + C_1/K_{G1} + C_2/K_{C1})} + \frac{E_{A2}(C_{i+2} - C_i)}{\left(K_{M2} + \sum_{i=3}^{\infty} C_i\right)(1 + C_1/K_{G2} + C_2/K_{C2})} + \frac{2E_{A3}C_2}{(K_{M3} + C_2)(1 + C_1/K_{G3})} \quad (41)$$

Where E_{A1} and E_{A2} are the maximum enzyme activities of E_1, E_2 and E_3 respectively, defined as:

$$E_{Ai} = k_i E_i$$

Assuming the association of the cellulases with cellulose fragments is the same, the following equation for rate of change of concentration, for glycosidic bond breakage for the number average degree of polymerization ($\overline{DP}$) in the range of i = 1 to ∞:

$$\frac{d}{dt}\left(\sum_1 C_i\right) = -\frac{d}{dt}\left(\sum_1 \{(i-1)C_i\}\right) = N_0 \frac{d}{dt}\frac{1}{\overline{DP}} = \frac{E_{A1}\sum_3\{(i-1)C_i\}}{(K_{M1} + \sum_3\{(i-1)C_i\})(1 + C_1/K_{G1} + C_2/K_{C1})} + \frac{E_{A2}\sum_3 C_i}{(K_{M2} + \sum_3 C_i)(1 + C_1/K_{G2} + C_2/K_{C2})} + \frac{E_{A3}C_2}{(K_{M3} + C_2)(1 + C_1/K_{G3})} = \frac{E_{A1}S_W}{(K_{M1} + S_w)Ih_1} + \frac{E_{A2}S_M}{(K_{M2} + S_M)Ih_2} + \frac{E_{A3}C_2}{(K_{M3} + C_2)Ih_3} \quad (42)$$

Where $\overline{DP} = \frac{\sum_1(iC_i)}{\sum_1 C_i} = \frac{N_0}{\sum_1 C_i}$, $N_0 = \sum_1(iC_i) = constant$, $S_W = \sum_3\{(i-1)C_i\}$, $S_M = \sum_3 C_i$, $Ih_1 = (1 + C_1/K_{G1} + C_2/K_{C1})$, $Ih_2 = (1 + C_1/K_{G2} + C_2/K_{C2})$, $Ih_3 = (1 + C_1/K_{G3})$.

For competitive inhibitions this becomes:

$$\frac{d}{dt}\left(\sum_{1} C_i\right) = -\frac{d}{dt}\left(\sum_{1}\{(i-1)C_i\}\right) = N_0 \frac{d}{dt}\frac{1}{\overline{DP}} = \frac{E_{A1}S_W}{(K_{M1}Ih_1 + S_w)} + \frac{E_{A2}S_M}{(K_{M2}Ih_2 + S_M)} + \frac{E_{A3}C_2}{(K_{M3}Ih_3 + C_2)} \quad 43$$

Their model found the degree of synergistic effect to be dependent upon the ratio of endocellulase to exocellulase in the mixture and the concentration of enzyme in the mixture. Okazaki and Moo-Young also noted the influence of degree of polymerization of substrate on the DSE, showing greater DSE with higher degree of polymerization.

The data presented for both of these models is all theoretical, with assumed kinetic parameters. Neither model includes a critical comparison of model predictions to experimental data. At the time of publication for each model, there was simply not appropriate data to compare to, as the required analytical techniques had not yet been developed (Dean and Rollings 1992).

Building further on the work by Suga et al., Dean and Rollings developed a model that included a more detailed description of endo-exo synergism and compared that model with experimental data (Dean and Rollings 1992).

$$\frac{dC_i}{dt} = \frac{-V_{max}(i-3)C_i}{\sum_{i=4}^{N}(i-3)C_i + K_m} + \frac{2V_{max}\sum_{j=i+2}^{N} C_j}{\sum_{i=2}^{N}(i-3)C_i + K_m} - \frac{V'_{max}C_i}{\sum_{i=2}^{N} C_i + K'_m} + \frac{V'_{max}C_{i+1}}{\sum_{i=2}^{N} C_i + K'_m} \quad 44$$

Where C_i is the concentration of species i, i is a counter corresponding to the polymer's degree of polymerization, t is time, K_m is the endo-acting enzyme's Michaelis constant, V_{max} is the endo-acting enzyme's rate constant determined by independent experiments and V'_{max} and K'_m are the exo-acting enzyme's rate constants.

The model used is very similar to the one published by Suga et al., but with the distinction that the initial conditions are set experimentally. Suga et al. assumed that at time t=0, all the polymers in the substrate were of the same molecular weight, which is not what would be observed experimentally. The initial condition in the Dean and Rollings model is the distribution of the molecular weights of the polymers in the substrate, experimentally determined using size exclusion chromatography coupled to a low-angle laser light scattering detector (SEC/LALLS). The kinetic parameters used had been determined experimentally. Using these initial conditions, the model could be solved numerically. Results from this model compared well at time points early in conversion, but failed to predict experimental data at longer times. The inconsistency can be partially attributed to substrate and product inhibition and enzyme deactivation, which were not accounted for in the model.

Fujii et al. developed another Michaelis-Menten based model for the mixture of endocellulase, exocellulase and β-glucosidase working synergistically (Fujii et al. 1991). The model used the following assumptions: 1) the endocellulase and exocellulase acted only on the cellulose surface; 2) the exocellulase acts only on the non-reducing ends of cellulose chains to form cellobiose and that cellobiose production adheres to the Michaelis-Menten mechanism; 3) in a solution of exocellulase only, the concentration of cellulose substrate for the enzyme does not change during the reaction; 4) the activity of the endocellulase does not create an appreciable amount of soluble sugars and does not

adhere to Michaelis-Menten kinetics; 5) in a mixture of endocellulase and exocellulase, the actions of each will create new binding sites for the other; 6) the rate of reaction of the endocellulase is independent of the concentration of substrate in the system; and 7) β-glucosidase will act on cellobiose to produce glucose and reduce cellobiose inhibition on the endo and exo cellulases (Fujii et al. 1991). Assumption 1 is a good assumption for modeling purposes, but binding studies have shown that purified cellulose substrates used in experiments do not conform to this. There is pore structure to consider, and while the enzymes will bind to the most easily accessible sites first, i.e. the ones on the cellulose surface, binding will continue in the pores and less accessible regions and hydrolysis will occur. The kinetic equations derived from this model are given as follows:

For the activity of the exocellulase, in accordance with assumptions 2 and 3:

$$\frac{dC}{dt} = \frac{V_m S_0}{\{K_M(1 + C/K_{i1} + S_0\}} \quad 45$$

Where C = 0 at t = 0 and S_0 is the initial mass concentration of substrate particles, assumed proportional to the number of non-reducing end groups initially exposed on the surface of the particles.

For a system of endocellulase and exocellulase systems, the following equations apply:

$$\frac{dS}{dt} = k_{en} E_{en} \left\{1 - {}^{C}/_{(C + K_{i2})}\right\} \quad 46$$

$$\frac{dC}{dt} = \frac{V_m S}{\left\{K_m \left(1 + {}^{C}/_{K_{i1}}\right) + S\right\}} \quad 47$$

Where $S = S_0$ and $C = 0$ at $t = 0$ and S designates the concentration of substrate, a sum of the non-reducing end groups of the original on the surface and of the newly formed non-reducing end groups by the action of the endocellulase.

The model was tested against activity assays performed on Avicel and CMC by a cellulase mixture. In this model, the experimental data fit the predicted data well, and the model predicted the effect of synergism shown for the production of reducing sugars for both a two component mixture of endo and exo cellulases and a second mixture which included β-glucosidase.

Limitations of Michaelis-Menten Based Models

Models based on Michaelis-Menten are inherently limited because the interaction of cellulases and cellulose is not a homogeneous reaction. In a heterogeneous reaction such as cellulases on cellulose, the classical chemical kinetics assumption of a uniformly mixed system does not apply. Michaelis-Menten requires an excess substrate to enzyme ratio condition for a quasi-steady state assumption. This condition is not achieved since the fraction of cellulose accessible to adsorption ranges from 0.002 for Avicel to 0.04 for regenerated amorphous cellulose. BMCC has a fraction of accessible cellulose of 0.03 (Hong et al. 2007). Even if excess substrate was achieved initially, it could not be maintained as the substrate is depleted during the course of hydrolysis. The quasi-steady state assumption is important to Michaelis-Menten kinetics, but cellulose hydrolysis by cellulases is a dynamic system, with the concentration of substrates for each cellulase changing during the course of the reaction as new binding sites are created through the actions of other cellulases in a synergistic mixture. Michaelis-Menten models in the literature have fit well to experimental data, as described, but have limitations and will likely not be applicable to more complicated lignocellulosic substrates.

Langmuir Based Models for Synergistic Interactions

Converse and Optekar developed a model for the synergistic interaction of endo and exo cellulases that acknowledged the competition between the two for available binding sites (Converse and Optekar 1993). The model was based on endocellulases breaking internal glycosidic bonds and exocellulases releasing cellobiose from cellulose chain ends with competitive adsorption between the two arising from assigning a stronger adsorption equilibrium constant for the exocellulase, so that it adsorbed more strongly than the endocellulase (Converse and Optekar 1993). The model assumes the two enzymes compete for the same adsorption sites, and that the hydrolysis of a bond will expose another bond for hydrolysis, since only a fraction of the bonds will be on the surface of the cellulose particle at time t=0. The model is based on the following reaction mechanisms:

$$EG_s + S_{1,f} \leftrightarrow EG_a \quad 48$$

$$CBH_s + S_{1,f} \leftrightarrow CBH_a \quad 49$$

$$EG_a \rightarrow S_2\left(+S_{1f}\right) + EG_s \quad 50$$

$$S_2 + CBH_a \rightarrow G(+S_{2)} \quad 51$$

Where EG is the endocellulase, S is the substrate, CBH is the exocellulase, and G is glucose. In this model, EG in solution, EG_s, is adsorbed reversibly on unoccupied intermonomer bonds on the surface of the substrate, $S_{1,f}$ to form EG_a, adsorbed endocellulase. The exocellulase is adsorbed similarly as shown in equation 49. The adsorbed EG_a acts as an enzyme-substrate complex and breaks the bond, forming cellulose polymer ends, S_2. This action does not necessarily reduce $S_{1,f,}$ since an intermonomer bond below the surface may now be exposed. This possibility is represented by the term $+S_{1,f}$ and shown in

equation 50. The adsorbed exocellulase reacts with the polymer ends to produce glucose, shown in equation 51. The term $+S_2$ is included to show that the number of chain ends on the polymer is not reduced by this reaction until the polymer chain is completely hydrolyzed. The kinetic model described by this reaction mechanism is shown below as equations 52-56.

The competitive adsorption of EG is governed by:

$$\frac{dEG_a}{dt} = \{(S_1 - CBH_a - EG_a)(EG_T - EG_a C_0) - K_{dEG} EG_a k_{aEG}\} \quad 52$$

Where EG_T is the total amount of endocellulase, C_0 is the initial concentration of cellulose, K_{dEG} is the desorption equilibrium constant for EG and k_{aEG} is the adsorption rate constant for EG.

The corresponding equation for CBH is:

$$\frac{dCBH_a}{dt} = \{(S_1 - CBH_a - EG_a)(CBH_T - CBH_a C_0) - K_{dCBH} CBH_a k_{aCBH}\} \quad 53$$

Where CBH_T is the total amount of exocellulase, K_{dCBH} is the desorption equilibrium constant for CBH and k_{aCBH} is the adsorption rate constant for CBH. To model competitive adsorption, these equations allow either enzyme component to compete for the available adsorption site.

The concentration of substrate is modeled by the following equation:

$$\frac{dS_1}{dt} = -P_f(k_1 EG_a + k_2 CBH_a S_2 C_0) \quad 54$$

The factor Pf accounts for the fact that often another intermonomer bond is below each one that is broken such that the concentration of such bonds does not decline every time one is broken. The generation of polymer chain ends is described by the following equation:

$$\frac{dS_2}{dt} = k_1 EG_a - \frac{k_2 S_2 CBH_a C_0}{DP} \quad 55$$

Where DP is the degree of polymerization. The second term on the right side of the equation is divided by the DP to account for the fact that a whole chain of glucose units must be produced before the chain end disappears. The formation of glucose is given by this equation:

$$\frac{dG}{dt} = k_2 CBH_a S_2 C_0 \quad 56$$

The model was compared to experimental data from Woodward et al. for verification (Woodward et al. 1988). The five equations that comprise the model give a good fit to the experimental data, but it does not appear to account for a saturation component to the curve, making the fit less good as time proceeds. The effect of enzyme concentration on degree of synergy and how the model predicted this effect was also investigated. The data for the degree of synergy in the Woodward study hit a maximum with respect to total enzyme concentration, with a decline at higher concentrations of enzyme likely being due to competitive adsorption (Woodward et al. 1988; Converse and Optekar 1993). This was modeled by having the desorption kinetic constant for the exocellulase be smaller than the desorption kinetic constant for the endocellulase. The ratio of the exocellulase bound to the endocellulase increases with increasing total enzyme concentration.

Understanding the mechanisms of synergism will contribute to an overall better understanding of designing cellulase cocktails for industrial purposes. As noted before, a key step to the reaction of cellulases and cellulose is the binding of cellulase to cellulose and the formation of the reactive complex. Adsorbed cellulase concentrations will change as hydrolysis proceeds and studying these variations and their implications on synergism is important to an overall understanding of the mechanisms behind synergism (Bansal et al. 2009). By developing a good model for synergistic binding, we can begin to understand how that binding will change as the cellulose surface is increasingly hydrolyzed.

Langmuir kinetics, as described above, can be appropriate for modeling single component cellulases binding on cellulose. In a mixture of cellulases, it is more appropriate to consider multiple component Langmuir kinetics. The assumptions required by a multiple kinetic model are as follows:

The system is at equilibrium, with the rate of adsorption equal to the rate of desorption.

1. All binding sites are equivalent
2. Each site can hold at most one unit of A or one unit of B at any time, but not both
3. There are no interactions between adsorbate units on adjacent sites.

The derivation for the equilibrium constants for A and B are similar to the derivation described in equations 8 – 10. The equilibrium constants for A and B are given by:

$$\frac{A_{ads}}{A_f S} = K_{eq}^{A} \tag{57}$$

$$\frac{B_{ads}}{B_f S} = K_{eq}^{B} \tag{58}$$

The total number of sites available is given by the total number of free sites, the sites occupied by A and the sites occupied by B:

$$S_0 = S + A_{ads} + B_{ads} \quad 59$$

By inserting the equilibrium equations and rearranging the terms as described before, competitive adsorption isotherms for A and B are determined:

$$\theta_A = \frac{K_{eq}^A A_f}{1 + K_{eq}^A A_f + K_{eq}^B B_f} \quad 60$$

$$\theta_B = \frac{K_{eq}^B B_f}{1 + K_{eq}^A A_f + K_{eq}^B B_f} \quad 61$$

From these general models and the Langmuir binding isotherm for cellulases on cellulose described by Bothwell et al. and shown in equation 16, we can make the following approximations for the simplest case of Langmuir binding in a mixture:

$$E_{1b} = \frac{(E_{1,m} + E_{2,m})K_a^1 E_{1,f}}{1 + K_a^1 E_{1,f} + K_a^2 E_{2,f}} \quad 62$$

$$E_{2b} = \frac{(E_{1,m} + E_{2,m})K_a^2 E_{2,f}}{1 + K_a^1 E_{1,f} + K_a^2 E_{2,f}} \quad 63$$

Where $E_{1,m}$ and $E_{2,m}$ are the maximum binding capacities for enzymes 1 and 2 and the sum of $E_{1,m}$ and $E_{2,m}$ is equal to S_0. For mixtures involving three or more enzymes, a general form of the Langmuir binding isotherm for an enzyme in that mixture is as follows:

$$E_{i,b} = \frac{(\sum_{i=1}^{n} E_{i,m}) K_a^i E_{i,f}}{1 + \sum_{i=1}^{n} K_a^i E_{i,f}} \quad 64$$

Where n is the number of enzymes in the solution.

In the case of cellulase hydrolysis by a mixture of endocellulases and exocellulases, the enzymes should not be competing for the same sites, but may block each other from appropriate binding sites due to their size and the availability of binding sites in a complicated pore structure (Bothwell et al. 1997). An implicit assumption in this kinetic framework is that adsorption equilibrium is established very quickly, compared to the start of the hydrolysis, such that the number of binding sites can be assumed constant (Bansal et al. 2009). At low temperatures, with correspondingly low hydrolysis activity, this assumption is valid, but the picture becomes much more complicated at higher temperatures and in synergistic mixtures, when hydrolytic activity is observed and the concerted efforts of some cellulases create new binding sites for others (Jung et al. 2002). Bothwell et al. proposed a nonlinear Langmuir binding model, shown in equations 18 and 19, which fit better to the experimental data than the linearized models. This model, if possible, should be amended to include multiple, competing adsorbates, and possibly applied to experimental data for mixtures of cellulases.

Biophysical Methods

As previously discussed, using fluorescently labeled enzymes in binding reactions makes it possible to measure the concentration of bound cellulase, making the dependent variable in the Langmuir binding isotherm a known quantity and therefore reducing the error associated with the calculated kinetic parameters. Accurate data for enzyme concentration, coupled with good spatial and

temporal resolution can be used to refine existing models of cellulase binding. This data can be obtained using biophysical techniques, including nanofabrication and microscopy.

Much of the understanding of cellulase systems, their modes of catalysis and the functions of their structural domains has been derived from protein engineering and X-ray crystallography. Elucidating the structure of the CDs and the CBMs has allowed for determination of alignment of cellulose polymers in the active sites of cellulases, the resolution of such characteristic features as "clefts" and "tunnels", and the identification of the amino acids playing a critical role in cellulose binding and hydrolysis on the cellulases (Henrissat 1991; Gebler et al. 1992; Mccarter and Withers 1994; Henrissat et al. 1995; Henrissat and Davies 1997; Wilson and Irwin 1999; Boraston et al. 2004; Moran-Mirabal et al. 2008). From the information obtained through crystallography, NMR and sequence data, CDs and CBMs are classified into families, with expected folds and hydrolysis reaction mechanisms. This information, however, is from bulk cellulase-cellulose measurements, obscuring the on-off rate of cellulases from different structures of cellulose and processive behavior. Greater spatial and temporal resolution is necessary to observe cellulase-cellulose interactions at the surface of cellulose morphological structures.

Imaging Techniques Applied to Cellulases

Effective visualization of cellulose hydrolysis by cellulases requires that three conditions be met: first, imaging must occur in an aqueous environment, ideally at ambient pressure; second, a suitable, immobilized substrate must be used; and finally, high resolution imaging techniques must be employed (Ding et al. 2008; Bubner et al. 2013). Although many advanced imaging techniques require vacuum chambers, extremely low temperatures or highly processes samples for achieving good resolution,

atomic force microscopy (AFM) and optical microscopy have emerged as effective visualization methods for observing cellulases in biologically relevant conditions (Lee et al. 1996; Moran-Mirabal et al. 2008; Bubner et al. 2013). These techniques have been utilized to study the interaction of cellulases and cellulose at sub-micron scales (Ding et al. 2008; Moran-Mirabal et al. 2008; Igarashi et al. 2009; Moran-Mirabal et al. 2009).

AFM has been successfully used to visualize cellulose degradation by cellulases. AFM is a type of scanning probe microscopy, which uses a microcantiliever with a nanoscale tip to scan a surface(Bubner et al. 2013). Deflections from the forces between the tip and the sample are measured by photodiodes through a reflected laser spot. AFM is useful for characterizing biomolecules because imaging can be accomplished under aqueous condition, which enables both static and dynamic observations of biological systems on a molecular level at environmental pressure and temperature (Bubner et al. 2013). Ding et al. have applied this system to visualize maize cells with cellulosomes, and recently high resolution images of cellulases on single fibers of bacterial cellulose were obtained using magnetic alternating current AFM (Ding and Himmel 2006; Quirk et al. 2010; Wang et al. 2012). High speed AFM makes it possible to image the dynamic behavior of individual cellulases in real time and Igarashi et al. used the technique to great effect to create movies of processive cellulases moving along cellulose fibers, hydrolyzing portions of the cellulose, and getting into ‘traffic jams’ and blocking the processive movements of other cellulases on the fiber (Igarashi et al. 2009; Igarashi et al. 2011). AFM techniques have also been used to try and visualize cellulase synergism. Ganner et al. showed that endoglucanases exclusively attacking the amorphous region of a cellulose substrate expose crystalline ‘nanofibers’ for cellobiohydrolases to attack (Ganner et al. 2012).

Fluorescence microscopy is another set of techniques for imaging the interaction of cellulases with cellulose. It is non-invasive and can be performed under biologically relevant conditions. Biomolecules can be labeled with a variety of fluorescent tags that do not interfere with their native activity. These molecules can then be illuminated through an objective with light of a wavelength specific to the excitation spectrum of the fluorescent tag. The tag then emits light of a longer wavelength than the excitation light that passes back through the objective and is collected by a camera (Bradbury and Evennett 1996). This system has been adapted and refined by Moran-Mirabal et al. for use with the cellulase-cellulose interaction (Moran-Mirabal et al. 2008; Moran-Mirabal et al. 2009).

Total internal reflection fluorescence microscopy (TIRF-M) is an optical technique that enables the visualization of a single molecule in a system of molecules, making observation of transient intermediates and the distribution of physical properties of a single molecule in a heterogeneous system possible, and avoiding ensemble averaging (Ding et al. 2008). Liu et al. combined TIRF-M and AFM to study the interactions of cellulase components with crystalline cellulose. They observed the surface structure of crystalline cellulose and changes made to the structure by the actions of *T. reesei* exocellulase CBHI and its CBM (Liu et al. 2010). Structural changes in the cellulose such as the decrease in the width of the fibrils and an increase in surface roughness were observed in real time. Additionally, a green fluorescent protein tagged CBM from *T. reesei* was observed exhibiting linear motion along the fibril. Liu et al. concluded that the combination of TIRF-M with AFM is a good tool for measuring the effects of cellulase hydrolysis on the morphology of crystalline cellulose. Dagel et al. expanded on this previous single molecule work by applying a technique known as defocused orientation and position imaging to localize CBMs to specific surfaces on the crystalline cellulose microfibril (Dagel et al. 2010). The observed systematic orientations that indicate the CBMs are binding to the two opposite

hydrophobic faces of the cellulose microfibril, with a well-defined orientation relative to the fiber axis, providing evidence for a binding mechanism that is driven by chemical and structural recognition of the cellulose surface by the CBM (Dagel et al. 2010).

Confocal microscopy is another fluorescence microscopy technique that is able to collect optical sections of thick specimens that can be reconstructed as a 3-D image, allowing for the observation of cellulases on larger cellulose structures, including biomass (Niggli and Lederer 1990; Moreno et al. 2006; Zhu et al. 2011). Whereas TIRF and AFM are effective for high resolution scanning of surface features, they are limited in their resolution in the Z direction (Bubner et al. 2013). Confocal microscopy has been employed by Zhu et al. to visualize *T. fusca* cellulase binding on particles of pretreated wood and by Singh et al. to demonstrate the effectiveness of their ionic liquid pretreatment on the cellulose structure of switchgrass (Singh et al. 2009; Zhu et al. 2011). Santa-Maria et al. integrated confocal microscopy with AFM to study changes in the microstructure of cellulose during hydrolysis by a purified cellobiohydrolase. They observed an early un-twisting of the bacterial cellulose microfibrils after approximately 30% of the hydrolysis completed and extensively thinned microfibrils as the hydrolysis reaction was nearing completion (about 80% hydrolysis) (Santa-Maria and Jeoh 2010). The combination of AFM and confocal enhanced their visual understanding of the changes to cellulose microstructure during cellulase binding and hydrolysis. Confocal microscopy has been extensively used by the Walker lab to study cellulase diffusion into cellulose pore structure and hydrolysis kinetics. Luterbacher et al. used a fluorescently spiked cellulase cocktail (Spezyme CP) to follow the concentration of cellulase bound on the cellulose substrate and follow the temporal morphological changes associated with cellulose hydrolysis (Luterbacher et al. 2013). More recently, Yang et al. used fluorescently labeled dextrans to visualize diffusion into the pore structure of filter paper by confocal microscopy, finding

diffusion influenced by steric hindrances between the diffusing solute and the walls of the pore structure, and between the solute molecules themselves (Yang et al. 2013). Moran-Mirabal et al. used a combination of fluorescence recovery after photobleaching (FRAP) techniques with single molecule tracking techniques to show that cellulases exhibit only limited surface diffusion when bound to crystalline cellulose and that a large fraction of the cellulases remain immobile at temperatures optimal for catalysis (Moran-Mirabal et al. 2011; Moran-Mirabal et al. 2013). They found that binding was only partially reversible, but that for processive cellulases, that reversibility increased with increasing temperature. The results challenged the accepted ideas of cellulase surface diffusion on cellulose originally published by Jervis et al. and indicate that the diffusion of cellulases and the motion of cellulose bound cellulases are more complicated that previously reported (Moran-Mirabal et al. 2013).

Fluorescence Detection of Bound Cellulases

In order to detect the change in concentration of cellulases bound on cellulose with time using an optical system, a few conditions must be met:

1. The cellulose must be immobilized on a solid support, so that the substrate will not drift in and out of focus in an aqueous solution.
2. The cellulases must be labeled such that they emit a detectable signal, with fluorescent tags that will not appreciably affect the size, charge, and activity of the native enzyme.
3. The effects of photobleaching must be accounted for and mitigated through the addition of an oxygen scavenger to the reaction, such as ascorbic acid; or the effects of photobleaching must be corrected for after the data has been collected.

Moran-Mirabal et al. satisfied the first condition by adapting a polymer lift-off technique with proven success for immobilizing biomolecules in well-defined spatial patterns (Moran-Mirabal et al. 2008). A polymer coating, in this case paralene, is evaporated onto a glass surface. A pattern is photolithographically applied to the coating, and then the pattern is etched away, leaving windows of exposed glass in the coating. A solution of cellulose can be applied to the entire surface, the polymer peeled away, and immobilized cellulose is left in the patterned windows (Moran-Mirabal et al. 2005; Moran-Mirabal et al. 2008). The cellulose left behind exhibits various identifiable morphologies, such as fibrils, bundles and mats.

Observation of the interaction between cellulases and cellulose using fluorescent spectroscopy requires bright molecules with full native activity. Proteins are often labeled with fluorescent dyes through covalent reaction with specific amino acids, however this reaction in bulk solutions can yield a mixture of enzymes with a spectrum of different degrees of labeling and enzymes without a label at all. This mixture can make characterizing the enzymes and accurately quantifying the detected concentrations difficult. Labeling in the bulk solution also risks labeling enzymes on amino acids in the active sites, thereby changing the native activity. Moran-Mirabal adapted this labeling technology by adsorbing *T. fusca* cellulases onto a cellulose substrate before applying the labeling reaction, thereby minimizing the possibility of labeling in the active site of the enzyme, and then separated the labeled enzymes using FPLC, to obtain populations of natively active enzymes with known degree of labeling. The enzymes and dyes used in this technique are outlined in Table 8 below:

Table 8: Properties of cellulases and fluorophores used in Moran-Mirabal et al.

Molecule	*Molecular Weight (Da)*	*Charge (at pH 7.0)*	*Lysine residues (accessible/total)*	*λEx (nm)*
Cel5A	46300	-16	3/10	-

Cel6B	59600	-37	4/11	-
Cel9A	90400	-52	10/20	-
AF350	410	0	-	346
AF488	643	-1	-	495
AF647	~1300	-3	-	650

(Moran-Mirabal et al. 2009)

This technique yields well characterized enzymes that can be used for epi-fluorescent imaging, or imaging methods requiring a greater degree of labeling and characterization, such as TIRF-M.

Photobleaching is a well-documented effect of fluorescence microscopy, wherein overexposure to light causes decay in the photon output of the molecules. The effect can be used to quantify two-dimensional lateral diffusion of fluorescent particles, such as diffusion and binding in a cell membrane (Axelrod et al. 1976; Sprague et al. 2004). However photobleaching can be problematic in time-lapse microscopy. To minimize the effects of photobleaching on labeled enzymes, the exposure of enzymes to light must be minimized and/or a chemical oxygen scavenger can be employed. In a time course experiment, the enzyme system must be exposed to light during data capture, but it is not necessary at any other time. The exposure time programmed to the camera should be as low as possible. In addition, ascorbic acid can be added at low concentrations to the buffer solution containing the enzymes as an oxygen scavenger (Moran-Mirabal et al. 2008).

Epi-fluorescent Microscope System

An appropriate microscope system is necessary to image the labeled and immobilized cellulase-cellulose reaction. Epi-fluorescence is a good technique for biological samples, because so many bio-molecules and structures can be tagged or stained with small fluorescent molecules that will not interfere with the biological system. Such a system must incorporate a microscope, camera, objective, illumination source,

filters and mirrors. The microscope necessary for epi-fluorescence may be either upright or inverted. In an inverted system, the sample is illuminated from below. The camera must have sufficient detection capabilities, to detect signal from very low concentrations of enzyme at the lowest possible exposure time. The objective is used for both illumination and signal collection in an epi-fluorescent system. In a system of multiple labels and enzymes, an objective that will minimize chromatic aberration is important. Such an objective will have the same field of focus for the colors being observed, minimizing signal collected out of focus. The illumination source should either be specific to the excitation wavelengths of the labels being observed, or coupled to appropriate filters, that will pass only the excitation wavelength. A dichroic mirror and filter set can be placed to collect and pass only the emission wavelength, minimizing signal from the excitation light. This system will effectively collect signal from a cellulase-cellulose system for hours-long time courses, yielding good temporal data for cellulase binding (Moran-Mirabal et al. 2008; Moran-Mirabal et al. 2009).

CHAPTER 3: AN OPTIMIZED MICROPLATE ASSAY SYSTEM FOR QUANTITATIVE EVALUATION OF PLANT CELL WALL DEGRADING ENZYME ACTIVITY OF FUNGAL CULTURE EXTRACTS

Introduction

Effective hydrolysis of plant cell wall biomass requires a cocktail of cell wall degrading enzymes, with various substrate specificities and modes of attack to hydrolyze cellulose and other polysaccharides in the cell wall structure. Cellulose utilizing organisms in nature produce enzyme cocktails with a variety of activities to access cellulose in the cell wall and degrade it. Although there is much diversity in cell wall degrading microbes, most industrial enzyme mixtures contain cellulases from just one organism, *T. reesei*. Certain plant pathogens may possess unique enzymes that might complement commercial enzyme preparations, resulting in faster and more complete biomass hydrolysis with less enzyme loading.

The objective of this research was to develop a standardized method for quantitative high throughput characterization of prospective microbial sources for enzymes capable of hydrolyzing plant cell wall polysaccharides, with the inclusion of typical biomass substrates. Specifically, the effects and interactions of fungal species, growth media, and assay temperature on hydrolysis rates of different polysaccharide substrates were examined in order to develop a standardized methodology for evaluating a large number of isolates. The DNS reducing sugar assay was modified for small hydrolysis reaction volumes in 96-well plates and non-standard enzyme substrates in order to more closely represent the types of lignocellulosic biomass being proposed for bioethanol production.

Materials and Methods

Fungal Cultures

Fusarium oxysporum f. sp. *loti* Fo060NY-93 (isolated from a stem of birdsfoot trefoil, *Lotus corniculatus* cv. "Empire"), *Gibberella zeae* Gz014NY-98 (isolated from a spike of wheat, *Triticum aestivum*., and *Sclerotinia sclerotiorum* Ss001NY-83 (isolated from a stem of soybean, *Glycine max*) were obtained from G. C. Bergstrom (Cornell University). *Trichoderma reesei* RUT-C30 was obtained from G. E. Harman (Cornell University). Fungal spores and/or mycelium were stored in 20% glycerol at -80 °C. Isolates were revived by plating onto 50 mm Petri dishes containing ¼ strength potato dextrose agar (PDA: 6 g potato dextrose broth (BD 254920), 16 g agarose, 1 L H_2O) and incubating at 25 °C until colonies had covered the surface. Mycelial plugs (6 mm) were transferred to Petri dishes containing agar modified from ATCC cellulose medium 907 (0.5 g $(NH_4)_2SO_4$, 0.5 g L-asparagine, 1 g KH_2PO_4, 0.5 g KCl, 0.41 g $MgSO_4 \bullet 7H_2O$, 0.1 g $CaCl_2$, 0.5 g yeast extract, 16 g agarose, 5 g cellulose, 1 L H_2O). Two variations of this medium with different carbon sources were used: either pure microcrystalline cellulose (Avicel, FMC type PH-101, 50 micron) or switchgrass (*Panicum virgatum* cv. “Blackwell”, 15 + 4 year stands, Pawling NY, Dutchess County, milled to pass through a 20 mesh screen). Fungi were grown on Avicel (Avi) and switchgrass (SG) agar for 10 days at 25 °C. In preliminary experiments, 10 day old cultures had the highest levels of reducing sugars produced when measured with the DNS assay when compared to 3 and 7 day old cultures regardless of culture media used. Cultures at 14 days showed no additional increase in reducing sugar production.

Extract Preparation

Two replicated Petri dish cultures of each species per media were combined for each extraction. This was repeated for five independent biological replicates. The initial PDA plug inoculum was removed, and the remaining cultures and agar were chopped and extracted in 25 ml of 0.1 *M* sodium acetate buffer with 0.02 *M* sodium chloride and 0.02% sodium azide at pH = 5.5, for 2.25 hours at room temperature to obtain a crude mixture of extracellular proteins. Extract aliquots were centrifuged in 2 ml microfuge tubes at 13,000 rpm for 5 min, and the resultant supernatants then added to a deep 2 ml, 96-well master plate (Whatman, 7701-5200, Maidstone, England). Aliquots of each extract were added directly to the plate. A second aliquot of each extract was passed through a syringe filter (0.2 µm, 13 mm HT Tuffryn membrane, Gelman Sciences Acrodisc (4454), Pall Corporation, East Hills, NY) prior to addition to the plate.

Hydrolysis Reactions

Hydrolysis reactions were carried out in 96-well flat-bottom plates (Corning Life Sciences 3370, Corning, NY). Each well contained 90 µl of carbohydrate substrate in 0.1 *M* sodium acetate buffer pH 5.5. Ninety µl of extract was added from the master plate to each well for a total reaction volume of 180 µl. Six assay substrates were evaluated: 1) filter paper (FP, 7 mm disk of Whatman #1 filter paper, 1001070, Maidstone, England) and suspensions (20 mg/ml) of 2) Avicel (Avi, FMC type PH-101 (50 micron)), 3) corn stalk (CS, Department of Plant Pathology, Cornell University) 4) switchgrass (SG), 5) carboxymethylcellulose (CMC, low-viscosity Sigma C5678, St. Louis, MO), and 6) arabinoxylan (AX, from oat spelt, Sigma X0627, St. Louis, MO). Biomass was milled using a Wiley mill to an 80 mesh screen size. One gram of each biomass sample was washed with 50 ml of ddH_2O prior to hydrolysis to remove soluble lignin and sugars that could react with DNS and increase background. To accurately transfer insoluble substrates to the 96-well plates, suspensions were continuously agitated in preparation

reservoirs with a magnetic stir bar. Negative controls of each extract (without substrate) and substrate in buffer (without extract) were included on each plate to identify background reducing activity. After preparing the hydrolysis reactions, plates were sealed with aluminum film (Axygen Scientific Inc. PCRAS200, Union City, CA) and incubated at 22, 37, and 50 °C. The CMC and AX plates were incubated for 2 h; FP and Avi plates were incubated for 20 h; and CS and SG plates were incubated for 80 h. Time points were selected to allow more complete hydrolysis and allow appropriate production of reducing sugars within the dynamic range of the standard curve used for calibration of the DNS assay. Reactions were stopped by freezing at -20°C.

Protein Quantification

Protein concentration was measured in 96-well microplates using a Sigma bicinchoninic acid (BCA) kit following manufacturer's instructions (Sigma, St. Louis, MO). Extracts were diluted 1:20 to achieve protein concentrations consistent with the assay's dynamic range for quantification, up to 20 μg/ml protein. Bovine serum albumen standards at concentrations of 0, 0.5, 5, 10, and 20 μg/ml were prepared in 0.1 *M* sodium acetate buffer pH 5.5 and replicated 3 times per plate. Plates were incubated at 60 °C for 1 h and absorbencies were measured at 562 nm on a Synergy HT Multi-Detection Microplate Reader (BioTek Instruments, Inc., Winooski, VT).

Reducing Sugar Quantification

The DNS reducing sugar assay was previously adapted to utilize a miniaturized 96-well microplate system (Decker et al. 2003; Xiao et al. 2004; Xiao et al. 2005). These methods were further modified to use crude extracts and finely ground biomass samples as substrates. DNS reagent was prepared as previously described (Miller 1959; Ghose 1987). The DNS reagent is nonspecific and reacts

with both five and six carbon reducing sugars. Although this assay does not allow discrimination among specific carbohydrates, it can be used to quantify hydrolysis of a wide range of polysaccharide substrates. Glucose standards of 0, 0.5, 1.0, 1.5, 2.0, and 3.0 mg/ml were prepared in 0.1 *M* sodium acetate buffer pH 5.5 and replicated three times per plate. Sixty µl of standards or reaction hydrolysate was added to 120 µl DNS reagent in a 96-well PCR microplate (Axygen Scientific Inc. PCR-96, Union City, CA) for a total reaction volume of 180 µl (Xiao et al. 2004; Xiao et al. 2005). DNS reactions were carried out in PCR thermocyclers (Biorad iCycler, Hercules, CA and MJResearch Inc PTC-100, Waltham, MA) by heating at 95 °C for 5 min followed by cooling to 4 °C for 1 min, and holding at 20 °C. Thirty-six µl of the completed DNS reaction was then added to 160 µl of ddH_2O in flat-bottom microplates (Corning Life Sciences 3370, Corning, NY) and absorbencies were measured at 540 nm.

Statistical Analysis

Data were analyzed using the statistical software package JMP (SAS Institute Inc., Carey, NC). To identify significant effects and interactions, data were fit to standard least squares models using the restricted maximum likelihood method. Experimental replicates and individual extracts were treated as random effects. For all responses analyzed, the effect of sample filtration and its interaction terms were not significant. Only unfiltered data was used for further analysis. The effects of fungal species (F), growth media (M), and their interaction were used to build a 4x2 factorial model for protein concentration (µg protein/ml extract). Log transformed reducing sugar concentrations (mM reducing sugar) had residuals with more normal distributions and equal variance than untransformed data. Insensitivity of the DNS assay and slight variation in the standard regression at very low reducing sugar concentrations resulted in estimation of a small number of activities less than or equal to zero. The minimum value was -0.14 mM. Log transformations are most effective when the smallest value is 1;

therefore the range was shifted by adding 1.14 to all data. The effects of assay substrate (S), fungal species (F), assay temperature (T), growth media (M), and their interactions were used to build a 6x4x3x2 full factorial model for sugar concentration. All effects were treated as nominal. Non-significant interactions were removed to build the final model.

Results and Discussion

Standards for BCA and DNS Assays

All standard regressions for both protein and sugar measurements were linear. To account for plate to plate variation and allow more accurate comparisons across plates, each plate contained internal standards. A representative linear regression of measured protein concentrations versus known concentrations of protein standards yielded a slope of 1.081 and an R^2 value of 0.996. A representative regression of measured glucose concentrations versus known concentrations of glucose standards yielded a slope of 1 and an R^2 value of 0.998.

Protein Content

Fungal species, growth media, and their interaction had a highly significant effect ($p < 0.0001$) on protein content (Table 9), as one might predict.

Table 9: Least squares model for the effects of fungal species (F) and growth media (M) on protein concentration of extracts (μg protein/ml extract).

Source	N_{parm}	*DF*	DF_{Den}	*F Ratio*	*p-value*
F	3	3	28	32.48	< 0.0001
M	1	1	28	28.27	< 0.0001
F x M	3	3	28	12.54	< 0.0001

In general, however, extracts from fungi grown on switchgrass media contained more protein than extracts grown on Avicel. There was greater species-to-species variation for Avicel-grown cultures than switchgrass-grown cultures (Figure 4). *T. reesei* extracts had slightly more protein than the other species. The effect of growth media was not significant for *S. sclerotiorum* or *T. reesei*, while *F. oxysporum* and *G. zeae* produced more protein when grown on switchgrass. Limited conclusions can be drawn from these differences in protein content, however; in addition to the hydrolytic enzymes of interest, the total protein content of the extracts also includes protein from the growth media, non-cellulolytic extracellular proteins, and some intracellular proteins released by cell lysis during extraction. Because certain carbohydrate binding modules bind tightly to their insoluble substrates, the extraction methodology may not capture the entirety of a given culture's hydrolytic system. Weakly bound enzymes could be over-represented in the extracts, while tightly bound enzymes may remain attached to insoluble particles in the media. Use of detergents or high temperatures to enhance extraction of these tightly bound enzymes could significantly affect their activity however, so the extraction used in this study may be a limitation of capturing the full hydrolytic potential. Furthermore, it is difficult to determine the specific composition of the mixture of hydrolytic enzymes, especially when testing a large number of fungal species in a high-throughput system. Crude protein measurements are not useful in this context to calculate specific enzyme activities and kinetic data, because such calculations are most meaningful when combined with an estimation of the amount of specific enzymes in the mixture assayed (Zhang et al. 2006). In this study, activity is estimated only based on reducing ends produced over time from a single time point after the reaction had occurred for a suitable period for reducing sugar production. Extracts that demonstrate superior reducing end production will be further characterized to identify individual enzyme components in future studies.

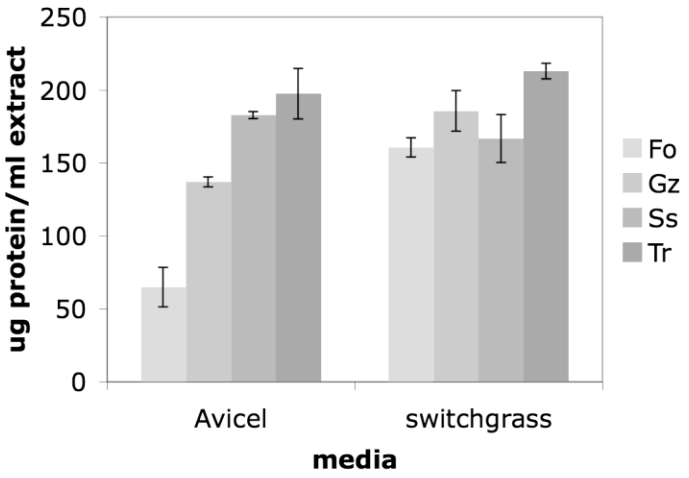

Figure 4: Protein content of fungal extracts when grown on Avicel and switchgrass media. Fo = *F. oxysporum*, Gz = *G. zeae*, Ss = *S. sclerotiorum*, Tr = *T. reesei*

Hydrolytic Activity

No reducing activity was detected in any of the negative controls. Quantification of reducing sugars using the DNS colorimetric reagent was highly reproducible both within a given extract (assay variation) and among replicated culture extractions (biological variation) (Table 10). Most coefficients of variation (CV = σ/μ) were low. A few outliers had relatively high values, however these samples also had the smallest means, leading to inflation of calculated CVs. Most of the variation observed in this study was due to differences in fungal growth among cultures and extraction methodology, not from reducing sugar quantification. Excluding *F. oxysporum* tested on Avicel at 22 °C, biological replicates had CVs less than 0.42 and experimental replicates had CVs less than 0.29. Variation among extract replicates was higher than among experimental replicates using a single extract, but results for both were highly reproducible.

Table 10: Comparison of variation within (assay) and among (biological) extracts for five replicated measurements. Mean µg reducing sugars/ml hydrolysate (µ), standard deviations (σ), and coefficients of variation (σ/µ) are presented for extracts of two fungi grown on Avicel medium, *F. oxysporum* (Fo A) and *T. reesei* (Tr A). Extracts were assayed on three substrates, carboxymethylcellulose (CMC), Avicel (Avi), and switchgrass (SG) at three temperatures, 22, 37, and 50 °C.

	Within extract						*Among extracts*					
		FoA			Tr A			Fo A			Tr A	
	µ	σ	CV	µ	σ	CV	µ	σ	CV	µ	σ	CV
CMC												
22	0.36	0.01	0.03	0.81	0.04	0.05	0.40	0.16	0.41	0.94	0.30	0.32
37	0.41	0.01	0.03	0.96	0.03	0.03	0.39	0.06	0.15	1.03	0.08	0.07
50	0.52	0.03	0.06	1.09	0.03	0.03	0.56	0.07	0.13	1.20	0.12	0.10
Avi												
22	0.03	0.02	0.68	0.16	0.01	0.08	0.02	0.02	1.05	0.25	0.05	0.19
37	0.08	0.01	0.12	0.43	0.02	0.05	0.06	0.03	0.40	0.53	0.13	0.24
50	0.23	0.06	0.28	1.30	0.10	0.08	0.16	0.07	0.41	1.43	0.19	0.13
SG												
22	0.17	0.01	0.04	0.34	0.02	0.05	0.12	0.03	0.27	0.37	0.05	0.13
37	0.26	0.01	0.05	0.48	0.05	0.10	0.19	0.05	0.26	0.47	0.03	0.07
50	0.26	0.02	0.08	0.69	0.02	0.03	0.21	0.06	0.28	0.60	0.08	0.13

The DNS assay has been criticized for its use in characterizing complex mixtures resulting from hydrolysis of lignocellulose. Although results from DNS correlate well with results from HPLC for analysis of simple sugars, this is not necessarily the case for lignocellulosic hydrolysates (Rivers et al. 1984). DNS is influenced by the degree of polymerization of reducing oligosaccharides and interference with compounds such as tannins found in the hydrolysate and/or growth media (Rivers et al. 1984; Breuil and Saddler 1985; Schwald et al. 1988). However, HPLC analysis can be time consuming and impractical for processing large numbers of samples in a high-throughput fashion (Chundawat et al. 2008). Despite its limitations, the DNS method is still used for rapid measurement of total reducing ends generated from a range of substrates, making it suitable for comparing relative activities of many samples using high-throughput screening methodology (Chen et al. 2008; Hu et al. 2008; Roman et al. 2008). The method adapted from Xiao et al. (2004,2005) is quick, reproducible, and the materials required are relatively inexpensive and available in most laboratories. In this study, controls were included to ensure that measured reducing sugars were a product of enzymatic polysaccharide hydrolysis, and not compromised by background interference from either the substrates or culture extracts. Upon identification of samples with promising CWDE systems, a more complete analysis of hydrolysis products using HPLC can be performed to determine specific polysaccharide production.

Individual activity measurements of polysaccharide hydrolysis under all conditions for five replicated culture extractions are given in Table 11. Activity tended to increase with increasing temperature and more sugars were released from relatively simple substrates such as CMC and AX than from complex biomass substrates like SG and CS. *T. reesei* is generally a consistently superior producer of enzymes for hydrolysis, however, the difference in activity between *T. reesei* and the other fungi diminished when tested on more complex assay substrates and growth media. *T. reesei* RUT-C30, a

hypersecretor of cellulases that is resistant to catabolite repression, does not appear to possess any new or altered enzymes than the parental strain QM6a (Ghosh et al. 1982; Sheir-Neiss and Montenecourt 1984). Thus, although it produces large amounts of cellulase, total activity may be limited by its ability to degrade the complex and heterogeneous structure of plant cell walls. As previously described, activities of hydrolytic enzyme mixtures on relatively simple substrates such as filter paper, Avicel, and CMC does not necessarily correlate with activities on more complex substrates such as biomass (Berlin et al. 2005; Chundawat et al. 2008). This underscores the importance of identification and development of enzymes complementary to the *T. reesei* system, which is efficient for cellulose hydrolysis but less so for heterogonous polysaccharide substrates. Individual comparisons using unpaired *t* tests showed that when grown on switchgrass media and assayed at 37 °C, *T. reesei* extracts had higher activity than *G. zeae* extracts on cellulosic substrates such as FP, Avi, and CMC ($p < 0.0001$) while *G. zeae* had higher activity than *T. reesei* on AX ($p = 0.0306$). There was no significant difference between the two species on CS ($p = 1.0000$) or SG ($p = 0.5047$). Switchgrass compared to Avicel growth media induced a significantly higher activity on AX at 37°C for *F. oxysporum* ($p = 0.0002$) and *G. zeae* ($p = 0.0508$), but not for *T. reesei* ($p = 0.4992$) or *S. sclerotiorum* ($p = 0.3799$). Switchgrass media also induced higher activities when tested on SG and CS for *F. oxysporum* ($p < 0.0001$ and $p = 0.0051$ respectively) and *G. zeae* ($p = 0.0018$ and 0.0632) but not for *T. reesei* ($p = 0.4520$ and 0.6685). Switchgrass cultures of *S. sclerotiorum* had lower activity on SG and CS than did Avicel cultures ($p = 0.0140$ and 0.0117). Activity on Avi was higher for *F. oxysporum* and *G. zeae* when fungi were grown on switchgrass ($p = 0.0075$ and 0.0431 respectively). However for *S. sclerotiorum* and *T. reesei* activity was higher when fungi were grown on Avicel ($p = 0.0004$ and 0.0052).

Table 11: Mean rates of polysaccharide hydrolysis under all conditions for five replicated culture extractions. Avicel (Avi) and filter paper (FP) were hydrolyzed for 20 hours, corn stalk (CS) and switchgrass (SG) were hydrolyzed for 80 hours, and carboxymethyl cellulose (CMC) and arabinoxylan (AX) were hydrolyzed for 2 hours. Standard deviations are presented in parentheses.

Assay temperature	*Growth media*	*Species*	*Activity on substrate μM reducing sugar released / minute*					
			Avi	FP	CS	SG	CMC	AX
22	Avicel	*F. oxysporum*	0.04 (0.08)	-0.04 (0.04)	0.35 (0.15)	0.14 (0.04)	18.41 (7.60)	38.12 (23.51)
		G. zeae	0.09 (0.08)	0.01 (0.07)	0.49 (0.13)	0.28 (0.04)	20.56 (10.25)	60.43 (28.90)
		S. sclerotiorum	0.76 (0.22)	0.55 (0.15)	0.52 (0.09)	0.28 (0.00)	34.53 (10.93)	48.49 (21.42)
		T. reesei	0.99 (0.18)	0.78 (0.06)	0.69 (0.10)	0.42 (0.06)	43.51 (13.83)	67.38 (33.55)
	Switchgrass	*F. oxysporum*	0.10 (0.06)	-0.01 (0.07)	0.51 (0.07)	0.35 (0.06)	20.26 (7.41)	87.43 (42.90)
		G. zeae	0.15 (0.07)	0.06 (0.08)	0.60 (0.13)	0.45 (0.06)	22.52 (8.59)	97.48 (48.43)
		S. sclerotiorum	0.31 (0.12)	0.23 (0.08)	0.42 (0.09)	0.23 (0.05)	29.68 (11.8)	52.7 (23.68)
		T. reesei	0.72 (0.16)	0.49 (0.11)	0.67 (0.12)	0.43 (0.04)	41.65 (10.4)	70.85 (40.62)
37	Avicel	*F. oxysporum*	0.25 (0.11)	0.14 (0.08)	0.42 (0.13)	0.22 (0.06)	18.02 (2.73)	34.48 (6.15)
		G. zeae	0.38 (0.15)	0.31 (0.11)	0.57 (0.11)	0.39 (0.06)	19.30 (1.01)	56.02 (7.99)
		S. sclerotiorum	1.62 (0.07)	1.35 (0.10)	0.55 (0.08)	0.33 (0.03)	35.40 (4.27)	47.93 (7.42)
		T. reesei	2.28 (0.25)	1.78 (0.25)	0.76 (0.18)	0.55 (0.04)	47.62 (3.55)	61.62 (7.74)
	Switchgrass	*F. oxysporum*	0.46 (0.09)	0.29 (0.05)	0.70 (0.10)	0.48 (0.05)	20.62 (2.08)	89.91 (18.68)
		G. zeae	0.52 (0.13)	0.45 (0.07)	0.72 (0.11)	0.55 (0.05)	22.10 (2.98)	97.66 (21.59)
		S. sclerotiorum	0.81 (0.16)	0.91 (0.14)	0.42 (0.04)	0.26 (0.04)	29.08 (2.80)	51.48 (8.41)
		T. reesei	1.72 (0.18)	1.30 (0.13)	0.72 (0.09)	0.53 (0.04)	44.33 (5.26)	67.99 (13.23)
50	Avicel	*F. oxysporum*	0.67 (0.31)	0.61 (0.27)	0.40 (0.14)	0.24 (0.07)	25.92 (3.26)	48.23 (7.86)
		G. zeae	0.62 (0.27)	0.71 (0.18)	0.42 (0.15)	0.28 (0.05)	27.45 (3.65)	81.11 (13.49)
		S. sclerotiorum	1.97 (0.16)	2.56 (0.55)	0.24 (0.08)	0.15 (0.01)	39.71 (5.83)	60.18 (5.17)
		T. reesei	6.64 (0.89)	5.94 (0.91)	0.91 (0.23)	0.70 (0.09)	55.71 (5.56)	97.27 (21.97)
	Switchgrass	*F. oxysporum*	1.14 (0.12)	1.11 (0.10)	0.59 (0.17)	0.42 (0.07)	27.74 (3.33)	122.56 (14.84)
		G. zeae	0.85 (0.22)	0.79 (0.13)	0.54 (0.18)	0.41 (0.05)	29.28 (4.55)	135.85 (23.30)
		S. sclerotiorum	1.06 (0.20)	1.31 (0.26)	0.19 (0.06)	0.13 (0.01)	34.71 (5.17)	69.04 (12.50)
		T. reesei	5.42 (0.51)	4.70 (0.34)	0.76 (0.16)	0.67 (0.10)	52.08 (7.11)	107.08 (24.39)

The least squares model identified the most significant effects and interactions. All four main effects (S, F, T, and M) were highly significant, as were several two and three factor interactions (Table 12). The T x M interaction was not significant, nor were higher order interactions containing this term. The interactions with fungal species, growth media, and assay temperatures group the six assay substrates into four major categories: 1) insoluble, primarily exo-glucanase hydrolyzed microcrystalline cellulose (Avi, FP), 2) insoluble, heterogeneous monocot biomass (CS, SG), 3) soluble, endo-glucanase hydrolyzed cellulose (CMC), and 4) miscible arabinoxylan (AX). Avicel-based growth media generally induced greater hydrolytic activity in *S. sclerotiorum* and *T. reesei* for all substrates except AX (Figure 5A-E). Switchgrass-based media showed a slight induction of hydrolytic activity for these two species on AX (Figure 5E). Switchgrass media induced higher activity compared to Avicel media in *F. oxysporum* and *G. zeae* on all substrates tested, particularly CS, SG, and AX (Figure 5D-F).

Table 12: Least squares model for the effects of assay substrate (S), fungal species (F), assay temperature (T), growth media (M), and their significant interactions on log transformed data (mM reducing sugars + 1.14).

Source	N_{parm}	*DF*	DF_{Den}	*F Ratio*	*p-value*
S	5	5	592	1861.77	< 0.0001
F	3	3	28	263.44	< 0.0001
T	1	1	592	354.40	< 0.0001
M	1	1	28	20.74	< 0.0001
S x F	15	15	592	60.06	< 0.0001
S x T	5	5	592	74.73	< 0.0001
S x M	5	5	592	37.47	< 0.0001
F x T	3	3	592	40.42	< 0.0001
F x M	3	3	28	56.06	< 0.0001
S x F x T	15	15	592	5.67	< 0.0001
S x F x M	15	15	592	3.07	<0.0001

Regulation of fungal CWDEs is controlled largely at the transcriptional level (Aro et al. 2005). Polysaccharides and smaller molecules derived from them can induce expression of genes coding for appropriate enzymes. Expression can also be repressed when those enzymes are not needed. Production of xylanases and other accessory CWDEs is controlled in part by the transcriptional activator Xyr1 in *T. reesei* and *G. zeae*, and the orthologous XlnR in *F. oxysporum* (Rauscher et al. 2006; Stricker et al. 2006; Brunner et al. 2007; Calero-Nieto et al. 2007; Calero-Nieto et al. 2008). Growth media is known to influence microbial enzymatic diversity and activity (Duff et al. 1987). Recent proteomic studies of *G. zeae* found at least 25 potential CWDEs expressed *in planta* during fungal infection of wheat heads and over 49 potential CWDEs expressed when grown on hop cell wall (Phalip et al. 2005; Paper et al. 2007). By comparison, only 9 potential CWDEs were expressed when *G. zeae* was grown on glucose (Phalip et al. 2005). These enzymes have important roles in plant-microbe interaction since at least 20 CWDEs have been identified as potential virulence factors in *G. zeae* (Cuomo et al. 2007). Similar results have been found in *S. sclerotiorum*; when grown on wheat bran, more xylanases were induced than when grown on filter paper or xylan (Olfa et al. 2007). For these reasons, when screening fungal cultures for novel enzymes it is important to consider the effect of growth media on protein induction.

The slight increase in activity observed in extracts of Avicel-grown *T. reesei* and *S. sclerotiorum* when assayed on the two biomass substrates tested is probably due to greater induction of cellulases, rather than induction of xylanases, which was not significantly different for the two media. In contrast, switchgrass-based media induced the species *F. oxysporum* and *G. zeae* to produce a suite of enzymes with higher activity on CS, SG, and AX (Figure 5C, D, F), but extracts from this media had little effect on hydrolysis of pure cellulosic substrates like Avi, FP, and CMC (Figure 5A, B, E). These data suggest that the increased sugar release by *F. oxysporum* and *G. zeae* extracts observed on biomass is due, at least in

part, to xylanase activity. The hydrolysis products of hemicellulose react with DNS in the same manner as cellulose hydrolysis products, contributing directly to the total sugar content measured in the assay. Removal of hemicellulose could also improve the accessibility of cellulose microfibrils, resulting in higher cellulase activity. While hemicellulase activity clearly contributes to overall biomass hydrolysis, other mechanisms such as removal of lignin via peroxidase or esterase activity could also be induced by microbial growth on biomass. Although the plant pathogens *F. oxysporum* and *G. zeae* have lower cellulase activity compared to *T. reesei* (Figure 5A, B, E), when grown on switchgrass media, they have comparable activity to *T. reesei* on biomass and higher activity on arabinoxylan, potentially due to the expression of different classes or larger concentrations of enzymes. This demonstrates that non-cellulolytic enzymes are being produced that contribute to overall biomass hydrolysis. These enzymes could potentially be used to complement and improve industrial enzyme preparations produced by *T. reesei*.

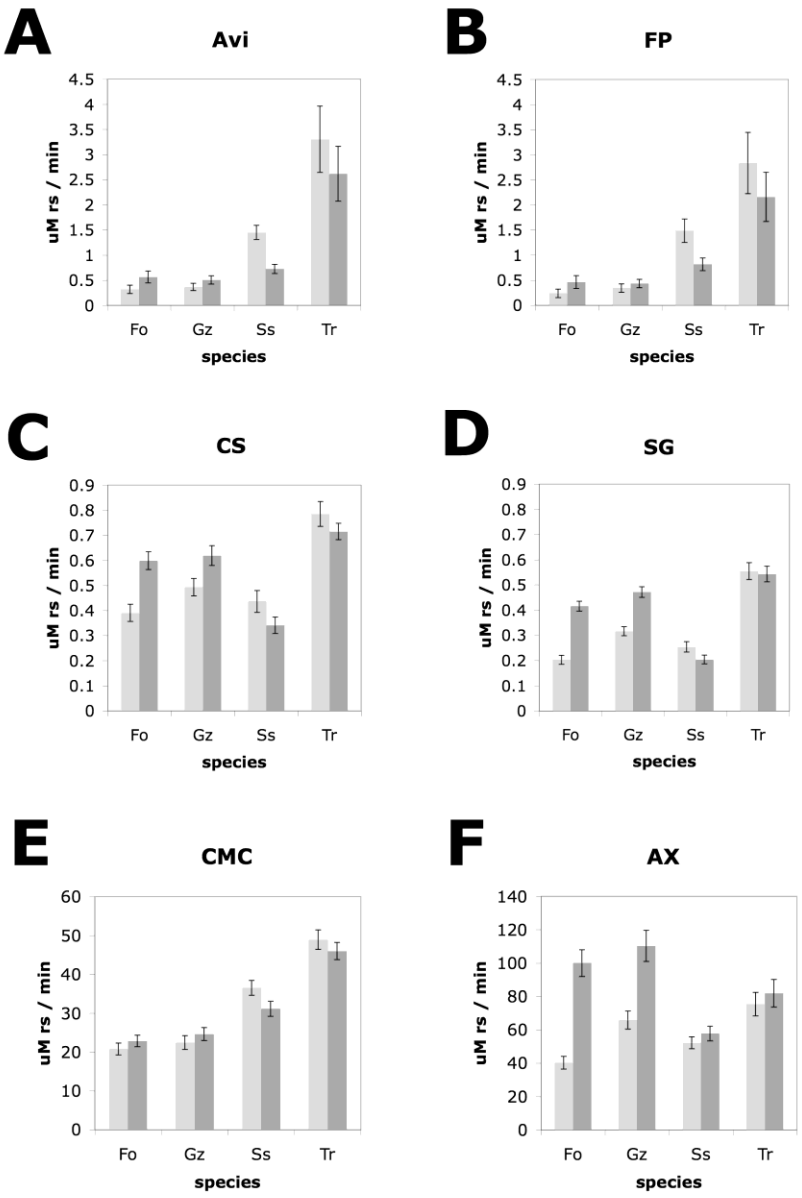

Figure 5: Effect of two growth media, Avicel (light gray) and switchgrass (dark gray), on polysaccharide hydrolysis rates by extracts of four fungi, *F. oxysporum* (Fo), *G. zeae* (Gz), *S. sclerotinia* (Ss), and *T. reesei* (Tr). Polysaccharide substrates include A) Avicel (A), B) filter paper (FP), C) corn stalk (CS), D) switchgrass (SG), E) carboxymethylcellulose (CMC); and F) arabinoxylan (AX). Avi and FP were hydrolyzed for 20 hours, CS and SG were hydrolyzed for 80 hours, and CMC and AX were hydrolyzed for 2 hours. Error bars indicate mean standard error.

Comparing the activities of these isolates grown on different growth media also illustrates the need to evaluate multiple growing conditions for enzyme activities. Growth and CWDE production may be reduced if the fungi cannot adequately degrade and utilize the complex polysaccharides. Furthermore, biomass may contain compounds that are inhibitory to fungal growth. By comparing activities produced on Avicel- and switchgrass-media with multiple substrates, we were able to note the differential activities that indicate presence of non-cellulolytic enzymes.

Extracts from all species showed increased hydrolysis rates with increasing temperature for the substrates Avi and FP (Figure 6A, B). Activity of *F. oxysporum* and *G. zeae* was not detectable at 22°C. On biomass, activity of *T. reesei* increased with increasing temperature, while *F. oxysporum*, *G. zeae*, and *S. sclerotiorum* had highest activity at 37°C (Figure 6C, D). *S. sclerotiorum* had similar activities at 22 and 37 ºC, and significantly reduced activity at 50°C. *F. oxysporum* and *G. zeae* had lower activities than *S. sclerotiorum* and *T. reesei* when tested on CMC (Figure 6E), but higher activities than *S. sclerotiorum* and comparable activity to *T. reesei* on AX (Figure 6F). On both of these substrates, there was no difference in activity at 22 and 37°C, but increased activity at 50°C. Although arabinoxylanase activity is highest at 50°C, this assay was only conducted for 2 h, compared to 80 h for the biomass assay. Short-term improvements in activity by increasing temperature may be outweighed by the long-term consequence of thermal instability. The pathogens used in this study were isolated from New York State, and have the ability to thrive on plant biomass at moderate temperatures (Sutton 1982). *G. zeae* overwinters on and within field residues of maize (*Zea mays*) and small grains, particularly in the recalcitrant nodal areas (Sutton 1982). It grows as a saprophyte during the fall, winter, and spring, during which time CWDEs may be very important for growth and reproduction. There is evidence that temperatures between 22-24°C favor outbreaks of ear rot (Sutton 1982; Paul et al. 2007). The fungus may benefit from copious

production of CWDEs during this rapid necrotrophic growth phase. Similarly, although *S. sclerotiorum* is not a competitive saprophyte in the soil, it grows rapidly in culture and *in planta* and relies on CWDE to facilitate rapid colonization of plants (Morrall and Dueck 1982; Hegedus and Rimmer 2005).

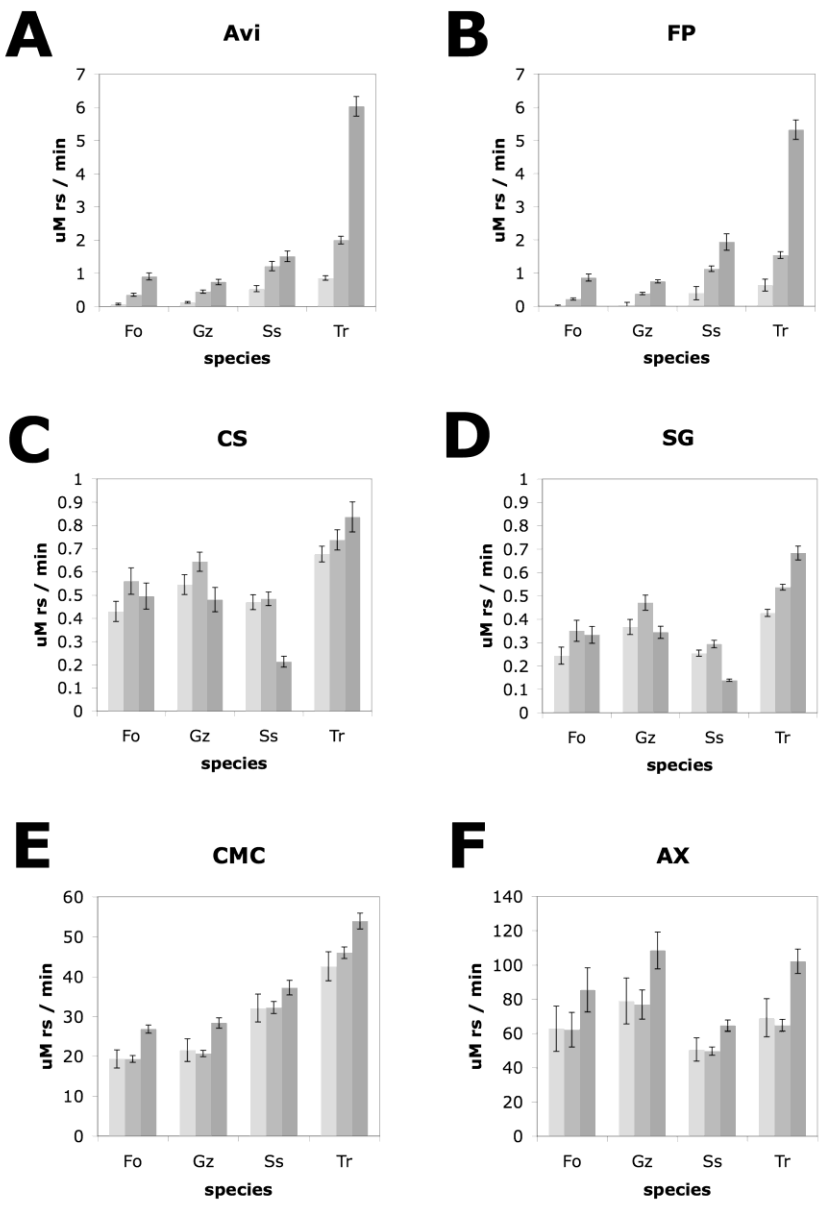

Figure 6: Effect of three temperatures, 22 (light gray), 37 (medium gray), and 50 °C (dark gray), on polysaccharide hydrolysis rates by extracts of four fungi, *F. oxysporum* (Fo), *G. zeae* (Gz), *S. sclerotinia* (Ss), and *T. reesei* (Tr). Polysaccharide substrates include A) Avicel (A), B) filter paper (FP), C) corn stalk (CS), D) switchgrass (SG), E) carboxymethylcellulose (CMC); and F) arabinoxylan (AX). Avi and FP were hydrolyzed for 20 hours, CS and SG were hydrolyzed for 80 hours, and CMC and AX were hydrolyzed for 2 hours. Error bars indicate mean standard error.

Enzyme activity is expected to increase with increasing temperatures, in some cases doubling with every 10°C increase up until a point of thermal inactivation (Fullbrook 1996; Rosgaard et al. 2006). Maximum activity for fungal cellulases has been observed between 45 and 55°C (Saddler and Gregg 1998; Tengborg et al. 2001). Hydrolysis at higher temperatures with increased enzyme activity could reduce the costs associated with producing ethanol from biomass by reducing reaction time and required enzyme loading. Much work has been done to improve the thermostability of cellulases and other hydrolytic enzymes at temperatures above 50°C (Ai and Wilson 2002; Gusakov et al. 2005; Voutilainen et al. 2007). In a conversion plant employing a separate hydrolysis and fermentation scheme, each step can operate at its optimum temperature, making enzymes active at 50°C or higher important for efficient hydrolysis (Tengborg et al. 2001). On the other hand, plants operating with a simultaneous saccharification and fermentation schemes will require enzymes that are most active between 35 and 38°C for maximum hydrolysis (Szczodrak and Fiedurek 1996; Tengborg et al. 2001). This is a compromise between the optimum temperature for hydrolysis and the optimum for fermentation, which is between 28 and 35°C (Szczodrak and Fiedurek 1996). It is possible that plant pathogens that thrive in mesophilic environments may provide enzymes that could be optimized for either operational scheme, as is already the case with *T. reesei*.

Conclusions

This research presents a rapid, quantitative, reproducible, and high-throughput platform for analyzing CWDE activities of fungal extracts. By choosing appropriate cell wall components as substrates, it is possible to gain insight into the mechanism of hydrolysis for complex and heterogeneous biomass materials. Though this study used only two complex biomass substrates for analysis, more complete information on CWDEs substrate specificity and activity could be obtained by using additional

biomass sources and pretreated biomass materials. Greater diversity of substrates will allow for better characterization and diversity of CWDEs for cellulolytic cocktails. Use of multiple fungal growth media and hydrolytic assay temperatures in this screening platform provides a more complete picture of substrate specificity and thermostability.

Microbes employ a variety of enzymes to deconstruct the plant cell wall and growth medium affects the activity observed in the final extracts. Complex polysaccharides such as those found in the cell wall can induce synthesis of enzymes preferentially hydrolyzing those sugars. In addition to substrate specificity, enzymes have temperature optima that may reflect the environment of the microbe that produces them. Enzymes of *T. reesei* are quite stable at higher temperatures, but improving thermal stability of novel accessory enzymes could be an important target for improving overall industrial biomass conversion. While the *T. reesei* enzyme system is quite efficient at degrading pure cellulose, there are opportunities to complement its enzyme systems with novel enzymes from other species. The fact that the plant pathogenic fungi used in this study compared favorably *to T. reesei* is supported by genomic and proteomic analyses demonstrating that plant pathogenic fungi are rich reservoirs of multiple classes of enzymes involved in cell wall breakdown (Phalip et al. 2005; Yajima and Kav 2006; Paper et al. 2007; Martinez et al. 2008). Identifying superior species and isolates is an important first step to obtaining novel cellulolytic enzymes.

Future studies based on this initial work will characterize individual enzyme components produced by plant pathogens identified as having good crude activity to obtain information on mode of catalytic behavior and specific activity. With this information, more complete enzyme cocktails could be developed, incorporating additional cellulases and accessory enzymes complementary to current

cellulolytic cocktails' activities. Plant pathogens present a unique opportunity for prospecting for novel cellulolytic and accessory enzymes for biomass hydrolysis (King et al. 2009).

CHAPTER 4: OBSERVING *THERMOBIFIDA FUSCA* CELLULASES CEL5A AND CEL6B BINDING ON SIMPLE AND COMPLEX BMCC MORPHOLOGICAL STRUCTURES USING EPI-FLUORESCENT MICROSCOPY

Introduction

Biological conversion of lignocellulosic biomass to fermentable sugars is chiefly accomplished by a class of enzymes called cellulases. At the most fundamental scale, cellulose hydrolysis occurs when cellulases bind to cellulose polymers and hydrolyze the β-1,4 linkages between glucose monomers (Ghosh and Singh 1993; Bayer et al. 1998; Wilson 2009). However, gaining access to polymers requires that cellulases diffuse and bind to complex three dimensional structures such as cellulose microfibers, mats, and particles. In addition, cellulases exhibit different binding characteristics depending on their reactive domains and evidence indicates the concerted effort of these different cellulases is required to efficiently hydrolyze cellulose polymers. Thus a mechanistic framework for cellulose hydrolysis is essential for improved design of cellulase cocktails for lignocellulosic biomass hydrolysis.

The kinetics of cellulose hydrolysis is dominated by a set of mass transport and reactions that take place across multiple physical phases that represent a heterogeneous catalysis system. Multiple enzymes with different modes of binding and hydrolysis, and varying sizes add an additional level of complexity that makes kinetic modeling challenging. Michaelis-Menten kinetics has been used extensively to model cellulose hydrolysis by cellulases (Suga et al. 1975; Okazaki and Moo-Young 1978; Gusakov et al. 1985; Nidetzky et al. 1994). However this kinetic framework is based on mass action laws for homogeneous reactions that cannot be directly applied to the heterogeneous cellulase-cellulose reaction. In this case the substrate, cellulose polymers in the plant cell wall, is embedded in a matrix of

hemicellulose and lignin, making access difficult without some pretreatment of the lignocellulose. The cellulose polymers themselves feature both macro-structures and pores that define the accessibility of the substrate to the enzymes. Previous studies show that surface accessibility is a key component to efficient lignocellulose hydrolysis (Jeoh et al. 2007; Zhu et al. 2011; Luterbacher et al. 2013). Cellulases hydrolyze cellulose most efficiently as part of a synergistic mixture, employing both endocellulases, which bind randomly along the cellulose polymer and hydrolyze β-1,4 linkages in the middle of the chain before either unbinding and diffusing away or processing to the next link for hydrolysis, and exocellulases, which bind at the ends of cellulose polymers and release smaller oligosaccharides from the ends of the chains. Together, these two modes of cellulolytic action enhance degradation, but there may be instances of steric hindrance on the cellulose surface and in the pore structure (Luterbacher et al. 2013). Developing a kinetic framework for cellulose hydrolysis by cellulases will require understanding the behavior of pure cellulase components, both endocellulase and exocellulase, and the behavior of these components in a mixture in addition to the effects of surface accessibility.

Langmuir kinetics provides a classical heterogeneous catalysis framework for the modeling of cellulases binding to cellulose (Bothwell and Walker 1995; Zhang and Lynd 2004; Bansal et al. 2009). The insoluble cellulose substrate with its macro and micro pores, defines the reactive space in which enzymes are transported, bind and depolymerize cellulose. The formation of a reactive enzyme-substrate complex is generally assumed to be a reversible mechanism, which is a core assumption of Langmuir kinetics. However, issues of steric hindrance and pore entrapment can yield binding kinetics that is not consisted with classic Langmuir kinetics. Thus, good temporal and spatial resolution of enzyme concentration within the pores and on the surface of insoluble cellulose is necessary to tease out molecular mechanisms involved in the enzymatic hydrolysis of cellulose. Previous studies in our

research group have documented and analyzed temporal cellulase binding data to develop an understanding of the molecular basis for enzyme-substrate interaction (Bothwell et al. 1997; Bothwell et al. 1997; Jeoh et al. 2002; Jung et al. 2002; Jung et al. 2003; Jeoh et al. 2006; Santhanam and Walker 2008). More recently, we have developed high spatial and temporal resolution methods based on advanced imaging techniques and biochemically well characterized fluorescently labeled cellulases to obtain additional insights (Moran-Mirabal et al. 2008; Moran-Mirabal et al. 2009; Moran-Mirabal et al. 2011; Luterbacher et al. 2013).

Cellulases can be labeled with small organic dyes of various colors in a way that will minimize the effect on native activity (Moran-Mirabal et al. 2009). These labeled cellulases can be incubated with immobilized cellulose on a solid substrate and observed for several hours until binding equilibrium is achieved. The increase in florescence intensity detected by the camera as photons can be correlated to increased cellulase surface concentration. This ability to locate and track labeled cellulases provides a unique approach to observing cellulase transport and binding, and allow for the testing of hypotheses about cellulases interactions with the structural features of cellulose particles and fibers.

The small organic dyes are subject to a process called photo-bleaching, wherein overexposure to light causes decay in the photon output of the molecules. This process is highly temperature dependent, with higher temperatures enhancing the bleaching effect. Photo-bleaching can be mitigated by the addition of ascorbic acid to the imaging buffer, but long term effects are still apparent in the temporal data. Additionally, the selection of the photon sampling space within the image can influence the quality of the signal detected. Larger spaces will contain more data points, but may also include more complicated cellulose structures, such as mats (Moran-Mirabal et al. 2008). Smaller sampling areas

contain less data, but also make it possible to interrogate small structures, such as fibrils, without much interference from other structures.

The goal of this study was to develop a method to effectively track cellulase binding in real time and tease out insights into cellulose-cellulase binding interaction. *Thermobifida fusca* (*T.fusca*) endocellulases and exocellulases are applied to immobilized cellulose substrates and binding is observed at three temperatures to build a kinetic framework for cellulase binding in pure components and in synergistic mixtures. The effects of photo-bleaching for each dye are measured and a correction is established to remove the artifact. The variations in image analysis methods are evaluated to glean the most relevant spatial and temporal data from each experiment. The synthesis of effectively collected spatial and temporal binding data with thoughtful analysis will contribute to greater understanding of the fundamental mechanisms governing cellulase-cellulose binding and hydrolysis.

Materials and Methods

Cellulase labeling and purification

T. fusca cellulases Cel5A and Cel6B were expressed and purified as described in Jeoh et al. 2002 (Jeoh et al. 2002). The cellulases were fluorescently labeled with amine–reactive dyes Alexa Fluor 488 and 647 (Invitrogen, Carlsbad, CA) at 10 μM concentration with labeling molar ratio (LMR) of 100:1 at 4°C for 24 hours using the solid phase (SP) labeling method of Moran-Mirabal et al. 2009 (Moran-Mirabal et al. 2009). Briefly, the cellulases were labeled using the SP technique to prevent labeling of the enzymes' active site. Labeled enzymes were separated using fast protein liquid chromatography (FPLC) into populations with distinct degrees of labeling (DoL) at 21°C. Protein concentration and DoL were measured for each labeled fraction. Only the fractions of enzymes with a DoL of 1 were used for the

experiments described in this paper. Hydrolytic activities of labeled cellulases were measured using BMCC and compared to that of unlabeled enzymes as described in Moran-Mirabal et al. 2009. No significant change in activities was observed (Moran-Mirabal et al. 2009). Labeled cellulase fractions were distributed into 50 µL aliquots at concentrations of 200 nM and stored at -20°C. For the experiments described in this paper, the 200 nM fractions were diluted in 50mM sodium acetate buffer to a final enzyme concentration of 2 nM.

Immobilized cellulose substrate preparation

A solution of 1mg/ml bacterial micro-crystalline cellulose (BMCC, Monsanto Cellulon, San Diego, CA) in water was pretreated as previously described in Jeoh et al. 2002 and Santhanam et al. 2008 (Jeoh et al. 2002; Santhanam and Walker 2008). A 50 µg/ml BMCC suspension in MilliQ water was sonicated for 5 min at 60% amplitude using a SPLt sonicator (Branson, Danbury, CT) to break up some of the more dense cellulose aggregates into less dense pieces, including some individual fibers. For the room temperature experiments, glass slide bottomed petri dishes (MatTek Corp., Ashland, MA) were used to prepare the immobilized cellulose substrate. For the 34° and 50 °C experiments, a Bioptechs temperature controlled fluidic chamber (FCS2 chamber assembly, Bioptechs, Butler, PA) was used with 40 mm 170 µm thick glass wafers (Bioptechs, Butler, PA) to prepare the immobilized cellulose substrate. In all cases, the glass substrates were pretreated in a Plasma Cleaner (Harrick, Ithaca, NY) to make a hydrophilic surface for depositing the BMCC. Five 10 µL drops of BMCC in water solution were placed on the glass surface, spread around, and allowed to lightly dry on a 70°C hotplate for 30 minutes for an initial cellulose loading of 2.5 µg. The substrates were rinsed with MilliQ water to remove any non-adhered cellulose and then incubated with a solution of 10% BSA (Fisher Scientific, Pittsburgh, PA) in 50 mM sodium acetate buffer overnight at room temperature to minimize non-specific adhesion of

cellulases onto the substrate surface. Following the incubation, the substrates were washed with 50 mM AA buffer (degassed 50 mM sodium acetate buffer pH 5.5 supplemented with 5 mM ascorbic acid) to remove the BSA. Ascorbic acid was added to scavenge oxygen in the buffer solution and reduce the effects of photo-bleaching during the experiment as described in Moran-Mirabal et al. 2008 (Moran-Mirabal et al. 2008). The samples were loaded onto the microscope and the temperature was held constant in the 34 and 50°C experiments by resistive heating provided by the FCS2 assembly.

Cellulase imaging

Binding time lapse experiments

For each experiment, an area of interest was selected on the cellulose substrate then the AA buffer was removed and replaced with 2.5 mL of the 2nM cellulase solution in 50 mM AA buffer for a total enzyme loading of 0.005 nmoles. In room temperature experiments the buffer was removed and cellulase solution was added using a 5 mL pipette and in the higher temperature experiments buffer was removed and cellulase solution was added using a syringe pump. Cellulase binding was observed using an Olympus IX-81 inverted microscope with ZDC focus correction, a motorized X–Y stage (ASI, Eugene, OR), and a 60x/1.2NA UPLSAPO Olympus water immersion objective (Olympus, Center Valley, PA). Appropriate filters were used for both excitation and emission for enzymes labeled in different colors, Semrock Brightline 485/20-25 and 523/45-25 for excitation and emission for the 488 channel respectively, Semrock Brightline 650/13-25 and 676/29-25 for excitation and emission in the 647 channel, and a Semrock 410/504/582/669 nm BrightLine quad-edge dichroic beamsplitter (Semrock, Rochester, NY). Olympus software (Olympus, Center Valley, PA) was used to control the filter wheels and shutters, allowing for data acquisition in both the 488 and 647 channels. Images were recorded on a

Hamamatsu ImageEM EMCCD camera (Hamamatsu Bridgewater, NJ) with exposures of 50 ms. Three exposures were taken and averaged to produce each frame to improve the signal to noise ratio. The sample was exposed to light only during image acquisition, a total of 150ms for each frame. Binding time-course experiments were run for up to 240 minutes for room temperature experiments, 180 minutes for 34° experiments and 20 minutes for 50° experiments. Images were obtained at pre-determined intervals to capture the binding phenomena at each temperature and saved as stacks of raw image data. In all experiments, the total exposure time was limited to 15 seconds (50 ms/frame, 3 frame average, 100 total frames).

Photo-bleaching measurement

Cellulose substrates and cellulase solutions were prepared as previously described in this chapter. Instead of applying the substrate to the microscope and observing the initial cellulase binding, the cellulases were allowed to bind overnight in a dark chamber to come to an equilibrium level of binding. Once an equilibrium level of binding had been achieved, the substrates were imaged using the Olympus IX-81 inverted microscope with the 60x/1.2NA UPLSAPO Olympus water immersion objective. Appropriate filters as previously described, were used for both excitation and emission for enzymes labeled in different colors and Olympus software was used to control the filter wheels and shutters, allowing for data acquisition in both the 488 and 647 channels. Images were recorded on a Hamamatsu ImageEM EMCCD camera with exposures of 50 ms. The sample was exposed to light only during image acquisition. The bound labeled enzymes were exposed to the same amount of light that they would receive over the course of the experiments previously described. For these experiments the total

exposure time was limited to 15 seconds (50 ms/frame, 3 frame average, 100 total frames). Photo-bleaching was measured at 23, 34 and 50°C for each enzyme and fluorophore.

Image analysis

All images were obtained as stacks of image files and were aligned and corrected for stage drift using ImageJ plugin StackReg (National Institutes of Health, USA). The signal intensities in the aligned images were pre-processed for analysis using a custom MATLAB program (The Mathworks, Natick, MA) adapted from Moran et al. 2008 to separate pixels into signal and background populations over the time-course for both the 488 channel and the 647 channel (Moran-Mirabal et al. 2008). First, the routine prompts the user to select the center point of a region to analyze. To document the effect of the number of pixels on the quality of the data produced, three different sizes were used for this region of interest, a 10 x 10 pixel, a 50 X 50 pixel, and a 100 x 100 pixel squares. Once the center point of each square was determined, the user is prompted to select background pixels from the region of interest to establish a threshold for separating signal pixels, with fluorescence detected from the bound cellulases, from background pixels, which have no detected signal from the fluorescent cellulases. Unbound cellulases in solution have negligible fluorescent signal in the plane of focus due to their low concentration in the chamber. The average intensity and the standard deviation of that intensity were measured for a selected background region for all time points in the series and the mean background was subtracted from each image to correct for fluctuations in illumination intensity. Saturated signal pixels were also removed during this pre-processing. Saturated areas occur when the fluorescence intensity signal from the bound cellulases exceeds the detection limit of the camera in a region, resulting in saturated pixels that limit the detection of changes in intensity in that area.

Signal pixels were assigned by generating a mask from the final image recorded during the time-course, to obtain good contrast between signal and background populations as described in Moran-Mirabal et al. 2008 (Moran-Mirabal et al. 2008). From the selected image, a threshold grayscale level was calculated and the image was separated into signal and background. A mask of signal pixels is generated and successively applied to all images recorded during the time-course. This was done to ensure that the same number of pixels are considered signal in all images contained within the stack. The program calculates the integrated mean and standard deviation of pixel intensities for the selected signal regions for each time point. All of the image data was subject to this image analysis program to obtain quantitative data for the binding time-course experiments and the photo-bleaching measurements.

Fluorescence intensity data from the photo-bleaching experiments for both AF488 and AF647 was imported into MS Excel to determine the temporal effect of photo-bleaching. The fluorescence signal intensities were plotted against the number of frames to show the decrease in detected fluorescence signal with increasing total light exposure over the course of the experiment. A linear regression was fit to the data. The slope, *m*, the y-intercept, *b*, and the R^2 value of the decrease in detected fluorescence were determined using the LINEST function in MS Excel. A linear function, shown below as equation 66, was used to correct for photo-bleaching in each frame in a series.

$$\hat{I}_t = \alpha I_t \qquad 65$$

Where I_t is the detected fluorescence intensity at time t, $\hat{I}_t$ is the corrected fluorescence intensity at time t, and α is the photo-bleaching correction factor. For each frame, the signal intensity is adjusted by

this correction to minimize the effect of photo-bleaching on the measurement. This process was repeated for each fluorophore, AF488 and AF647, at each temperature, 23°, 34°, and 50°C.

The time course fluorescence signal intensity data for each experiment was imported into MS Excel and the data was compiled according to cellulase, either Cel5A or Cel6B and label color, either AF488 or AF647. The pre-processed signal intensities from the binding time-course experiments were corrected for photo-bleaching in each data set. The resulting sets of corrected fluorescence intensity data were normalized to 1 to facilitate comparisons between experiments with different numbers of signal pixels and therefore different levels of detected fluorescence intensities. These photo-bleaching corrected and normalized fluorescence data sets were plotted against the time-course to show the increase in fluorescence in the selected region of interest with time, corresponding to the increasing concentration of bound cellulases.

Results

Photo-bleaching Corrections

As noted earlier, bleached fluorophores are not detected by the camera and therefore are not measured, though they occupy a binding site on the substrate. Thus, it is necessary to correct for the effects of bleached enzymes on overall cellulase concentration measurements. Temperature also affects the photons emitted by each fluorophore, with reduced signal at higher temperatures. This loss of signal can also be corrected for once the bleaching characteristics are documented.

Photo-bleaching was measured by preparing a BMCC substrate as described earlier, applying a solution of labeled cellulases, and allowing the mixture to bind until equilibrium occurs, by allowing the apparatus to incubate overnight in a dark chamber. The BMCC substrate was placed on microscope

stage, as described earlier, and the bound labeled enzymes were exposed to the same amount of light that they would receive over the course of an experiment. For all experiments and fluorophores, bleaching was measured at 23, 34 and 50°C. For these experiments the total exposure time was limited to 15 seconds (50 ms/frame, 3 frame average, 100 total frames). Figure 7 is a representative plot of the loss of fluorescence intensity with time for Cel5A labeled with AF488 at 50°C for one of the experiments described, before the photo-bleaching correction is applied.

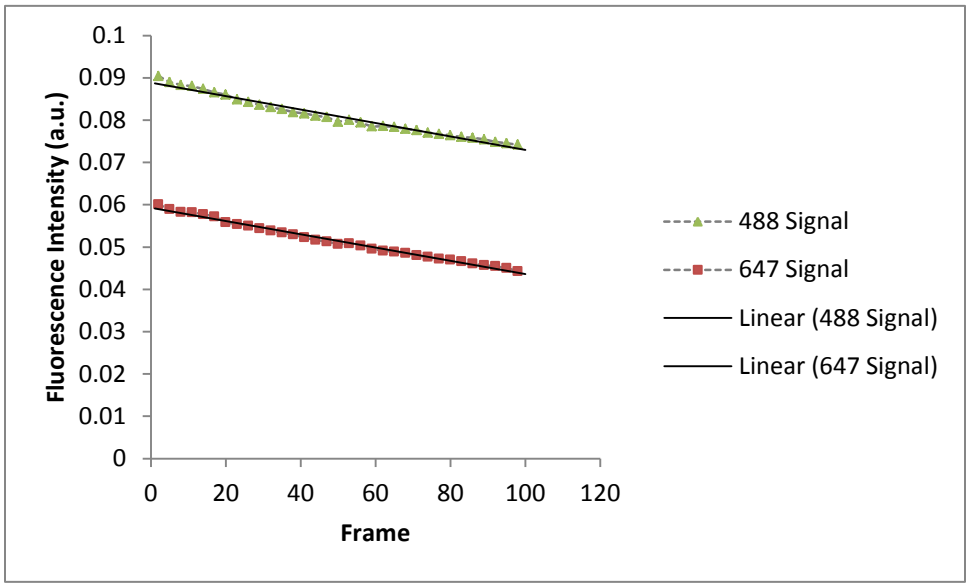

Figure 7: Loss of detected fluorescence signal for AF488 (green triangles) and AF647 (red squares) at 50°C over the course of 100 frames. Each frame is an average of three 50ms exposures, 150ms per frame. For 100 frames, the total time the sample is exposed to light is 15 seconds. At 50°C, 20% of the signal is lost in the 488 channel and 30% in the 647. The decay in the detected signal is linear in this time frame, and so a correction function can be applied to the data.

The detected loss of fluorescence signal over the course of the experiment due to photo-bleaching was linear for all temperatures; thus, a linear regression was fitted to these data. The values for the slope, *m*, the y-intercept, and r^2 are shown in Table 13 below for all temperatures and fluorophores. The slope, *m*,

is a measure of the loss of fluorescence intensity in each frame. Thus, we can use *m* to correct the experimental data for loss of fluorescence.

Table 13: Values of *m* for each fluorophore for each temperature. These values are used in eq. 1 to correct the experimental data for the effects of photo-bleaching.

	AF 488			AF 647		
Temperature	**Slope, *m***	**y-intercept**	**r^2**	**Slope, *m***	**y-intercept**	**r^2**
23°C	-0.00136	1.020	0.970	-0.00091	1.018	0.934
34°C	-0.00027	0.980	0.990	-0.00036	0.971	0.985
50°C	-0.00175	0.981	0.972	-0.00259	0.975	0.990

Two scenarios for photo-bleaching correction were derived: first, an assumed steady-state correction, depicted as follows in Figure 8:

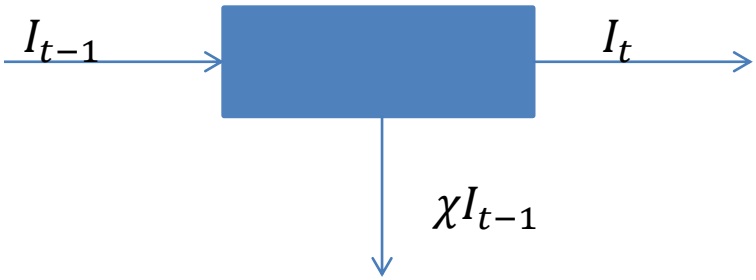

Figure 8: Depiction of a steady-state loss of fluorescence due to photo-bleaching, where: I_t is the signal at time t, I_{t-1} is the signal at time t-1 (preceding frame), and χ is the fraction of bleached fluorophores
We know that I_t is equal to the signal at time t-1, minus some fraction of bleached fluorophores:

$$I_t = I_{t-1} - \chi I_{t-1} \qquad 66$$

The corrected signal $\widehat{I_t}$ is the signal recorded at time t, plus the signal from the fraction of bleached fluorophores added back in.

$$\hat{I}_t = I_t + \chi I_{t-1} \quad (67)$$

Such that $\widehat{I_t}$ is simply equivalent to I_{t-1}.

Fluorophore bleaching is more generally defined as an exponential decay dictated by a characteristic bleaching time assuming constant illumination:

$$I_t = I_0 e^{-t/\tau} = I_0 e^{-f/\varphi} \quad (68)$$

Where I_0 is the fluorescence intensity at time t=0, τ is the characteristic decay time, and where in the second expression f is the number of frames after the initial intensity and φ the characteristic decay in frames. Assuming the fluorescence decay is slow in the time course experiments considered, Equation 69 can be expanded according to the Taylor series as follows:

$$I_t \approx I\left(1 - \frac{f}{\varphi}\right) = I(1 - \chi f) \quad (69)$$

If we consider just the intensities in the frame at time t and the frame at time t-1 (f=1) this becomes

$$I_t = I_{t-1}(1 - \chi) \quad (70)$$

This can be rearranged to

$$I_{t-1} = \frac{1}{1 - \chi} I_t \quad (71)$$

Combining (71) with (66) and (67) we get

$$\hat{I}_t = \frac{1}{1-\chi} I_t \qquad 72$$

The fractional intensity loss per frame corresponds to χ, and the accumulated loss of fluorescence intensity due to photobleaching over the time course is χf, where f is the frame number. From the linear regression data, we know that the slope *m* is the fractional intensity loss per frame χ for each fluorophore and temperature. We can define α_d as the quantity $\frac{1}{1-\chi f}$ so that the correction given by (72) becomes

$$\hat{I}_t = \alpha_d I_t \qquad 73$$

The value for α_d is defined using a calibration standard, the known quantity of fluorescence decay for the fluorophores over time and will be a distinct value for each fluorophore, the 488 tag and the 647 tag, denoted by *d*. In the time course investigated in this experiment, the decay is linear, and α can be defined in terms of the slope of the decay curve. The data and corrected values from photo-bleaching experiments using equal concentrations of Cel5A labeled with 488 tags and 647 tags at each temperature are shown below in Figure 9.

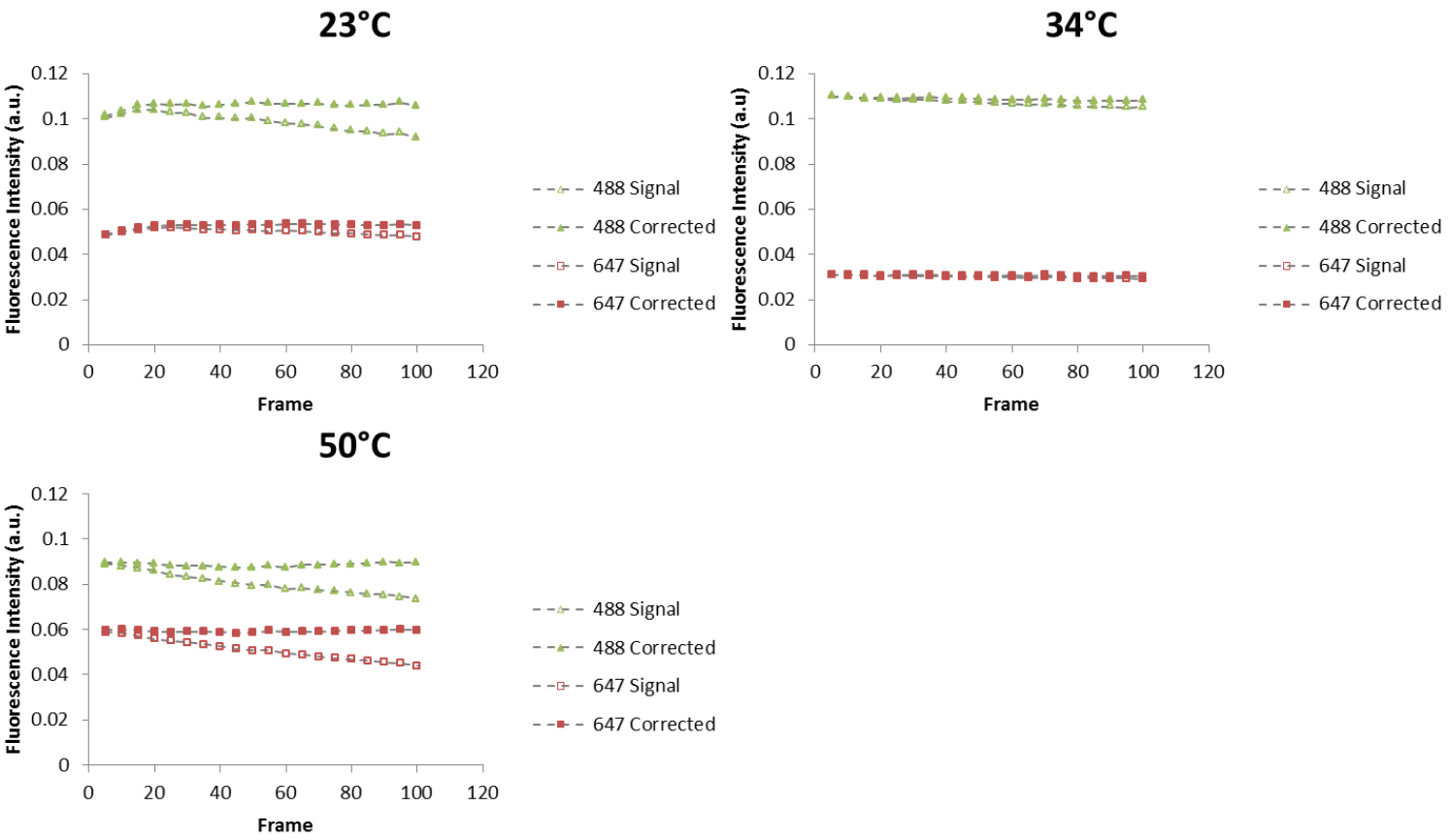

Figure 9: Photo-bleaching correction data for all temperatures, 23°, 34°, and 50°C. Raw signal data for Cel5A labeled with 488 is shown with unfilled green triangles; photo-bleaching data corrected for Cel5A labeled with 488 is shown as filled green triangles. Raw signal data for Cel5A labeled with 647 is shown as unfilled red squares, photo-bleaching corrected data for Cel5A labeled with 647 is shown as filled red squares.

The severity of the photo-bleaching effect varied with temperature. At room temperature (23°C), there was a 15% loss of signal in the 488 channel after 100 frames, and a 10% loss after 100 frames in the 647 channel. At 34°C there was a 3% loss in the 488 channel after 100 frames and a 4% loss in the 647 channel after 100 frames. At 50°C, the loss of signal after 100 frames was 20% in the 488 channel and 30% in the 647.

Though the photobleaching correction data was collected at steady state, the experimental data is being collected while additional fluorescence intensity is added to the system via cellulase binding on the cellulose substrate, as depicted in Figure 10:

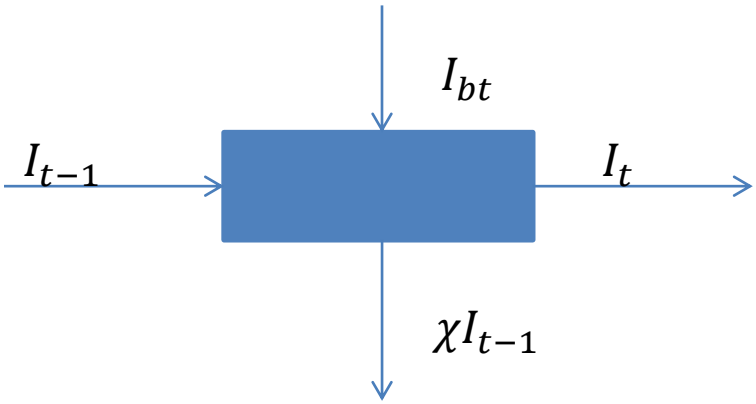

Figure 10: Depiction of the non-steady state loss of fluorescence intensity signal due to photobleaching. Where I_t is the signal at time t, I_{t-1} is the signal at time t-1 (preceding frame), χ is the fraction of bleached fluorophores, and I_{bt} is the signal from the newly bound fluorophores
In this situation, the fluorescence intensity I at time t is defined as follows:

$$I_t = I_{t-1}(1-\chi) + I_{bt} \tag{74}$$

From (67) we know the corrected signal should be whatever the signal was in the preceding frame, plus whatever the signal from the newly bound enzymes is

$$\hat{I}_t = I_{t-1} + I_{bt} \tag{75}$$

We can rearrange (74) to get

$$I_{t-1} = \frac{I_t - I_{bt}}{1-\chi} \tag{76}$$

Substituting (76) into (75) we get

$$\hat{I}_t = \frac{I_t}{1-\chi} - \frac{I_{bt}}{1-\chi} + I_{bt} \quad (77)$$

By multiplying the I_{bt} term by $\frac{1-\chi}{1-\chi}$ we can rearrange (77) as follows

$$\hat{I}_t = \frac{I_t}{1-\chi} - \frac{I_{bt}}{1-\chi} + \frac{(1-\chi)I_{bt}}{1-\chi} \quad (78)$$

This simplifies to

$$\hat{I}_t = \frac{I_t}{1-\chi} - \frac{\chi I_{bt}}{1-\chi} \quad (79)$$

We have already defined α_d as the quantity $\frac{1}{1-\chi f}$ over the time course of the experiment, thus (79) simplifies to

$$\hat{I}_t = \alpha_d I_t - \alpha_d \chi I_{bt} \quad (80)$$

The values for α and χ have been previously defined from the linear slope of the decay data in Table 13.

For Cel5A, the correction during the dynamic binding will be very small, as the binding all occurs very early in the time course, when the value for χ_t is low. The value of $\alpha_d\chi_t$ is low during this period, and the correction will be dominated by $\alpha_d I_t$. Thus, the dynamic binding for Cel5A can likely be approximated by the steady state correction shown in (73). For Cel6B, the steady state correction will probably be fine for fibers, but since the mat structures continue to bind throughout the time course, it's possible the value for $\alpha_d\chi$ for 647 will become significant. However, since the rate of binding slows as the time course progresses, the value for I_{bt} will become smaller, and the value for the corrected signal will be

dominated by the value of $I_{t-1,}$ the signal from the enzymes that are already bound. In this case the correction for dynamic binding could still be approximated using the steady-state correction.

Additionally, assuming I_0 is the intensity at time 0, then in frame 1, all new fluorescence imaged in that frame is due to binding rather than photobleaching and I_1 does not need to be corrected. However, after acquiring I_1, a certain fraction of the fluorophores has been bleached, and those fluorophores can be approximated by $\hat{I}_1 = \alpha_d I_1$. The next frame, I_2, needs to be corrected, but only for the fraction that has been bleached from I_1 such that $\hat{I}_2 = I_2 + \alpha_d I_1$. If this process is done iteratively, the correction does not require knowing anything other than the bleaching constant. This is a simplified correction and assumes bleaching occurs instantaneously after image acquisition. In practice, because the image acquisition takes some finite time, 50ms in this case, it approximates well in the early frames of the time course data.

Influence of sampling size on structural information

High temporal and spatial resolution data can be obtained from a time-course series of fluorescent images. The goal is to maximize the fluorescent signal collected. Larger collection areas have more signal pixels, but also more background pixels without information. Smaller collection areas have less background, but have more variability in signal quality. To obtain the most useful information, it is important to understand the effect of the number of pixels in a sampled area has on the detected signal from that area.

In this study, we evaluated the best collection area size for detecting the signal from cellulases bound to individual BMCC fibers and the signal from more complex BMCC mats. Once the cellulase binding experiments were completed, the images were aligned in ImageJ and analyzed to separate

signal pixels from background pixels. An area of interest was selected from each image set and the temporal change in fluorescence intensity was measured. The shape of this area of interest was confined to a square, with the coordinates of the center of the square provided by the user. Once the center was determined, the size of the analysis square was varied from 10x10, 50x50, and 100x100 pixels. Each pixel in this analysis corresponds to a length of 166.67 nm and each image is originally 512x512 pixels. Each experiment in the room temperature (23°C) data set was subjected to this analysis. Representative figures from an individual data set are shown below in Figures 11 and 12.

Figure 11 below shows the position of each square on a sample image from the data set on the left and the corresponding time course data from that experiment on the right, for both Cel5A and Cel6B on BMCC mats. Mat is a term used to describe regions of high BMCC density, with many BMCC fibers clustered together and layered on the glass substrate. The representative images were taken from the frame with the highest detected signal, to highlight the cellulose morphologies studied. The data have been corrected for photo-bleaching.

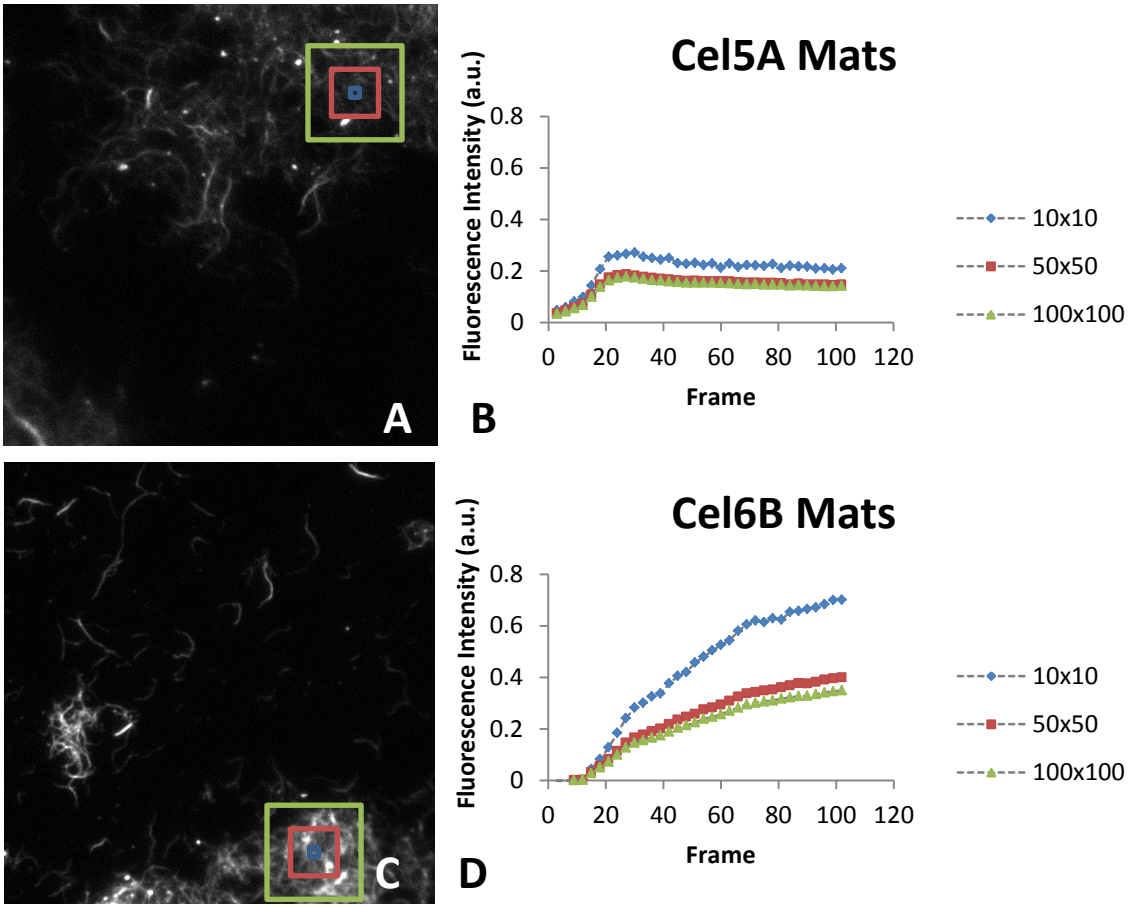

Figure 11: 10x10, 50x50, and 100x100 pixel sampling squares superimposed on representative images from cellulase binding time course experiments shown on BMCC mats for both Cel5A (A) and Cel6B (C). Graphs show time course data for entire experiment for Cel5A (B) and Cel6B (D) on BMCC mats at 23°C. These figures are representative of the three replicates used for this data set.

Figure 12 shows similar data as figure 11 above, but for BMCC fibers. Fibers are the most basic BMCC morphology, with a maximum binding capacity that can be studied within the time courses described. The term fibers describes single lengths of BMCC that are distinct within the region analyzed. Fibers are low density BMCC on the glass substrate.

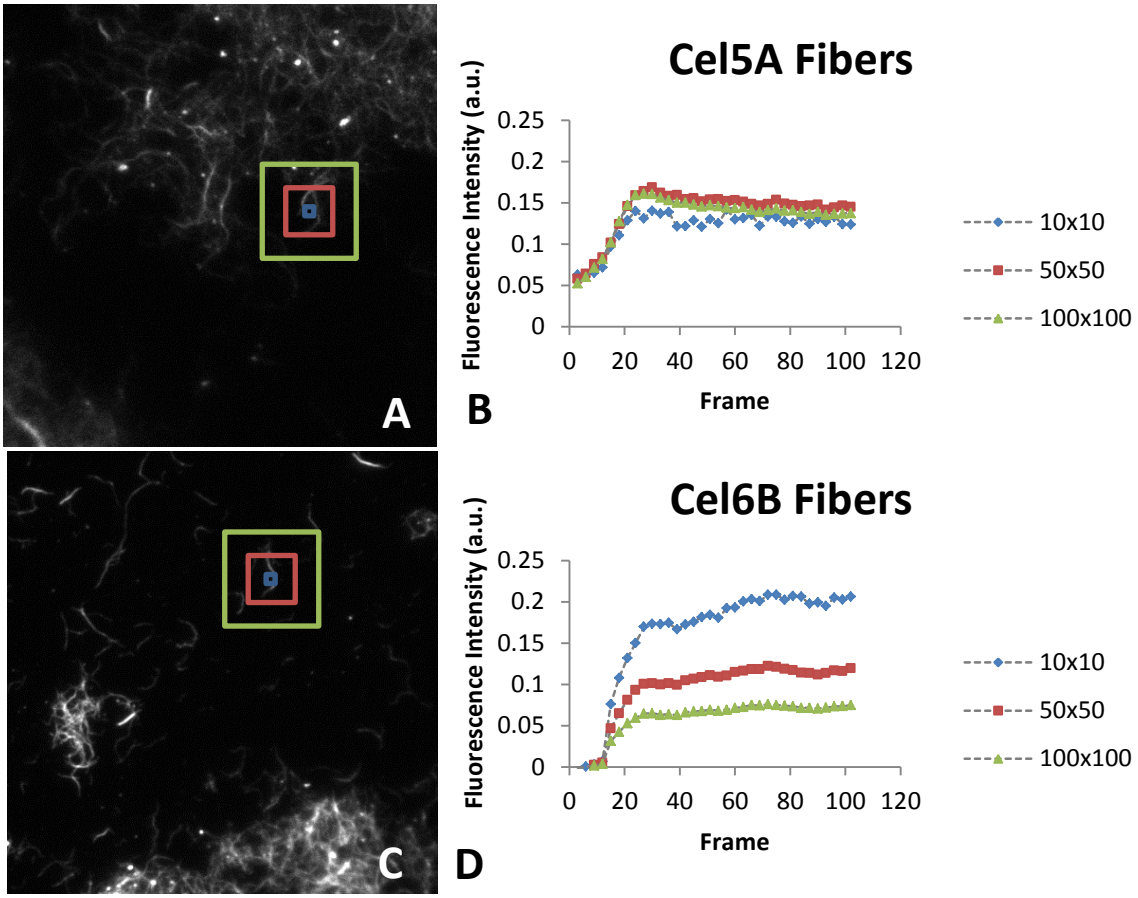

Figure 12: 10x10, 50x50, and 100x100 pixel sampling squares superimposed on representative images from cellulase binding time course experiments shown on BMCC fibrils for both Cel5A (A) and Cel6B (C). Graphs show time course data for entire experiment for Cel5A (B) and Cel6B (D) on BMCC fibrils

The size of the sampling region has little effect on the data produced by the analysis of the structures within that region for Cel5A on both fibers and mats. There is a more pronounced effect of sampling size on the data produced by this analysis for Cel6B, with the 10x10 square showing higher fluorescence intensity for both fibers and mats. The 100x100 squares for Cel6B on both fibers and mats showed the lowest fluorescence intensity of the three squares analyzed. In each case, however, the shape of the curve was consistent across all three squares. To maximize the number of both signal and background pixels, the 100x100 squares were selected to use for all further data analysis. Though the

fluorescence signal due to increasing cellulase concentration on the BMCC fibers is the experimental response we are looking for, background pixels are important for the image preprocessing and minimizing the effects of fluctuations in illumination intensity. Thus, the 100x100 pixel squares were selected to maximize both signal and background data.

T. fusca Cel5A and Cel6B time course binding results on BMCC fibers and mats

The variations in BMCC fiber and mat sizes and density meant the data from each individual experiment varied in fluorescence intensity, even within one temperature data set for one cellulase. Photobleaching corrected experimental data for the endocellulase Cel5A binding at room temperature (23°C), 34°C, and 50°C is shown in Figure 13 on both fibers and mats. Each figure shows the data sets used to calculate an average binding curve for Cel5A at 23°C and at 50°C and the binding curve for Cel5A at 34°C.

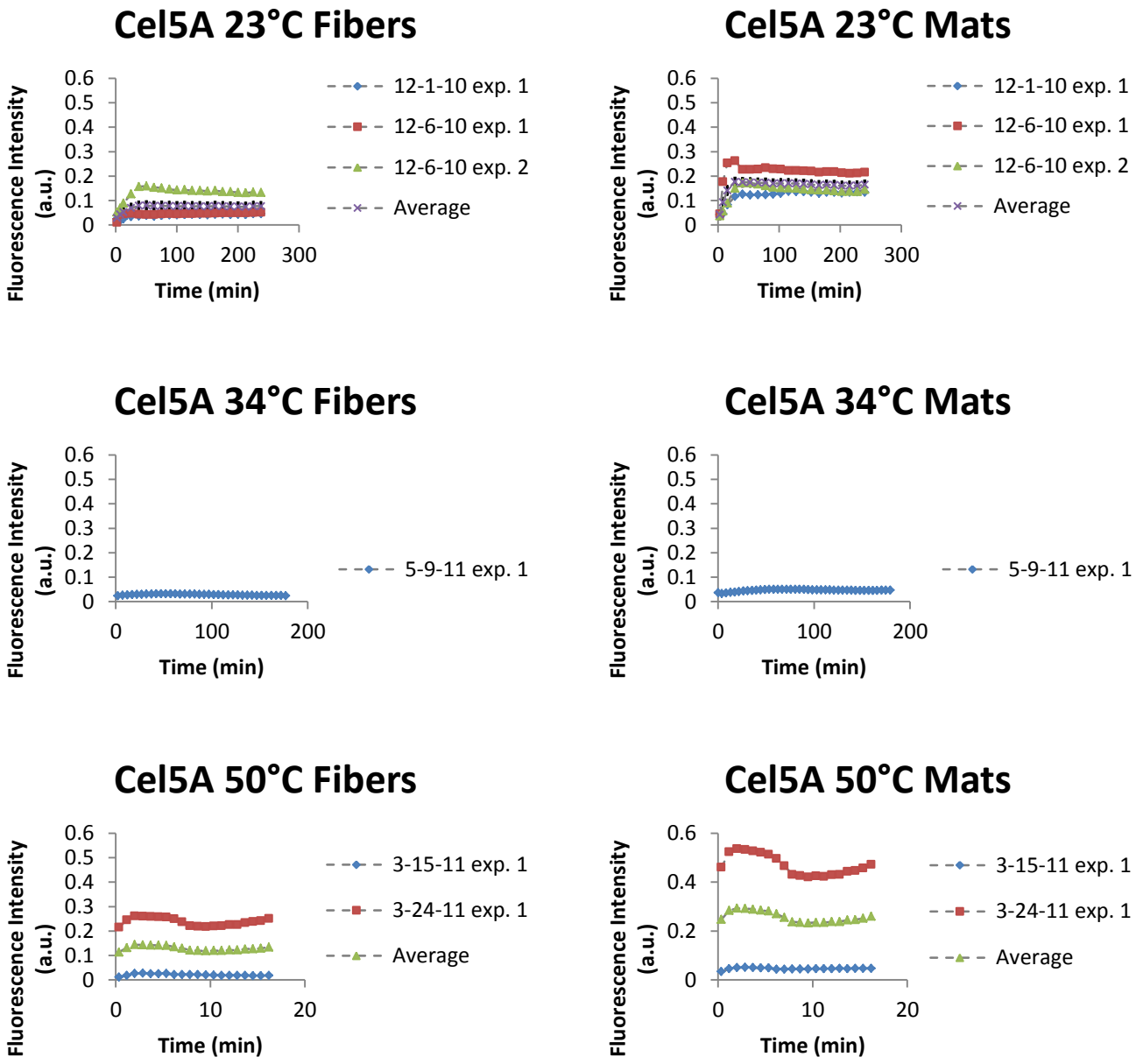

Figure 13: Raw fluorescence signal data for Cel5A alone binding on BMCC fibers and mats at 23°C, 34°C, and 50°C. Each individual experiment is noted by the date and number if applicable. Raw signal data varies in intensity due to the heterogeneity of the BMCC substrates between experiments.

Photobleaching corrected experimental data for the exocellulase Cel6B binding at room temperature (23°C), 34°C, and 50°C is shown in Figure 14 on both fibers and mats. Each figure shows the data sets used to calculate an average binding curve for Cel5A at each temperature.

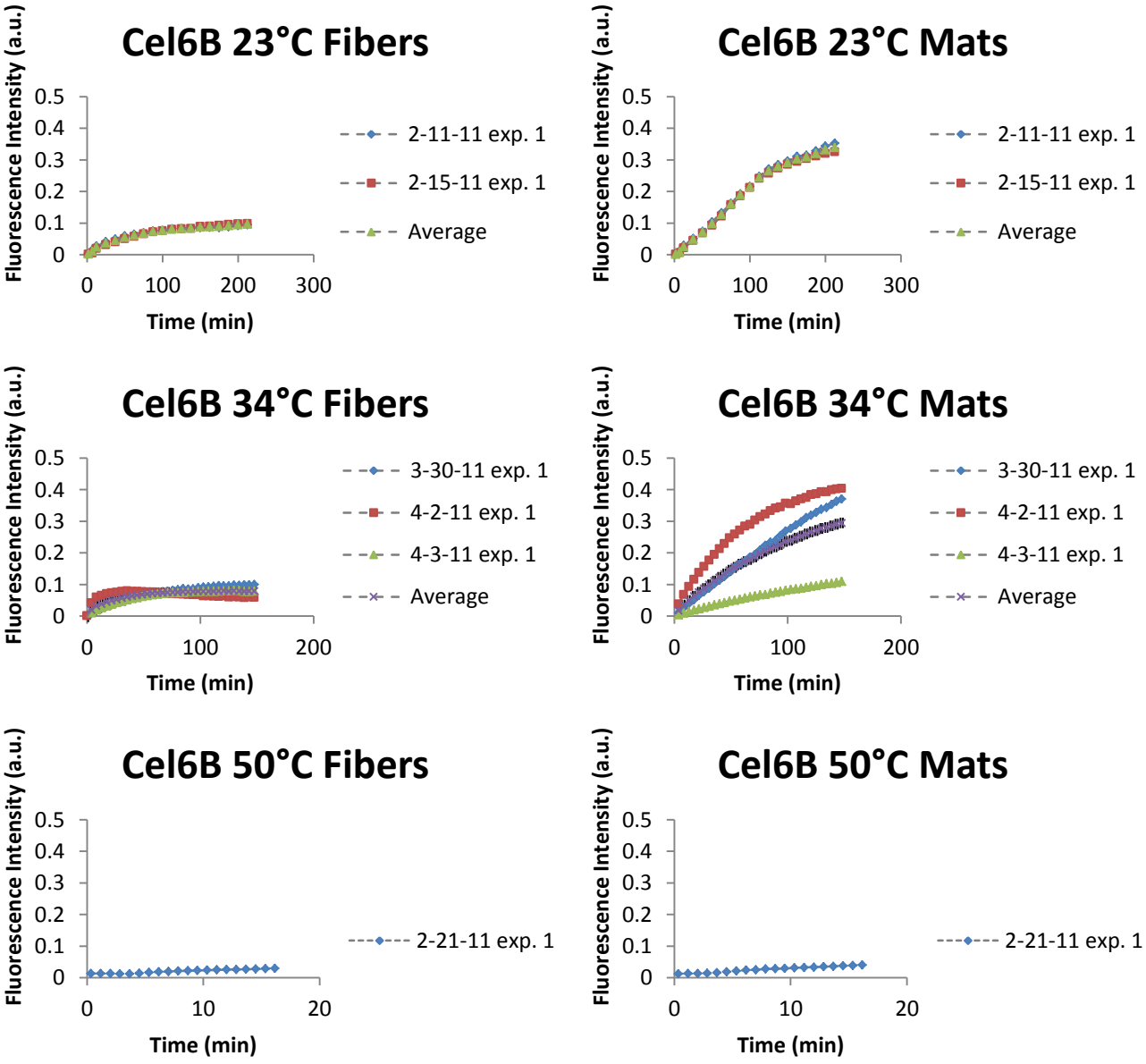

Figure 14: Raw fluorescence signal data for Cel6B alone binding on BMCC fibers and mats at 23°C, 34°C and 50°C. Each individual experiment is noted by the date and number if applicable. Raw signal data varies in intensity due to the heterogeneity of the BMCC substrates between experiments.

Figures 13 and 14 show the effect of BMCC substrate heterogeneity on the experimental data produced by this method. As discussed, BMCC fibers are a less dense cellulose morphology, with a larger portion of readily accessible surface area available for cellulase binding, but the structures are small, and have fewer binding sites overall, making them less fluorescent than the mat structures for both Cel5A and Cel6B once cellulase binding is completed. The fluorescence response from mat structures varies widely depending on the density of the BMCC deposited in the area of the substrate imaged. More dense BMCC mat structures have more overall binding sites available and therefore have a greater fluorescence response. Though the fluorescence intensity data varies by experiment, the average data set for each cellulase at each temperature can tell us something about the trends in binding. The average data sets for cellulase binding for both Cel5A and Cel6B on fibers and mats at 23°C, 34°C, and 50°C is shown in Figure 15 below. Table 14 shows the time to reach 95% of the maximum detected concentration of bound cellulases for both Cel5A and Cel6B at each temperature based on the average data sets.

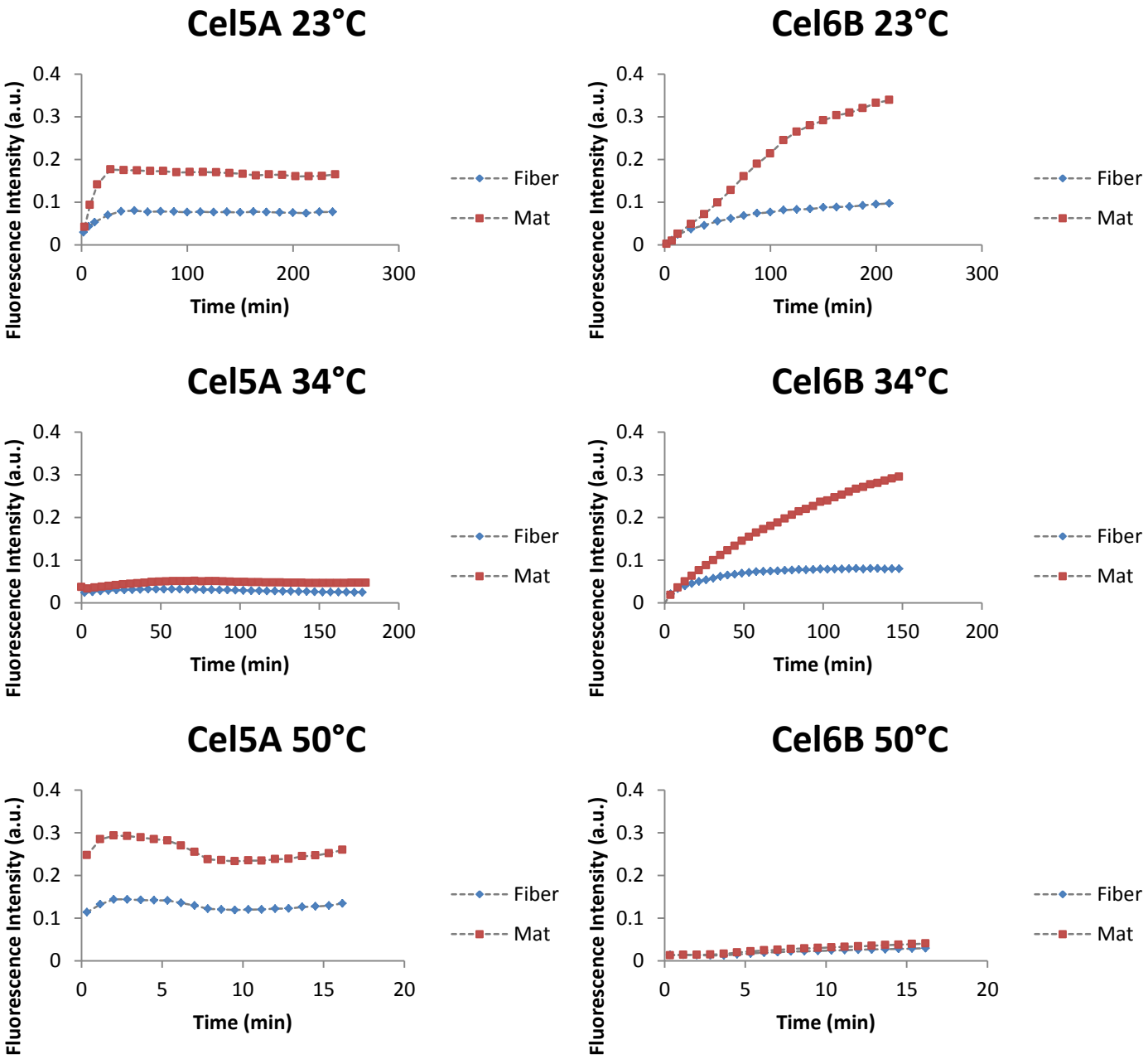

Figure 15: Binding data for Cel5A at 23°C, 34°C, and 50°C for both fiber and mat structures and binding data for Cel6B at 23°C, 34°C, and 50°C for both fiber and mat structures. Fiber data is shown with a blue diamond, mat data is shown with a red square.

Table 14: Time (in minutes) to reach 95% of maximum bound cellulase concentration for Cel5A (left side of table) and Cel6B (right side of table) at 23°C, 34°C, and 50°C.

Cel5A			Cel6B		
Temperature	**Fibers**	**Mats**	**Temperature**	**Fibers**	**Mats**
23°C	27.5	27.5	**23°C**	185	190
34°C	35	44	**34°C**	65	140
50°C	2.167	1.83	**50°C**	14.33	14.83

From Table 14 we observe that Cel5A binding is rapid and the time to reach 95% of the steady-state intensity tends to decrease with increasing temperature. Given the high affinity and accessibility of Cel5A, much of the initial binding is occurring during enzyme loading and is not reflected in the data set, leading to an initial observed binding measurement that is greater than 0 at all temperatures. Cel5A can still be seen to rapidly reach a peak detected amount of bound cellulase in all cases. Interestingly, there is not much difference in the rate of binding on the fiber vs. the mat structure, despite the greater accessibility of binding sites on the surface of fibers than those contained within a mat structure. Cel6B binding exhibited a much lower rate of initial binding than Cel5A, and generally exhibited much higher initial binding rates on fibers than on mats at both room temperature and at 34°C. Cel6B binds to the mat structure at a fairly constant rate, and does not appear to reach an equilibrium level of bound enzyme during the time course observed. The one exception is the result obtained at 50°C where the rates on the two structures are comparable and the times to reach 95% of steady-state intensity are comparable (see Table 14). This behavior is likely due to diffusion limitations associated with steric hindrance of the cellulases in the pores of the mat structure.

Previous studies in the Walker lab have shown that a maximum level of initially bound cellulase is achieved after about two hours of binding, with the bound concentration decreasing gradually over

the next 15-20 hours (Jung et al. 2003; Jeoh et al. 2006). Cellulase binding observed in the first two hours of this study, is consistent with the published data. However, previous studies did not have the resolution in temporal data to the show the different initial rates of binding observed in Cel5A and Cel6B. The advantage of this study, and of the fluorescence microscopy technique, comes from collecting images and binding data as early as 1 minute after the addition of a cellulase solution to the cellulose substrate, and at 1 minute intervals thereafter, throughout the course of the binding experiment. Additionally, previous studies had no way of discerning binding patterns on different cellulose morphological structures. That Cel6B binds at different rates on fibers and mats is a result uniquely observable by fluorescence microscopy.

Cellulose morphology affects cellulase binding through varying levels of easily accessible binding sites. For this study we focused on two morphologies, fiber and mat structures, which can be imaged simultaneously. Fibers are the most accessible with a large portion of available surface area, while mats are more complicated structures with a macro and micro-pores that define what fraction of the substrate is accessible for enzyme binding. Fibers are our most basic resolution for cellulase binding, and a peak detected level of cellulase binding can be observed on these structures. In the binding data collected and analyzed, the mat data sets had more signal pixels than the fiber data sets, since while the fiber structures are have more readily available surfaces for binding, the mats are more dense and have more surfaces for binding overall. The rate of diffusion into these mat structures is limited however. Previous work by the Walker lab has shown that the diffusion of cellulases into the cellulose pore structure can be influenced by steric hindrances (Yang et al. 2013). In this study, only initial binding of cellulases on cellulose was observed, and the rates and extents of any cellulose hydrolysis were not measured. Hydrolysis of the β-1,4 linkages between glucose monomers on the surface of the cellulose

micro-fibers will expose more cellulase binding sites. Though the time course experiments in this study were shorter than would be required for observing significant cellulose hydrolysis, it has been observed by others that this is a key rate-limiting step to cellulose degradation, rather than the initial binding itself (Luterbacher et al. 2013).

Conclusions

In this study, we have presented a method of observing cellulase binding on BMCC with high temporal and spatial resolution using fluorescence microscopy at various temperatures. Cellulose fiber and mat structures can be easily discerned from these images and studied. The fluorescence response of the bound cellulase is very dependent on the density of the BMCC structures available for image processing. Though the BMCC morphologies vary in size and density in each experiment, quantitative information on the rate and extent of cellulase binding can be gleaned from the consistency of the shape of the binding curves for each enzyme at each temperature. The resulting images were used to generate quantitative cellulase binding data sets for binding on both fiber and mat macrostructures. The observed effects of photobleaching can be easily corrected through the use of linear regression data. Selected regions of interest can be used to select either BMCC fibers or mats for analysis, and in this study, these regions were 100 by 100 pixel squares to maximize the number of signal and background pixels. We can conclude from the data sets that the *T. fusca* endocellulase Cel5A shows a rapid initial binding phase without any apparent hindrance from the cellulose structure regardless of the temperature of the binding reaction, while Cel6B binds more rapidly on fibers than on the mat structures at lower temperatures, while binding at a similar rate on both mats and fibers at 50°C. In summary, this study demonstrates that effectively collected spatial and temporal binding data from a

fluorescence microscopy system can be combined with thoughtful analysis to contribute to greater understanding of the fundamental mechanisms governing cellulase-cellulose binding and hydrolysis.

CHAPTER 5: INVESTIGATING SYNERGISTIC BINDING BY MIXTURES OF *THERMOBIFIDA FUSCA* CELLULASES CEL5A AND CEL6B ON SIMPLE AND COMPLEX CELLULOSE STRUCTURES USING EPI-FLUORESCENT MICROSCOPY

Introduction

Individual cellulases hydrolyze cellulose relatively slowly, but mixtures of cellulases and other plant cell wall degrading enzymes have been observed to act synergistically to enhance rates and extents of hydrolysis. In nature, cellulose degrading organisms, such as plant pathogenic fungi, produce a cocktail of enzymes, including cellulases with varying modes of action and accessory enzymes for biomass hydrolysis (Phalip et al. 2005; Paper et al. 2007; King et al. 2009; King et al. 2011). In cellulase synergism, it is assumed that the actions of endocellulases create more available sites for exocellulases to act, thereby increasing the overall activity of the mixture to an extent that is greater than the sum of the activities of the individual enzymes (Irwin et al. 1993; Walker et al. 1993; Santhanam and Walker 2008). Elucidating the molecular mechanisms that give rise to synergistic behavior is an important research goal and could contribute to the design of more efficient cellulase cocktails for lignocellulose degradation.

A major question is to what degree does cellulose morphological structure influence accessibility to cellulose polymers, how this accessibility changes with different cellulases, and how does this affect the ability of cellulases to act synergistically. In the case of cellulase hydrolysis by a mixture of endocellulases and exocellulases, binding site accessibility may be affected by steric hindrance within the porous structure of the cellulose substrate, the availability of sites in a complicated cellulose structure, and the rate of enzyme diffusion into the cellulose structure (Bothwell et al. 1997;

Luterbacher et al. 2013; Luterbacher et al. 2013; Yang et al. 2013).The adsorption of cellulases onto the cellulose polymer is a key step in the hydrolysis reaction and due to the dynamic nature of cellulose hydrolysis, the adsorbed concentrations of cellulases will change as the reaction proceeds. Understanding the mechanism of this dynamic binding will help to elucidate the synergistic interactions that yield enhanced hydrolysis of lignocellulosic biomass.

Jeoh et al. hypothesized that the effects of synergism are related to cellulase binding in mixtures. They observed cellulase binding on BMCC using mixtures of *Thermobifida fusca* cellulases Cel5A, Cel6B and Cel9A, representing a classical endocellulase, an exocellulase and a processive endocellulase respectively, at 5 and 50°C (Jeoh et al. 2002). Their observations revealed that the activity of endocellulases increases the number of available binding sites for exocellulases in a mixture. From these observations, they obtained a measure of the degree of synergistic binding (DSB) throughout a time course and gained some insight on whether one or both cellulases in a mixture exhibited increased binding due to synergism. Cellulase binding on cellulose is a dynamic system where temperature has a strong influence on binding and catalytic activity (Jeoh et al. 2002; Jeoh et al. 2006; Moran-Mirabal et al. 2011). Also, synergism decreases as the cellulose substrate becomes more recalcitrant, but the results they observed with Cel9A in the binary mixture on the more recalcitrant cellulose suggested endo-endo synergism (Jeoh et al. 2006).

The goal of this study was to effectively track cellulase binding for two different cellulases in a mixture in real time and tease out insight into cooperative or competitive cellulase binding in the absence and presence of hydrolytic activity. Mixtures of fluorescently labeled *T.fusca* endocellulases and exocellulases were applied to immobilized cellulose substrates and binding was observed via fluorescence microscopy at room temperature and at 50°C to build a kinetic framework for cellulase

binding in in synergistic mixtures. Using fluorescence microscopy to observe cellulase binding on simple and complex cellulose structures increases the spatial and temporal resolution of the binding data, and allows us to calculate the DSB and gain insights into the dynamic nature of cellulase binding with excellent temporal resolution (Moran-Mirabal et al. 2008; Moran-Mirabal et al. 2011; Zhu et al. 2011; Moran-Mirabal et al. 2013; Yang et al. 2013). The synthesis of high resolution spatial and temporal binding data with thoughtful analysis will contribute to greater understanding of the fundamental mechanisms governing cellulase synergism and could contribute to the design of more efficient cellulase cocktails for lignocellulose hydrolysis.

Materials and Methods

Cellulase labeling and purification

T. fusca cellulases Cel5A and Cel6B were expressed and purified as described in Jeoh et al. 2002 (Jeoh et al. 2002). The cellulases were fluorescently labeled with amine–reactive dyes Alexa Fluor 488 and 647 (Invitrogen, Carlsbad, CA) at 10 μM concentration with labeling molar ratio (LMR) of 100:1 at 4°C for 24h using the solid phase (SP) labeling method of Moran-Mirabal et al. 2009 (Moran-Mirabal et al. 2009). Only the fractions of enzymes with a degree of labeling of 1 were used for the experiments described in this paper. Hydrolytic activities of labeled cellulases were measured using BMCC and compared to that of unlabeled enzymes as described in Moran-Mirabal et al. 2009. No significant change in activities was observed (Moran-Mirabal et al. 2009). For the experiments described in this paper, the 200 nM fractions were diluted in 50 mM sodium acetate buffer for a final total enzyme concentration of 2 nM. For all experiments described in this chapter Cel5A was labeled with AF 488 dye and Cel6B was labeled with the AF 647 dye. A 1:1 Cel5A to Cel6B molar ratio was used in all experiments. The total enzyme loading for all experiments was 2 nM.

Immobilized cellulose substrate preparation

A solution of 1mg/ml bacterial micro-crystalline cellulose (BMCC, Monsanto Cellulon, San Diego, CA) in water was prepared as previously described in Jeoh et al. 2002 and Santhanam et al. 2008 (Jeoh et al. 2002; Santhanam and Walker 2008). A 50 µg/ml BMCC suspension in MilliQ water was sonicated for 5 min at 60% amplitude using a SPLt sonicator (Branson, Danbury, CT) to break up some of the more dense cellulose aggregates into less dense pieces, including some individual fibers. For the room temperature experiments, glass slide bottomed petri dishes (MatTek Corp., Ashland, MA) were used to prepare the immobilized cellulose substrate. For the 50 °C experiments, a Bioptechs temperature controlled fluidic chamber (FCS2 chamber assembly, Bioptechs, Butler, PA) was used with 40 mm 170 um thick glass wafers (Bioptechs, Butler, PA) to prepare the immobilized cellulose substrate. In all cases, the glass substrates were pretreated in a Plasma Cleaner (Harrick, Ithaca, NY) to make a hydrophilic surface for depositing the BMCC. Five 10 µL drops of BMCC in water solution were placed on the glass surface, spread around, and allowed to lightly dry on a 70°C hotplate for 30 min for an initial cellulose loading of 2.5 µg. The substrates were rinsed with MilliQ water to remove any non-adhered cellulose and then incubated with a solution of 10% BSA (Fisher Scientific, Pittsburgh, PA) in 50 mM sodium acetate buffer overnight at room temperature to minimize non-specific adhesion of cellulases onto the substrate surface. Following the incubation, the substrates were washed with 50 mM ascorbic acid (AA) buffer (degassed 50 mM sodium acetate buffer pH 5.5 supplemented with 5 mM AA) to remove the BSA. Ascorbic acid was added to scavenge oxygen in the buffer solution and reduce the effects of photo-bleaching during the experiment as described in Moran-Mirabal et al. 2008 (Moran-Mirabal et al. 2008). The samples were loaded onto the microscope and the temperature was held constant by resistive heating provided by the FCS2 assembly.

Cellulase imaging

Binding time lapse experiments

For each experiment, an area of interest was selected on the cellulose substrate then the AA buffer was removed and replaced with the 2 nM total cellulase solution in 50 mM AA buffer. In room temperature experiments the buffer was removed and cellulase solution was added using a 5 mL pipette and in the higher temperature experiments buffer was removed and cellulase solution was added using a syringe pump. Cellulase binding was observed as previously described. Olympus software (Olympus, Center Valley, PA) was used to control the filter wheels and shutters, allowing for data acquisition in both the 488 and 647 channels. Images were recorded on a Hamamatsu ImageEM EMCCD camera (Hamamatsu Bridgewater, NJ) with exposures of 50 ms. Three exposures were taken for each frame and averaged to improve the signal to noise ratio. The sample was exposed to light only during image acquisition, a total of 150 ms for each frame. Binding time-course experiments were run for up to 240 min for room temperature experiments and 20 min for 50° experiments. Images were obtained at pre-determined intervals to capture the binding phenomena at each temperature and saved as stacks of raw image data. In all experiments, the total exposure time was limited to 15 s (50 ms/frame, 3 frame average, 100 total frames).

Relative fluorescence intensity measurement

DTAF labeled cellulose was prepared as described in Santhanam et al. was applied to the prepared glass substrates and the cellulases were allowed to bind overnight to come to an equilibrium (Santhanam and Walker 2008). For these measurements, an equimolar mixture of cellulase Cel5A labeled with AF488 and Cel5A labeled with AF647 was applied to the substrate. Once an equilibrium level of binding was achieved, the substrates were imaged using the Olympus IX-81 inverted microscope

with the 60x/1.2NA UPLSAPO Olympus air objective as described earlier. Images were recorded on a Hammamatsu ImageEM EMCCD camera with exposures of 50ms. The sample was exposed to light only during image acquisition. 100 total frames were recorded with three 50ms exposures averaged to produce each frame.

Image analysis

Images were pre-processed as previously described in Chapter 4. Briefly, stacks of image files and were aligned and corrected for stage drift using ImageJ plugin StackReg (National Institutes of Health, USA). The signal intensities in the aligned images were pre-processed for analysis using a custom MATLAB program (The Mathworks, Natick, MA) adapted from Moran et al. 2008 to separate signal pixels from background pixels (Moran-Mirabal et al. 2008). The average intensity and the standard deviation of that intensity were measured for a selected background region for all time points in the series and the mean background was subtracted from each image to correct for fluctuations in illumination intensity. Saturated signal pixels were also removed during this pre-processing, as previously described. Signal pixels were assigned by generating a mask from the final image recorded during the time-course, to obtain good contrast between signal and background populations as described in Moran-Mirabal et al. 2008 (Moran-Mirabal et al. 2008). From the selected image, a threshold grayscale level was calculated and the image was separated into signal and background. A mask of signal pixels is generated and successively applied to all images recorded during the time-course. The program calculates the integrated mean and standard deviation of pixel intensities for the selected signal regions for each time point. All of the image data was subjected to this image analysis program to obtain quantitative data for the binding time-course experiments and the relative

fluorescence measurements. The pre-processed signal intensities from the binding time-course experiments were corrected for photo-bleaching in each data set as previously described in Chapter 4.

Relative fluorescence between the two fluorophores was obtained by determining the ratio of the AF488 signal to the AF647 signal for each frame from the data recorded in the relative fluorescence measurements described for each temperature as shown in equation 81 below:

$$\beta_t = S_{488t} \div S_{647t} \quad 81$$

Where S_{488t} is the signal in the 488 channel in frame t, S_{647t} is the signal in the 647 channel in frame t, and β_t is the ratio of the signal in each channel in frame t. The average value across the entire time course was determined from the value for equation 81 for each frame.

$$\bar{\beta} = \frac{\sum_{t=0}^{t=n} \beta}{n} \quad 82$$

Where n is the number of frames in the time course. Experimental data sets were corrected using the average value for the ratio of signal in the 488 channel to signal in the 647 channel over 100 frames, to mitigate the difference in detected signal between the two fluorophores. Briefly, the signal data from the 647 channel was multiplied by $\bar{\beta}$ in the steady state system to compensate for the less intense fluorescence signal from fluorophores in the 647 channel as follows:

$$S'_{647,t} = \bar{\beta} \times S_{647,t} \quad 83$$

Where $S'_{647,t}$ is the corrected signal in the 647 channel. This correction facilitates comparison between enzymes labeled with 488 and enzymes labeled with 647 in the same experimental data set.

These photo-bleaching and relative fluorescence corrected fluorescence data sets were plotted against the time-course to show the increase in fluorescence in the selected region of interest with time, corresponding to the increasing concentration of bound cellulases.

Results

Binding time course data for Cel5A and Cel6B individually and in mixtures compared

Fluorescence intensity versus time is plotted in Figure 16 for labeled Cel5A on both fibers and mats for Cel5A alone and in a 1:1 mixture with Cel6B at the same molar concentration. The total enzyme loading in all cases is 2 nM.

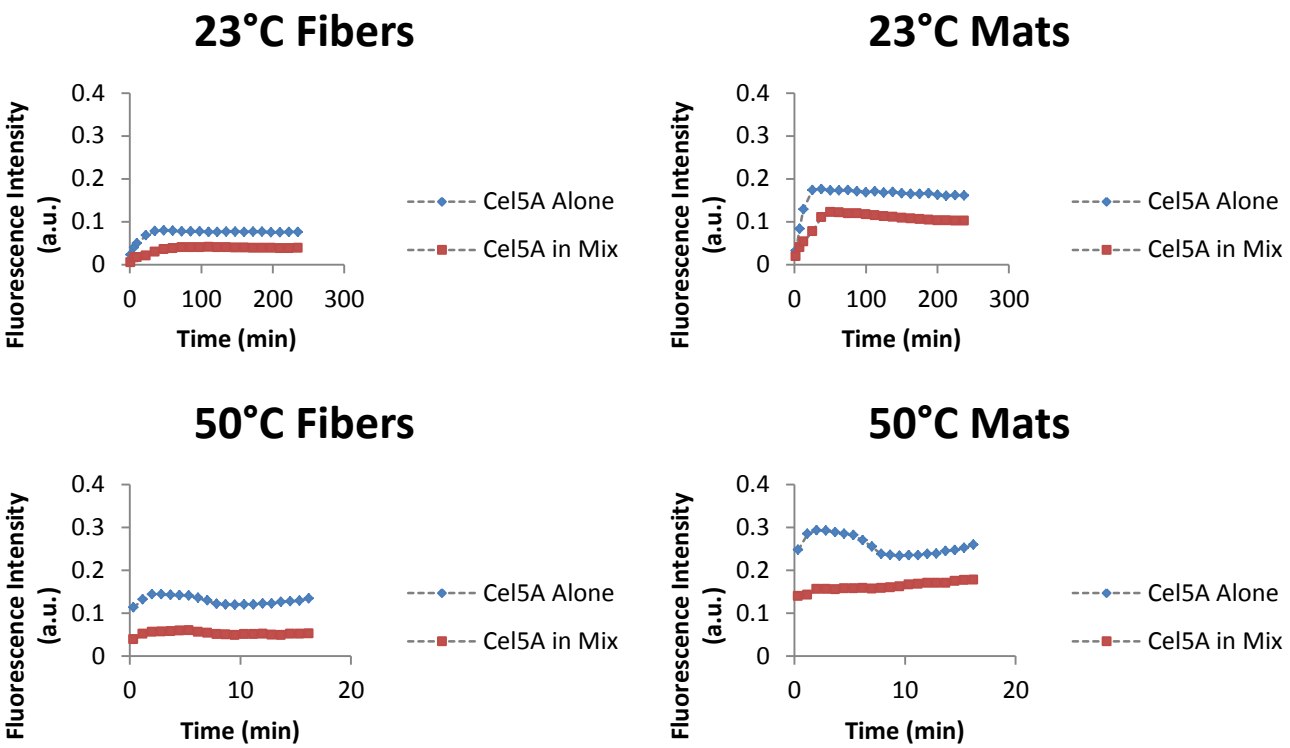

Figure 16: Binding data for Cel5A individually (blue diamonds) and in a 1:1 mixture with Cel6B (red squares) on both BMCC fibers and mats at 23, 34, and 50°C. Fluorescence intensity in arbitrary units is plotted vs. time in minutes. The difference in the x-axis time course is due to the shorter time required for binding at high temperatures and the rate of fluorophore bleaching at high temperatures. This bleaching effect is discussed in Chapter 4.

The binding time course was 240 minutes for the 23°C and 16.5 minutes at 50°C. The different time courses reflect how temperature influences the rate of binding, specifically, binding is faster at higher temperatures. The Cel5A binding time courses show a consistent shape between the individual component data and the mixtures data for each temperature, with a rapid increase in binding to an equilibrium level of binding that then holds steady throughout the course of the experiment. The average fluorescence intensity for Cel5A alone is consistently higher than the fluorescence intensity for

Cel5A in a 1:1 mixture with Cel6B at both 23°C and 50°C on both BMCC fibers and mats. On both fibers and mats Cel5A is binding to a lesser extent in a mixture than it is when it is alone. From these results, it is possible to conclude that some competitive binding with Cel6B may be occurring on the cellulose surface. The total enzyme loading is consistent for both the studies of Cel5A and Cel6B alone and the 1:1 mixture studies, with a 2 nM solution of cellulases being applied to the substrate in all experiments, so there is no effect from a variation in total enzyme loading. Further, as discussed in Chapter 4, there is some constant α_d that makes it possible to determine the concentration of fluorescently labeled cellulases, but at this time it is unknown. At room temperature (23°C), Cel5A binds at a slower initial rate in the 1:1 mixture with Cel6B than it does alone. There is little difference in the rate of binding at 50°C, regardless of whether Cel5A is the sole component or is in a 1:1 mixture with Cel6B, in both cases Cel5A reaches its equilibrium level of binding almost immediately. This trend was consistent for both fiber structures and mats.

Figure 17 below shows the fluorescence time course data for Cel6B labeled with AF 647 both alone and in a 1:1 mixture with Cel5A on both fibers and mats.

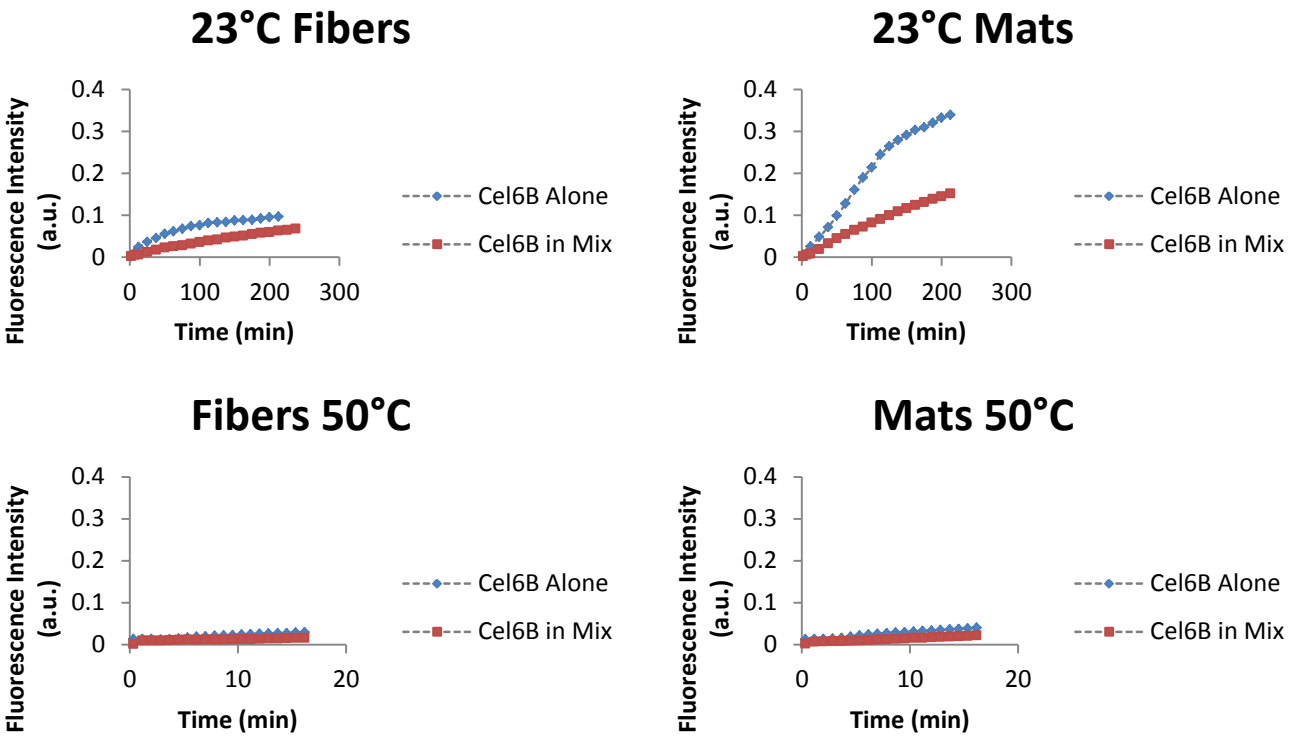

Figure 17: Binding data for Cel6A individually (blue diamonds) and in a 1:1 mixture with Cel5A (red squares) on both BMCC fibers and mats at 23, 34, and 50°C. Fluorescence intensity in arbitrary units is plotted vs. time in minutes.

Similar to the Cel5A data, Cel6B alone seems to bind at a greater extent on both fibers and mats at 23°C than Cel6B in a mix. This result on fibers indicates competitive binding with Cel5A in a mixture at 23°C. Competitive binding is also occurring on the BMCC mat structures for Cel5A and Cel6B at 23°C. Interestingly, Cel6B at 50°C on both BMCC fibers and mats shows no difference in binding between Cel6B alone and in a 1:1 mix with Cel5A. Moran-Mirabal et al. showed that the fraction of Cel6B reversibly bound on BMCC decreases with increasing temperature, while the fraction of Cel5A that is

reversibly bound remains constant at room temperature and at 50°C (Moran-Mirabal et al. 2011). Irreversibly bound Cel6B could be inhibiting Cel5A binding at 50°C.

Table 15 shows the time in minutes to reach 95% of the maximum detected concentration of bound cellulases for both Cel5A and Cel6B at each temperature individually and in a 1:1 mixture of Cel5A and Cel6B.

Table 15: Time (minutes) to reach 95% of the equilibrium level of binding on both mats and fibers at 23, 34, and 50°C for Cel5A and Cel6B alone and in synergistic mixtures of Cel5A and Cel6B (equimolar mixtures). To compare times between Cel5A and Cel6B individually and in mixtures, in each case, the lower time to 95% is highlighted.

	Fibers					Mats			
Temperature (°C)	Cel5A alone	Cel5A in mix	Cel6B alone	Cel6B in mix		Cel5A alone	Cel5A in mix	Cel6B only	Cel6B in mix
23	32	65	185	197.5		20	42.5	190	197.5
50	1.67	2.67	14.3	15.2		1	11.67	14.83	16

As in the single component experiments described in Chapter 4, the time to 95% of maximum recorded binding decreases with increasing temperature on both BMCC fibers and mats. Cel5A reaches 95% of the equilibrium amount of bound enzyme faster than Cel6B does in all cases. At room temperature, Cel5A is slower to reach 95% of equilibrium in the mixture than in the single component on both fibers and mats. At 50°C on fibers, there is little difference in the time to 95% of maximum binding, but there is a large difference in time on mats. As previously discussed, BMCC mat structures are dense, with lots of surface area and potential binding sites that are contained in a matrix of BMCC fibers tangled together. While these binding sites are available, there may be steric hindrances between the cellulases that slow diffusion into the BMCC mat structure, or interactions between the BMCC and the cellulases that influence the rate of diffusion into the mat structure and therefore the rate of cellulase binding on the

mat structure. The binding curve for Cel5A at 50°C on mats in Figure 16 illustrates that this is not necessarily due to slower binding, but due to Cel5A increasing in bound concentration throughout the time course observed for the mixture rather than the quick peak and equilibrium reached for Cel5A alone. It is possible that this change in the shape of the binding curve is due to the synergistic activities of Cel5A and Cel6B together, creating new binding sites for Cel5A and therefore allowing it to continue binding throughout the time course observed. For Cel6B on both fibers and mats, though the individual component experiments show faster binding according to the data in Table 15, the difference is not very large. In mixtures and alone, Cel6B reaches its maximum bound concentration faster at 50°C than at 23°C.

Relative fluorescence intensity

Though we can gain insights into the binding behavior of Cel5A and Cel6B from their individual binding curves shown in Figures 16 and 17, understanding how the concentration of each enzyme changes during the time course in a 1:1 mixture of Cel5A and Cel6B may also provide useful information. Previous work in the Walker lab has shown that in mixtures, Cel5A is only 10-15% of the total bound cellulase concentration, regardless of the initial loading ratio of Cel5A in a mixture with Cel6B, Cel9A, or Cel6B and Cel9A (Jeoh et al. 2002; Santhanam and Walker 2008). In order to compare the fluorescent signal from Cel5A labeled with AF 488 with the fluorescent signal from Cel6B labeled with AF 647, we must first adjust the fluorescence intensity values for the more efficient capture of AF 488 signal than AF 647 signal by the imaging set up.

From the photobleaching data shown in the preceding chapter, it is apparent that the signal from 488 labeled cellulases is more strongly detected by the camera than the signal from 647 labeled enzymes, even in equal concentrations. To simplify comparison between differently labeled populations,

a relative fluorescence intensity factor was calculated to make up for the weaker signal detection of 647 labeled enzymes. Similar to the photo-bleaching experiments, equal concentrations of Cel5A labeled with 488 and Cel5A labeled with 647 were applied to a BMCC substrate in the experimental setup previously described and allowed to reach equilibrium with an overnight incubation. Once equilibrium had been reached, the substrates were loaded onto the microscope as described, and the signal from each population of Cel5A was measured with the camera. Reaction temperature also alters the amount of photons emitted by each fluorophore. Reported in Figure 18 are the ratios between the AF488 and AF647 signal at 23° and 50°C.

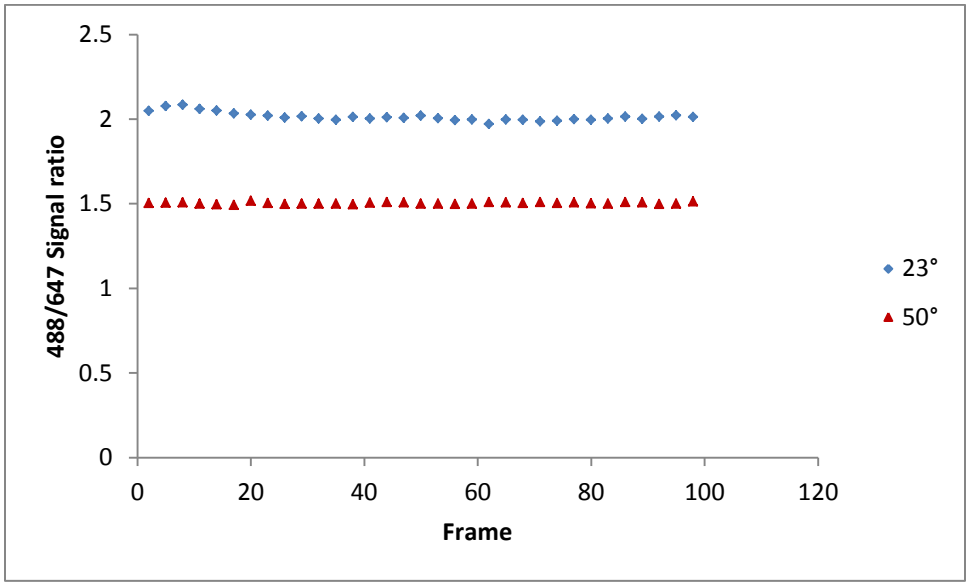

Figure 18: Relative fluorescence data for all temperatures. The ratio of AF488 signal to AF647 signal is shown in filled blue diamonds for data at 23°. The ratio of AF488 signal to AF647 signal is shown as filled red triangles for 50°.

The ratio of signal in the 488 channel to signal in the 647 channel is stable over the course of the 100 frames imaged. The average value for the ratio of 488 signal to 647 signal across all the frames was obtained from the data shown in Figure 18 and used as the correction factor to adjust the signal in the

647 channel to compensate for the lower fluorescence detection in the 647 channel. Table 16 below shows the 488/647 signal correction factors. These correction factors were used to adjust the value of the 647 signal in each frame, so that it would be possible to directly compare the signal from the 488 channel and the 647 channel and the corresponding relative amounts of detected bound cellulase. The 647 signal for each frame in the experimental time-course was multiplied by this correction factor.

Table 16: Relative fluorescence correction factors for 647 data at 23° and 50°C.

Temperature	488/647 Signal Correction	
23°C	2.015	±0.025
50°C	1.502	±0.006

Binding time course data for both Cel5A and Cel6B in a 1:1 mixture

Figure 19 below shows the binding time course data for a 1:1 mixture of Cel5A labeled with AF 488 and Cel6B labeled with AF 647 on both fibers and mats for 23 and 50°C. All data have been corrected for photobleaching and for the difference in relative fluorescence between the AF 488 tag and the AF 647 tag to facilitate comparisons between the data sets.

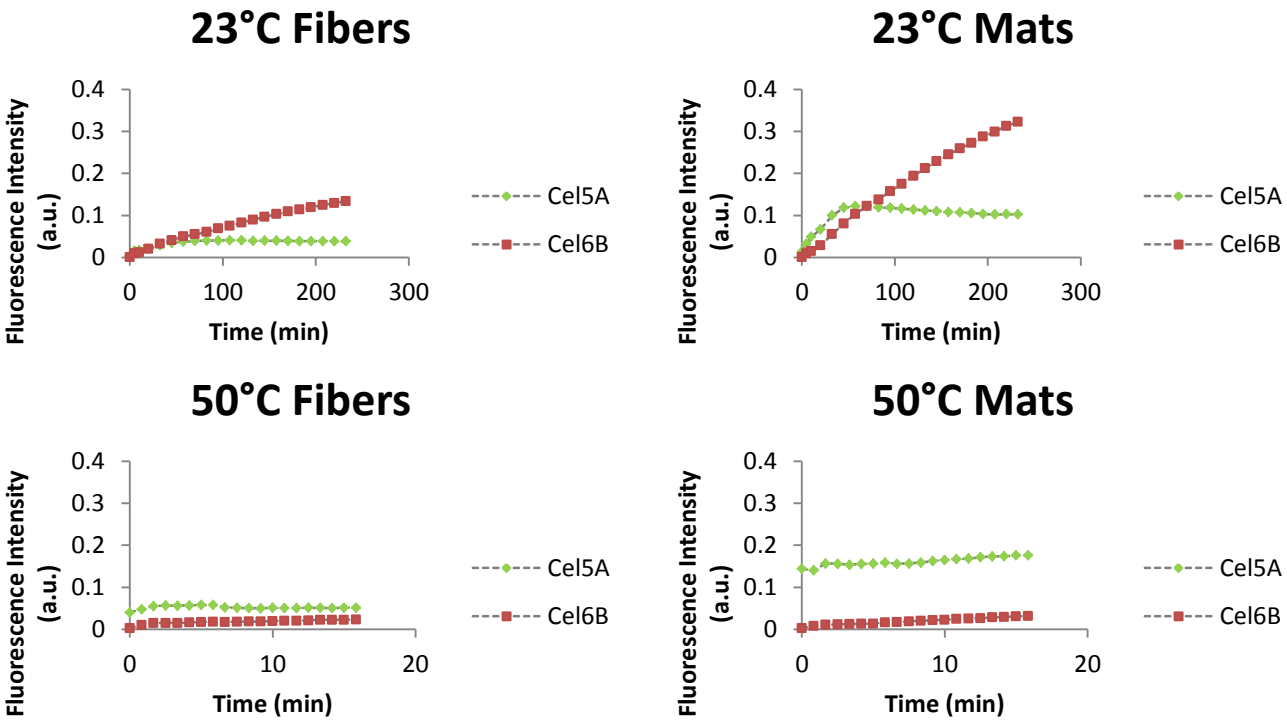

Figure 19: Binding data for equimolar mixtures of Cel5A labeled with AF 488 and Cel6B labeled with AF 647 at 23°C and 50°C for both fiber and mat structures. Cel5A labeled with AF 488 data is shown with a blue diamond, Cel6B labeled with AF 647 data is shown with a red square.

From the data shown in Figure 19, the percent of the total bound enzyme on each BMCC structure was calculated for both Cel5A and Cel6B in the mixture. Figure 20 below shows the percentage of the total cellulase signal that can be attributed to Cel5A and Cel6B in the equimolar mixture experiments at 23 and 50°C on fibers and on mats. Even though each enzyme is 50% of the total initial cellulase concentration applied to the cellulose substrate, the equilibrium bound concentration is not 50% of each. Rather, it varies by temperature and cellulose structure. The total bound cellulase is assumed to be the total fluorescence signal at each time point, such that:

$$S_{total,t} = S_{488t} + S'_{647,t} \qquad 84$$

Since the intensity of the signal in each channel corresponds to the concentration of bound fluorescent enzyme we can correlate the percentage of signal in each channel with the concentration of the enzyme it represents.

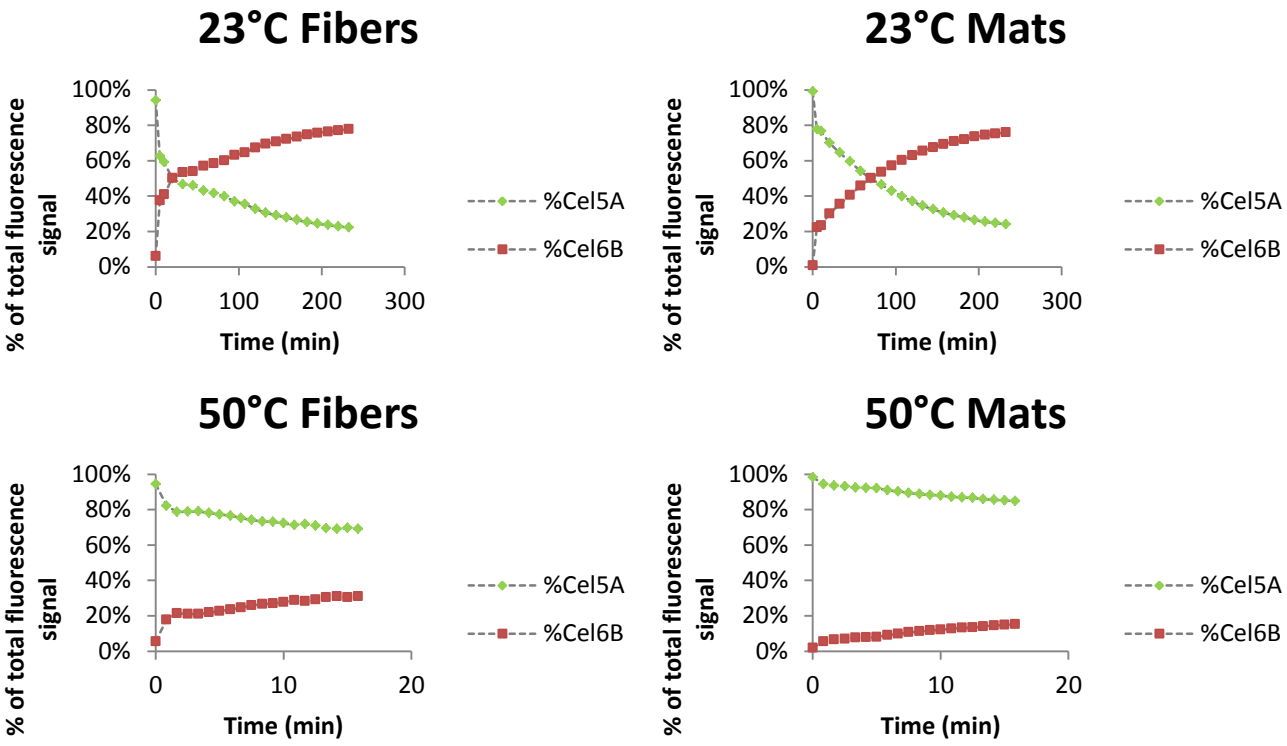

Figure 20: Percentage of total bound cellulase from an equimolar mixture of Cel5A and Cel6B. Cel5A data is shown as green diamonds, Cel6B data is shown as red squares.

In each case, although the initial mixture of cellulases applied to the substrate was 50% Cel5A and 50% Cel6B, the bound concentration is not split 50-50. The concentration of bound enzyme varies throughout the time course observed for both BMCC fibers and mats at 23°C and 50°C. In all cases, Cel5A starts as the dominant signal. At the end of the 240 minutes of binding observed at 23°C, the bound concentration of cellulases was portioned as approximately 70-80% Cel6B and 20-30% Cel5A for both fibers and mats. After 16.5 minutes of binding observed at 50°C the bound concentration was

approximately 70% Cel5A and 30% Cel6B on fibers, and 85% Cel5A and 15% Cel6B on mats. The time course at 50°C was limited due to photobleaching effects. Though the two time courses look very different from one another, limiting the 23°C time course to the first 20 minutes of data yields curves that look very similar to the 50°C data, so it is possible to imagine that with more time, the fraction of each cellulase bound on BMCC fibers and mats at 50°C would be similar to the bound concentrations at 23°C. The very early stages of binding are dominated by Cel5A binding rapidly to the cellulose substrate, while the concentration of Cel6B increases gradually with time. Ganner et al. saw similar results in their AFM studies of an endoglucanase and a cellobiohydrolase binding. In their study, the endoglucanase bound rapidly to the amorphous fraction of the cellulose substrate, hydrolyzing it and revealing more crystalline cellulose nanofibers for cellobiohydrolase binding (Ganner et al. 2012). Such synergistic actions may be occurring in this system, particularly at 50°C. This data corresponds with the binding time course data shown in Figure 19, where Cel5A has a rapid initial binding event and then reaches an equilibrium level of binding and Cel6B binds more slowly in the initial phases, but continues to bind throughout the time course observed on fibers. On mats however, the data from figure 19 indicates that the concentration of both Cel5A and CEel6B bound on the BMCC was continuing to increase after the 16.5 minutes observed, possibly due to new binding sites being made available due to synergistic actions. Jeoh et al. observed a binding time course for a mixture of Cel5A and Cel6B at 50°C for 16 hours and found that Cel6B was bound at a greater concentration than Cel5A after 45 minutes and peak binding for both Cel5A and Cel6B occurred at 2 hours (Jeoh et al. 2006). However, the 45 minute time point was their first data point in the time course. The advantage of this method is the excellent temporal resolution early in the binding time course, and the data presented in this chapter combined with the data presented in Jeoh et al. begins to paint a picture of Cel5A and Cel6B binding in a mixture when hydrolysis activity is present.

Though the initial rates of binding in synergistic mixtures are generally slower than the rates of binding individually for both Cel5A and Cel6B, another important parameter in cellulase binding studies is the extent of binding, or the concentration of bound enzyme on the substrate. The techniques described in this chapter and the preceding chapter are of limited effectiveness in determining an absolute concentration of cellulase bound to the BMCC substrate. The amount of BMCC bound in each experiment varies. However, the data can tell us something about the relative amount of bound cellulase in mixtures and in the individual component experiments at various time points during the observed time courses. By normalizing each data set to its highest detected fluorescence signal, which corresponds to the highest concentration of bound enzyme in each data set, we can compare relative extent of binding at various time points. Using this information, we can calculate the degree of synergistic binding (DSB) based on the fluorescence intensity data by adapting the following equation from Jeoh et al. (Jeoh et al. 2002):

$$DSB = \frac{E_{b,mix}}{\sum_{i=1}^{2}\left(E_{b,single}\right)_i} \quad 85$$

Where $E_{b,mix}$ is the concentration of bound enzyme in the mixture and $E_{b,single}$ is the concentration of bound cellulase in a single component reaction (Jeoh et al. 2002). The concentration of bound enzyme is proportional to the fluorescence intensity by some constant value, α_d, such that:

$$E_b = \alpha_d I_b \quad 86$$

Where I_b is the fluorescence intensity corresponding to E_b. Thus, we can substitute the value $\alpha_d I_b$ for E_b in equation 85, simplify, and get the following approximation for DSB:

$$DSB = \frac{I_{b,mix}}{\sum_{i=1}^{2}\left(I_{b,single}\right)_i} \quad 87$$

$I_{b,\,mix}$ is equivalent to S_{total} from equation 84 and $I_{b,single}$ is equivalent to the signal from Cel5A and Cel6B in the individual experiments, S_{Cel5A} and S_{Cel6B}. Thus we can calculate DSB from the normalized fluorescence signal at each point in the time course as follows:

$$DSB_t = \frac{S_{total,t}}{S_{Cel5A,t} + S_{Cel6B,t}} \quad 88$$

For both Cel5A and Cel6B we can compare the fluorescent signal at each time point in the 1:1 mixture experiments with the same time point in the individual component experiments. Observing the DSB throughout a time course can provide some insight on whether one or both cellulases in a mixture exhibited increased binding due to synergism and when that enhanced binding occurred. The advantage of using fluorescence microscopy to image cellulase binding on the BMCC substrates is the excellent temporal resolution that can be achieved. Cellulase binding on BMCC is a dynamic event, with binding rates and extents affected by cellulose structure and temperature (Moran-Mirabal et al. 2011). The value for the DSB can be calculated for every time point in the experiment and that data is represented in Figure 21 below

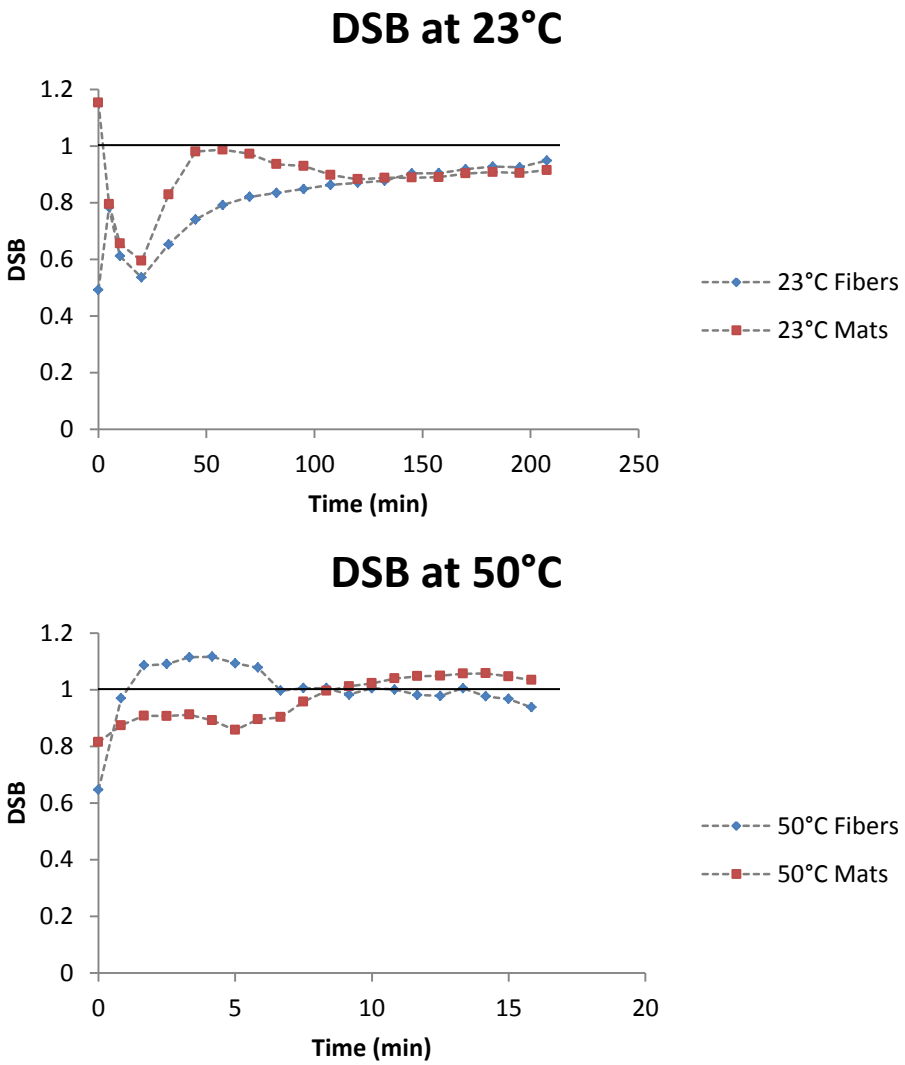

Figure 21: DSB calculated at each time point for an equimolar mixture of Cel5A and Cel6B at 23°C and 50°C on both fibers and mats. DSB > 1 indicates synergistic binding, depicted by the black line drawn to guide the eye.

There is no synergistic effect on binding observed for a 1:1 mixture of Cel5A and Cel6B at 23°C on either fibers or mats. Indeed, limiting the 23°C data to just the first 20 minutes of binding shows a DSB of approximately 0.5, indicating competitive binding at this temperature, on both fibers and mats. At 50°C, however, there is observed DSB on both fibers and mats in the 16.5 minutes of binding

observed, indicating cooperative binding between the Cel5A and the Cel6B. This result is consistent with the observations of Jeoh et al, who calculated a DSB of 0.11 for a 1:1 mixture of Cel5A and Cel6B at 5°C, indicating no synergistic binding, and DSB of 1.44 for the same mixture at 50°C (Jeoh et al. 2002). At 50°C, the DSB on mats increases throughout the time course. This is likely due to the synergistic effects of hydrolytic action by both Cel5A and Cel6B, creating new binding sites through cellulose hydrolysis. BMCC mats are dense cellulose structures, with much of the surface area contained within a matrix of overlapping and tightly packed BMCC fibers, and enhanced hydrolytic activity in a mixture of cellulases expands the available surface area and the number of cellulase binding sites. On fibers at 50°C, there is an initial increase in DSB early in the time course, then a decrease in the later stages of the experiment, after about 5 minutes. Fibers have readily available surface areas and binding sites, with little hindrance from the BMCC structure, so it follows that there might be a limit to the binding enhancement by a mixture of Cel5A and Cel6B when there is also hydrolytic activity once all of the initial binding sites are occupied.

Conclusions

In this study we have observed the effects of the presence of both Cel5A and Cel6B in a mixture on the rate and extent of cellulase binding. Fluorescence microscopy techniques combined with fluorescently labeled *T. fusca* cellulases Cel5A and Cel6B were applied to immobilized BMCC substrates at 23°C and 50°C to investigate cellulase binding with and without hydrolytic activity on cellulose fiber and mat structures. The concurrent binding by Cel5A and Cel6B in a mixture can be observed for both fibers and mats using two different fluorescent tags imaged together. The difference in the relative fluorescence of these tags can be accounted for and corrected, to provide insights into the rates and extents of binding by both Cel5A and Cel6B in a 1:1 mixture. The fluorescent binding data collected

provides a picture of cellulase binding with excellent spatial and temporal resolution, making it possible to discern binding on various cellulose structures in a dynamic process.

This work builds on previous observations by the Walker lab on cellulase binding and improves our understanding of the effect of cellulose morphological structures. Jeoh et al. saw similar results for an equimolar mixture of Cel5A and Cel6B binding at 50°C, with enhanced binding by the mixture over the extent of each cellulase binding alone (Jeoh et al. 2002). The advantage of the techniques used in this study is the spatial and temporal resolution which allows us to draw insights into the effects of cellulose structure on binding and the dynamic nature of the cellulase binding itself (Moran-Mirabal et al. 2008; Moran-Mirabal et al. 2011; Zhu et al. 2011; Luterbacher et al. 2013; Yang et al. 2013). In this study, cellulase binding and DSB was observed in the very early minutes of the binding reaction on two different cellulose morphological structures. The bound concentration of Cel5A in particular, is affected by cellulose structure and density. The bound concentration of Cel5A increased throughout the time course on mats, while remaining stable throughout the time course on fibers. This is likely due to enhanced hydrolysis activity by Cel5A and Cel6B together on the BMCC mats, which have more opportunity for the creation of new binding sites as compared to fibers. This spatial resolution enhances our understanding of the effect of cellulose structure on cellulase binding.

Additionally, we can observe how the DSB changes throughout the time course with hydrolytic actions of the cellulases in the mixture with the temporal resolution afforded by the fluorescence microscopy techniques. The concentration of bound cellulase at each time point can be correlated to the fluorescence intensity observed, making quantitative analysis of the DSB possible. Consistent with results reported by Jeoh et al., enhanced DSB was observed for a 1:1 mixture of Cel5A and Cel6B at 50°C on both fibers and mats (Jeoh et al. 2002; Jeoh et al. 2006). Interestingly, the DSB changed throughout

the time course, with enhanced binding observed early in the time course for fibers, and an increasing enhancement observed for mats. Again, the morphological structure of the cellulose substrate influences the cellulase binding.

This study lays the foundation for using fluorescent imaging techniques to expand on both Jeoh et al and Santhanam et al's ternary mixture cellulase studies to better understand the dynamic nature of cellulase binding in a mixture that is closer to what is observed in nature (Jeoh et al. 2002; Santhanam and Walker 2008). The spatial and temporal resolution of the binding data obtained from fluorescence microscopy techniques provides new insights into the dynamic binding behavior of a synergistic mixture of Cel5A and Cel6B.

CHAPTER 6: CONCLUSION AND FUTURE DIRECTIONS

The objective of the research presented in this dissertation was to explore the influence of cellulose morphological structure and lignocellulosic biomass complexity on cellulase binding and hydrolysis to improve our understanding of the synergistic activities of plant cell wall degrading enzymes required for biomass hydrolysis. To this end, a high throughput screening method to screen fungal plant pathogens on real biomass substrates was established, and a method to use fluorescence microscopy techniques to observe cellulase binding on BMCC fibers and mats with excellent spatial and temporal resolution was developed and then applied to the study of dynamic synergistic binding by a mixture of an endocellulase and an exocellulase. The greater the level of complexity in the cellulose substrate, the more important the synergistic actions of a mixture of cellulases and other plant cell wall degrading enzymes becomes to effectively hydrolyzing the cellulose polymer to its glucose monomers.

Building on the imaging methods presented here will lead to a better understanding of the influence of cellulose morphology on cellulase hydrolytic activities individually and in synergistic mixtures. As discussed, a major limitation of the imaging method presented is the lack of a closed mass balance to produce quantitative hydrolytic activity data. Developing a method to accurately measure the amount of cellulose adhered to the glass slide substrate after washing away non-adhered cellulose will be critical to know the initial amount of cellulose surface area available to the enzymes in solution. Additionally, measuring the quantity of cellulose left on the glass slide substrate after the binding and hydrolysis assays will be a key piece of closing the cellulose mass balance and understanding the rate of hydrolytic activities. At the same time, finding the actual concentration of cellulase enzymes bound to the surface of cellulose fibers and within cellulose mats will be important for understanding the ability

of cellulases to move within a more complicated cellulose structure. This information could provide insights into the effects of cellulose surface interactions, pore structure, and cellulase-cellulase steric hindrance on cellulolytic activity.

Despite the limitations in measuring the amounts of cellulose and cellulase in the system, the methods developed here could be used as they are to investigate the influence of cellulose morphology on cellulase binding in a mixture of three cellulases. *T. fusca* cellulase Cel9A, a processive endocellulase, could be labeled with a third color of Alexa Fluor dye that will not interfere with the fluorescence signal from either the cellulases labeled with the AF 488 or the AF 647. The molar ratios of the cellulases in this ternary system could be varied to begin to optimize the ratio of endo-acting cellulases to exo-acting. This study would build on the work begun in Santhanam et al. by improving the temporal resolution of the initial binding stages studied and looking at the influence of cellulose morphology on cellulase synergism in a ternary mixture (Santhanam and Walker 2008). Indeed, it is possible to speculate that many different dyes could be employed to investigate complicated systems of fluorescently labeled enzymes on the cellulose substrates, provided the dyes' excitation and emission spectra do not overlap significantly. Other plant cell wall degrading enzymes could be labeled and binding on real biomass substrates could be studied, as long as conditions to control for any auto-fluorescence in the biomass samples were met. The multiple enzyme imaging and analysis methods developed here could be used to produce new insights into the influence of substrate complexity on cellulase binding and hydrolysis and the effects of synergism in synergistic mixtures of multiple enzymes.

A major outcome of the research and method developed by Dr. Brian King and myself was the determination of hydrolytic activities for 156 species of fungi and oomycetes by King et al. using our method to identify promising sources for plant cell wall degrading enzymes complementary to those

currently available (King et al. 2011). This large scale screening effort identified several isolates of plant pathogenic fungi that were showed high hydrolytic activity on biomass. Several other studies have focused on screening collections of cellulose acting enzymes from microbial sources on a small scale in a high throughput manner (Cianchetta et al. 2012; Fer et al. 2012; Chang et al. 2013; Lucena et al. 2013; Romano et al. 2013). A limitation of isolating and growing a microbial source of cellulases in a laboratory setting is that often, some strains of microbes of interest cannot be reliably grown in pure cultures (Rappé and Giovannoni 2003). To this end, mining the genomic data of complex microbial ecosystems has emerged as a method to find novel sources of cellulases (Duan and Feng 2010). DNA extracted from environmental sources, such as soil or the guts of ruminants, can be used to construct metagenomic libraries in cloning vectors for isolating and identifying novel biocatalysts by function or sequence-based approaches (Duan and Feng 2010). Searching environmental genomic data complements high throughput screening methods for identifying highly active cellulose and other plant cell wall degrading enzymes. Using a library of genomic data as a first pass, promising candidates can be identified and crude enzyme extracts can be prepared from source clones and screened using the methods described in Chapter 3.

The field of cellulase imaging has grown and expanded by leaps and bounds in the three decades of visualized cellulase research. Fluorescence microscopy techniques, like the ones described in Chapter 4 of this dissertation, allow for the observation of micro-scale cellulase-cellulose interactions in an aqueous environment with excellent spatial and temporal resolution. AFM studies are able to investigate dynamic biological systems on a molecular scale under environmental conditions such as temperature and pressure in an aqueous environment (Bubner et al. 2013). High speed (HS) AFM, which can capture on the order of 10 images per second, is able to image individual cellulases in real time,

leading to the recording of some incredible movies showing cellulases processing along cellulose fibers (Igarashi et al. 2009). One of the great remaining challenges to obtaining valuable, quantitative image data is the cellulose substrate used in the imaging experiments. Cellulase activity and adsorption measured during an experiment are dependent on the type of cellulose used as the substrate (Igarashi et al. 2006; Bubner et al. 2012).The conclusions reached in Chapters 4 and 5 of this dissertation show the impact of cellulose morphological structure on cellulase binding, and this is only looking at BMCC. Cellulose substrates using in imaging studies are obtained from bacterial cellulose, algal cellulose, and plant cellulose, each with advantages and disadvantages, and each with its own requirements for substrate preparation (Bubner et al. 2013). Factors affecting cellulase binding and activity, such as crystallinity index, degree of polymerization, and the presence of lignin or hemicellulose are dependent on the source of the cellulose substrate and any pretreatments required to make the cellulose more accessible or immobilize it for imaging studies (Bubner et al. 2013). Despite these challenges, a wealth of cellulase-cellulose interaction information has been gleaned from imaging studies, and more is promised to follow. Emerging super-resolution fluorescence microscopy methods are able to visualize cellulases on a molecular scale, down to 10-20 nm resolution. Single molecule imaging by fluorescence microscopy or by HS-AFM can show cellulase processivity in real time (Igarashi et al. 2011; Moran-Mirabal et al. 2013). Confocal fluorescence microscopy and AFM techniques can both reveal high resolution information about the degradation of biomass by cellulolytic activities on a larger scale (Santa-Maria and Jeoh 2010; Zhu et al. 2011; Ding et al. 2012; Luterbacher et al. 2013; Yang et al. 2013). As imaging technologies advance, we will learn more about the nano-scale degradation of cellulose by cellulases and better understand the surface interaction that drive cellulase diffusion into the cellulose structure.

Classical cellulase synergism is understood to require the simultaneous actions of three types of cellulases. Endoglucanases randomly cleave bonds in the cellulose polymer, exoglucanases attack cellulose polymer chain ends, and β-glucosidases convert the cellobiose produced by the actions of the endo and exo acting glucanases to cellulose (Lynd et al. 2002; Merino and Cherry 2007; Horn et al. 2012). While the mechanism is well understood, several questions and challenges remain and are impeding our transition to a bio-based economy. Cellulose is effectively degraded by a combination of endo and exo acting glucanases, but conversion is typically less than 100%, closer to 70-80% of the available cellulose (Rosgaard et al. 2007; Klein-Marcuschamer et al. 2012). Improving cellulase accessibility to hydrolysable sites within the cellulose structure will lead to improved conversion efficiencies, but understanding how cellulase synergism is affected by cellulose structure is a key step in this process. The results presented in Chapter 5 show the DSB is influenced by the cellulose structure observed, whether binding is on BMCC fibers or mats. Cellulase binding on fiber structures benefitted early in the time course observed from synergistic actions, while binding was enhanced throughout the time course observed for mat structures in a synergistic mixture. An AFM study by Ganner et al. showed the effect of cellulose structure (amorphous or crystalline) on cellulase synergism and activity (Ganner et al. 2012). The endoglucanase exclusively attacked amorphous regions of the cellulose substrate, exposing crystalline nanofibers for the cellobiohydrolase to act upon. This activity was critical for making the crystalline fibers available to the cellobiohydrolase, as it was found to be barely active alone (Ganner et al. 2012).

Recently, the identification and characterization of bacterial and fungal proteins, classified early as family 33 carbohydrate binding module (CBM33) and family 61 glycoside hydrolase (GH61) respectively, have been shown to play a significant role in the degradation of cellulose and indicate that

the classical model of endo-exo synergism may need to make room for another player (Cantarel et al. 2009; Vaaje-Kolstad et al. 2010; Forsberg et al. 2011; Horn et al. 2012). These proteins use an oxidative mechanism that depends on the presence of divalent metal ions and an electron donor to cleave crystalline polysaccharide chains (Vaaje-Kolstad et al. 2010). The characterization of their activity has led to these proteins being reclassified as AA10 (formerly CBM33) and AA9 (formerly GH61) in the CAZY database (Cantarel et al. 2009). Their flat substrate binding sites are theorized to attach to flat crystalline surfaces on the substrate, where they disrupt packing and increase substrate accessibility (Horn et al. 2012). Genes encoding for these proteins are abundant in cellulose utilizing microorganisms, and recent transciptomics and proteomics studies have shown the expression of some AA9s (formerly GH61) and AA10s (formerly CBM33) is induced by cellulose and/or co-regulated with the expression of cellulases (Foreman et al. 2003; Eastwood et al. 2011; Macdonald et al. 2011; Adav et al. 2012; Horn et al. 2012). Classical synergy is enhanced by the presence of these proteins acting on the substrate surface and introducing additional breaks in the polysaccharide chains, and the addition of these proteins to the biorefinery tool box will increase the efficiency and yield of biochemical cellulose conversion to glucose.

This is an exciting time to be working in the field of cellulases and cellulose hydrolysis. Rapidly advancing imaging technology is allowing us to visualize cellulose hydrolysis by cellulases in ways that were never possible, achieving sub 20 nm resolution and making it possible to watch cellulases process along crystalline cellulose substrates. Using both fluorescence microscopy and AFM, it is possible to track the changes to the cellulose structure in real time as the degradation proceeds. This temporal resolution makes it possible to understand the role of various cellulases in a synergistic mixture as hydrolysis occurs. The advent of readily available genomic data and the rapid reduction in cost of sequencing will make it possible to explore new regions and environments for novel cellulases or

complementary enzymes to reduce costs and enhance cellulose degradation on an industrial scale. The synthesis of new scientific knowledge gained from metagenomic data and real-time visualizations of enzyme and substrate interactions will advance the field in new ways, ushering in a new era for the bioeconomy.

```
%Cellulase binding imaging analysis for epi-fluorescent data
%April 13, 2012
%by Marie Donnelly, adapted from Moran-Mirabal et al. (2008)
%Analyze background first, get statistics on background, then select an
%area for cellulase fluorescent signal analysis by selecting a single pixel
%to be the center of a box
%Currently, this box is defined as 100px X 100px, but can be adjusted in
%line 41
%Should work for dual color analysis, both 488 and 647

close all;
clear all;

Experiment488 = '488.tif'; %Takes 488 stack of images and names file
Experiment647 = '647.tif'; %Takes 647 stack of images and names file
info488 = imfinfo(Experiment488); %Stores image file name for 488 stack
info647 = imfinfo(Experiment647); %Stores image file name for 647 stack
totalfiles488 = size(info488); %Stores the number of images in 488 stack
totalfiles647 = size(info647); %Stores the number of images in 647 stack
Total = totalfiles488(1,1);
Final488 = im2double(imread(Experiment488,Total)); %'imread' Reads the final image (i.e. most
intense) in the stack, 'im2double' converts that image to double precision and stores it
Final647 = im2double(imread(Experiment647,Total));
Integral488 = sum(sum(Final488)); % Assigns a value to fluorescence intensity in final image in 488 stack
Integral647 = sum(sum(Final647)); % Assigns a value to fluorescence intensity in final image in 647 stack

if Integral488 > Integral647 % Chooses the more intense signal (greater value in final image) to use for
selecting areas for analysis
   Original = Final488;
else
   Original = Final647;
end

SatMask = im2bw(Original,0.9999); %Creates a mask removing saturated pixels (signal>0.9999) by
converting grayscale image to a binary image
%figure('Name','Saturation Mask'), imshow(SatMask); %Displays saturation mask
OriginalwoSat = Original - SatMask; %Uses saturation mask to remove saturated pixels from image for
analysis
figure('Name','Select Local Background'), imshow(imadjust(OriginalwoSat)); %Prompts user to select
background pixels from the entire image
[Background, rectback] = imcrop(imadjust(OriginalwoSat)); %Selects and stores background pixels from
a rectangle selection tool
BackAvg = mean2(Background); %Average of background pixels
```

BackStd = std2(Background); %Standard deviation of background pixels
figure('Name','Select Pixel at Center of Area to Analyze'), imshow(imadjust(OriginalwoSat)); %Prompts user to select signal pixels for analysis
[x,y] = ginput(1); %Stores center pixel of area to analyze
[OrCrop,rect] = imcrop(imadjust(OriginalwoSat),[x-50 y-50 100 100]); %Selects and stores signal pixels in a square of the size specified by the last two numbers in the imcrop command, with the center specified by the user in the ginput line
Crop = imadjust(OrCrop); %Stores the selcted region
level2 = BackAvg + 8*BackStd; %Creates a threshold for declaring a pixel a signal, any pixel with signal greater than this level will be counted
BW2 = im2bw(Crop, level2); %Creates a binary image from the selected region with only pixels that have a signal greater than the level specified
L = bwlabel(BW2,8); % Labels connected components in the selected region for analysis defined, 8-connected objects
stats = regionprops(L,'Area'); %Measures the number of pixels in the region
idx = find([stats.Area] > 25); %Finds regions with area greater than 25
SignalMask = ismember(L,idx); %Creates a binary image containing only regions with area greater than 25
Sample = SignalMask .* Crop; %Combines the cropped area with the mask indicating signal regions
figure('Name','Signal pixels'),imshow(Sample); %Displays the pixels analyzed as signal

for n = 1:Total;
Im488 = im2double(imread(Experiment488,n)); %Reads each image in 488 stack
Im647 = im2double(imread(Experiment647,n)); %Reads each image in 647 stack
Crop488 = imcrop(Im488,rect); %Applies the cropped area for analysis to each image in 488 stack
Crop647 = imcrop(Im647,rect); %Applies the cropped area for analysis to each image in 647 stack
Back488 = imcrop(Im488,rectback); %Applies the cropped area for background to each image in 488 stack
Back647 = imcrop(Im647,rectback); %Applies the cropped area for background to each image in 647 stack
Bav488 = mean2(Back488); %Gets the average value for background from all pixels in 488 stack
Bsd488 = std2(Back488); %Gets standard deviation for background in 488 stack
Signal488 = Crop488 .* SignalMask; %Applies signal mask to cropped area for analysis to each image in 488 stack
Sav488 = mean2(nonzeros(Signal488)); %Gets the average value for signal from all pixels in cropped area for analysis in 488 stack
Ssd488 = std2(nonzeros(Signal488)); %Gets the standard deviation for signal from all pixels in cropped area for analysis in 488 stack
Bav647 = mean2(Back647); %Gets the average value for background from all pixels in 647 stack
Bsd647 = std2(Back647); %Gets standard deviation for background in 647 stack
Signal647 = Crop647 .* SignalMask; %Applies signal mask to cropped area for analysis to each image in 647 stack
Sav647 = mean2(nonzeros(Signal647)); %Gets the average value for signal from all pixels in cropped area for analysis in 647 stack

Ssd647 = std2(nonzeros(Signal647)); %Gets the standard deviation for signal from all pixels in cropped area for analysis in 647 stack

Data(n,1) = n; %Frame count A(X)
Data(n,2) = Bav488; %Background average 488 B(Y)
Data(n,3) = Bsd488; %Background standard deviation 488 C(Y)
Data(n,4) = Sav488; %Signal average 488 D(Y)
Data(n,5) = Ssd488; %Signal standard deviation 488 E(Y)
Data(n,6) = 0; %F(Y) Placeholder column
Data(n,7) = Bav647; %Background average 647 G(Y)
Data(n,8) = Bsd647; %Background standard deviation 647 H(Y)
Data(n,9) = Sav647; %Signal average 647 I(Y)
Data(n,10) = Ssd647; %Signal standard deviation 647 J(Y)
Data(n,11) = 0;
Data(n,12) = (Data(n,4)-Data(n,2)); %Signal-background 488
Data(n,13) = Data(n,9)-Data(n,7); %Signal-background 647

end

AverageBackground488 = mean2(Data(:,2)) %Computes average value of background values for all images in 488 stack
StdDevBackground488 = std2(Data(:,2)) %Computes std dev of background values for all images in 488 stack
AverageBackground647 = mean2(Data(:,7)) %Computes average value of background values for all images in 488 stack
StdDevBackground647 = std2(Data(:,7)) %Computes std dev of background values for all images in 488 stack
Y1 = (Data(:,12)); % Signal-background 488
Y3 = Data(:,2); %background 488
Y2 = Data(:,9)-Data(:,7); %Signal-background 647
Y4 = Data(:,7); %background 647
Y5 = Y1./Y2; % Ratio of 488 signal/647 signal
Y6 = Data(:,4); %Raw signal 488
Y7 = Data(:,9); %Raw signal 647
X = Data(:,1);
figure(), plot(X,Y1,':sg');% Signal-background 488
hold on;
%plot(X,Y6,'-r*');%Raw signal 488
%hold on;
plot(X,Y2,'-r*');%Signal-background 647
hold on;
plot(X,Y3,':db');%background 488
hold on;
plot(X,Y4,'-mo');%background 647
%figure(),plot(X,Y5,':db');% Ratio of 488 signal/647 signal

```
LargeArea = Data;
Savename = 'LargeArea';
save(Savename,'LargeArea','-ascii');
xlswrite('LargeArea',Data); %Writes an MS Excel file containing data set
```

REFERENCES

Adav, S., Ravindran, A. and Sze, S. (2012). "Quantitative proteomic analysis of lignocellulolytic enzymes by *Phanerochaete chrysosporium* on different lignocellulosic biomass." J Proteomics **75**: 1493 - 1504.

Ai, Y.-C. and Wilson, D. B. (2002). "Mutation and expression of N233C-D506C of cellulase Cel6B from *Thermobifida fusca* in *Escherichia coli*." Enzyme and Microbial Technology **30**(6): 804-808.

Annis, S. L. and Goodwin, P. H. (1997). "Recent advances in the molecular genetics of plant cell wall-degrading enzymes produced by plant pathogenic fungi." European Journal of Plant Pathology **103**: 1-14.

Aro, N., Pakula, T. and Penttila, M. (2005). "Transcriptional regulation of plant cell wall degradation by filamentous fungi." FEMS Microbiology Reviews **29**: 719-739.

Atalla, R. H., Hackney, J. M., Uhlin, I. and Thompson, N. S. (1993). "Hemicelluloses as structure regulators in the aggregation of native cellulose." International Journal of Biological Macromolecules **15**(2): 109-112.

Atalla, R. H. and Vanderhart, D. L. (1984). "Native cellulose: A composite of two distinct crystalline forms." Science **223**(4633): 283-285.

Axelrod, D., Koppel, D. E., Schlessinger, J., Elson, E. and Webb, W. W. (1976). "Mobility measurement by analysis of fluorescence photobleaching recovery kinetics." Biophysical Journal **16**(9): 1055-1069.

Bansal, P., Hall, M., Realff, M. J., Lee, J. H. and Bommarius, A. S. (2009). "Modeling cellulase kinetics on lignocellulosic substrates." Biotechnology Advances **Volume 27**(Issue 6): 833-848.

Bayer, E. A., Chanzy, H., Lamed, R. and Shoham, Y. (1998). "Cellulose, cellulases and cellulosomes." Current Opinion in Structural Biology **8**(5): 548-557.

Beldman, G., Voragen, A. G. J., Rombouts, F. M. and Pilnik, W. (1988). "Synergism in cellulose hydrolysis by endoglucanases and exoglucanases purified from *Trichoderma viride*." Biotechnology and Bioengineering **31**: 173-178.

Berlin, A., Balakshin, M., Gilkes, N., Kadla, J., Maximenko, V., Kubo, S. and Saddler, J. (2006). "Inhibition of cellulase, xylanase, and β-glucosidase activities by softwood lignin preparations." Journal of Biotechnology **125**: 198-209.

Berlin, A., Gilkes, N., Kilburn, D., Bura, R., Markov, A., Skomarovsky, A., Okunev, O., Gusakov, A., Maximenko, V., Gregg, D., Sinitsyn, A. and Saddler, J. (2005). "Evaluation of novel fungal cellulase preparations for ability to hydrolyze softwood substrates- evidence for the role of accessory enzymes." Enzyme and Microbial Technology **37**(2): 175-184.

Berlin, A., Maximenko, V., Gilkes, N. and Saddler, J. (2007). "Optimization of enzyme complexes for lignocellulose hydrolysis." Biotechnology and Bioengineering **97**(1): 287-296.

Boraston, A. B., Bolam, D. N., Gilbert, H. J. and Davies, G. J. (2004). "Carbohydrate-binding modules: Fine-tuning polysaccharide recognition." Biochem. J. **382**(3): 769-781.

Bothwell, M. K., Daughhetee, S. D., Chaua, G. Y., Wilson, D. B. and Walker, L. P. (1997). "Binding capacities for *Thermomonospora fusca* E3, E4 and E5, the E3 binding domain, and *Trichoderma reesei* CBHI on avicel and bacterial microcrystalline cellulose." Bioresource Technology **60**(2): 169-178.

Bothwell, M. K. and Walker, L. P. (1995). "Evaluation of parameter estimation methods for estimating cellulase binding constants." Bioresource Technology **53**(1): 21-29.

Bothwell, M. K., Walker, L. P., Wilson, D. B., Irwin, D. C. and Price, M. (1993). "Synergism between pure *Thermomonospora fusca* and *Trichoderma reesei* cellulases." Biomass and Bioenergy **4**(4): 293-299.

Bothwell, M. K., Wilson, D. B., Irwin, D. C. and Walker, L. P. (1997). "Binding reversibility and surface exchange of *Thermomonospora fusca* E3 and E5 and *Trichoderma reesei* CBHI." Enzyme and Microbial Technology **20**(6): 411-417.

Bradbury, S. and Evennett, P. (1996). Contrast techniques in light microscopy, Bios Scientific Publishers.

Breuil, C. and Saddler, J. N. (1985). "Comparison of the 3,5-dinitrosalicylic acid and Nelson-Somogyi methods of assaying for reducing sugars and determining cellulase activity." Enzyme and Microbial Technology **7**: 327-332.

Brunner, K., Lichtenauer, A., Kratochwill, K., Delic, M. and Mach, R. (2007). "Xyr1 regulates xylanase but not cellulase formation in the head blight fungus *Fusarium graminearum*." Current Genetics **52**(5): 213-220.

Bubner, P., Dohr, J., Plank, H., Mayrhofer, C. and Nidetzky, B. (2012). "Cellulases dig deep: In situ observation of the mesoscopic structural dynamics of enzymatic cellulose degradation." Journal of Biological Chemistry **287**(4): 2759-2765.

Bubner, P., Plank, H. and Nidetzky, B. (2013). "Visualizing cellulase activity." Biotechnology and Bioengineering **110**(6): 1529-1549.

Calero-Nieto, F., Di Petro, A., Roncero, M. I. G. and Hera, C. (2007). "Role of the transcriptional activator XlnR of *Fusarium oxysporum* in regulation of xylanase genes and virulence." Molecular Plant Microbe Interactions **20**(8): 977-985.

Calero-Nieto, F., Hera, C., Di Pietro, A., Orejas, M. and Roncero, M. I. G. (2008). "Regulatory elements mediating expression of xylanase genes in *Fusarium oxysporum*." Fungal Genetics and Biology **45**(1): 28-34.

Cantarel, B. L., Coutinho, P. M., Rancurel, C., Bernard, T., Lombard, V. and Henrissat, B. (2009). "The Carbohydrate-Active enZymes database (CAZy): An expert resource for glycogenomics." Nucl. Acids Res. **37**(suppl_1): D233-238.

Carrasco, J. E., Sáiz, M. C., Navarro, A., Soriano, P., Sáez, F. and Martinez, J. M. (1994). "Effects of dilute acid and steam explosion pretreatments on the cellulose structure and kinetics of cellulosic fraction hydrolysis by dilute acids in lignocellulosic materials " Applied Biochemistry and Biotechnology **45/46**(1): 23-34.

Chang, C., Sustarich, J., Bharadwaj, R., Chandrasekaran, A., Adams, P. D. and Singh, A. K. (2013). "Droplet-based microfluidic platform for heterogeneous enzymatic assays." Lab on a Chip **13**(9): 1817-1822.

Chang, V. S. and Holtzapple, M. T. (2000). "Fundamental factors affecting biomass enzymatic reactivity " Applied Biochemistry and Biotechnology **84-86**(1-9): 5-37.

Chen, M., Zhao, J. and Xia, L. (2008). "Enzymatic hydrolysis of maize straw polysaccharides for the production of reducing sugars." Carbohydrate Polymers **71**(3): 411-415.

Chundawat, S. P. S., Balan, V. and Dale, B. E. (2008). "High-throughput microplate technique for enzymatic hydrolysis of lignocellulosic biomass." Biotechnology and Bioengineering **99**(6): 1281-1294.

Cianchetta, S., Galletti, S., Burzi, P. L. and Cerato, C. (2012). "Hydrolytic potential of *Trichoderma* sp. strains evaluated by microplate-based screening followed by switchgrass saccharification." Enzyme and Microbial Technology **50**(6–7): 304-310.

Converse, A. O. and Optekar, J. D. (1993). "A synergistic kinetics model for enzymatic cellulose hydrolysis compared to degree-of-synergism experimental results." Biotechnology and Bioengineering **42**(1): 145-148.

Cosgrove, D. J. (2005). "Growth of the plant cell wall." Nat Rev Mol Cell Biol **6**(11): 850-861.

Coughlan, M. (1985). "The properties of fungal and bacterial cellulases with comment on their production and application." Biotechnology and Genetic Engineering Reviews **3**: 39-109.

Coward-Kelly, G., Aiello-Mazzari, C., Kim, S., Granda, C. and Holtzapple, M. (2003). "Suggested improvements to the standard filter paper assay used to measure cellulase activity." Biotechnology and Bioengineering **82**(6): 745-749.

Coyle, W. T. (2010). Next-generation biofuels near-term challenges and implications for agriculture. Outlook, USDA Economic Research Service**:** 26 pp.

Cuomo, C. A., Guldener, U., Xu, J.-R., Trail, F., Turgeon, B. G., Di Pietro, A., Walton, J. D., Ma, L.-J., Baker, S. E., Rep, M., Adam, G., Antoniw, J., Baldwin, T., Calvo, S., Chang, Y.-L., Decaprio, D., Gale, L. R., Gnerre, S., Goswami, R. S., Hammond-Kosack, K., Harris, L. J., Hilburn, K., Kennell, J. C., Kroken, S., Magnuson, J. K., Muehlbauer, G., Munsterkotter, M., Nelson, D., O'donnell, K., Ouellet, T., W., Q., Quesneville, H., Roncero, M. I. G., Seong, K.-Y., Tetko, I. V., Urban, M., Waalwijk, C., Ward, T. J., Yao, J., Birren, B. W. and Kistler, H. C. (2007). "The *Fusarium graminearum* genome reveals a link between localized polymorphism and pathogen specialization." Science **317**: 1400-1402.

Dagel, D. J., Liu, Y.-S., Zhong, L., Luo, Y., Himmel, M. E., Xu, Q., Zeng, Y., Ding, S.-Y. and Smith, S. (2010). "In situ imaging of single carbohydrate-binding modules on cellulose microfibrils." The Journal of Physical Chemistry B **115**(4): 635-641.

Davies, G. and Henrissat, B. (1995). "Structures and mechanisms of glycosyl hydrolases." Structure **3**(9): 853-859.

Dean, S. W. and Rollings, J. E. (1992). "Analysis and quantification of a mixed exo-acting and endo-acting polysaccharide depolymerization system." Biotechnology and Bioengineering **39**(9): 968-976.

Decker, S. R., Adney, W. S., Jennings, E., Vinzant, T. B. and Himmel, M. E. (2003). "Automated filter paper assay for determination of cellulase activity." Applied Biochemistry and Biotechnology **105**: 689-703.

Ding, S.-Y. and Himmel, M. E. (2006). "The maize primary cell wall microfibril: A new model derived from direct visualization." Journal of Agricultural and Food Chemistry **54**(3): 597-606.

Ding, S.-Y., Liu, Y.-S., Zeng, Y., Himmel, M. E., Baker, J. O. and Bayer, E. A. (2012). "How does plant cell wall nanoscale architecture correlate with enzymatic digestibility?" Science **338**(6110): 1055-1060.

Ding, S.-Y., Xu, Q., Crowley, M., Zeng, Y., Nimlos, M., Lamed, R., Bayer, E. A. and Himmel, M. E. (2008). "A biophysical perspective on the cellulosome: New opportunities for biomass conversion." Current Opinion in Biotechnology **19**(3): 218-227.

Duan, C.-J. and Feng, J.-X. (2010). "Mining metagenomes for novel cellulase genes." Biotechnology Letters **32**(12): 1765-1775.

Duff, S. J. B., Cooper, D. G. and Fuller, O. M. (1987). "Effect of media composition and growth conditions on production of cellulase and beta-glucosidase by a mixed fungal fermentation." Enzyme and Microbial Technology **9**(1): 47-52.

Duff, S. J. B. and Murray, W. D. (1996). "Bioconversion of forest products industry waste cellulosics to fuel ethanol: A review." Bioresource Technology **55**(1): 1-33.

Eastwood, D., Floudas, D., Binder, M., Majcherczyk, A., Schneider, P., Aerts, A., Asiegbu, F., Baker, S., Barry, K. and Bendiksby, M. (2011). "The plant cell wall-decomposing machinery underlies the functional diversity of forest fungi." Science **333**: 762 - 765.

Esquerre-Tugaye, M.-T., Boudart, G. and Dumas, B. (2000). "Cell wall degrading enzymes, inhibitory proteins, and oligosaccharides participate in the molecular dialogue between plants and pathogens." Plant Physiology and Biochemistry **38**: 157-163.

Fales, S. L., Hess, J. R. and Wilhelm, W. W. (2007). Convergence of agriculture and energy: Ii. Producing cellolosic biomass for biofuels. Council for Agricultural Science and Technology (CAST) commentary. Ames, Iowa, CAST. **QTA2007-2**.

Fer, M., Préchoux, A., Leroy, A., Sassi, J.-F., Lahaye, M., Boisset, C., Nyvall-Collén, P. and Helbert, W. (2012). "Medium-throughput profiling method for screening polysaccharide-degrading enzymes in complex bacterial extracts." Journal of Microbiological Methods **89**(3): 222-229.

Foreman, P. K., Brown, D., Dankmeyer, L., Dean, R., Diener, S., Dunn-Coleman, N. S., Goedegebuur, F., Houfek, T. D., England, G. J., Kelley, A. S., Meerman, H. J., Mitchell, T., Mitchinson, C., Olivares, H. A., Teunissen, P. J. M., Yao, J. and Ward, M. (2003). "Transcriptional regulation of biomass-degrading enzymes in the filamentous fungus *Trichoderma reesei*." Journal of Biological Chemistry **278**(34): 31988-31997.

Forsberg, Z., Vaaje-Kolstad, G., Westereng, B., Bunaes, A., Stenstrom, Y., Mackenzie, A., Sorlie, M., Horn, S. and Eijsink, V. (2011). "Cleavage of cellulose by a CBM33 protein." Prot Science **20**: 1479 - 1483.

Fujii, M., Homma, T., Ooshima, K. and Taniguchi, M. (1991). "A kinetic model of the synergism of endo- and exoglucanase and β-glucosidase on hydrolysis of cellulose." Applied Biochemistry and Biotechnology **28-29**(1): 145-156.

Fullbrook, P. D. (1996). Practical limits and prospects (kinetics). Industrial enzymology. T. Godfrey and S. West, New York: Stockton Press**:** 609.

Ganner, T., Bubner, P., Eibinger, M., Mayrhofer, C., Plank, H. and Nidetzky, B. (2012). "Dissecting and reconstructing synergism: In situ visualization of cooperativity among cellulases." Journal of Biological Chemistry **287**(52): 43215-43222.

Gao, D., Chundawat, S. P. S., Krishnan, C., Balan, V. and Dale, B. E. (2010). "Mixture optimization of six core glycosyl hydrolases for maximizing saccharification of ammonia fiber expansion (AFEX) pretreated corn stover." Bioresource Technology **101**(8): 2770-2781.

Gebler, J., Gilkes, N. R., Claeyssens, M., Wilson, D. B., Beguin, P., Wakarchuk, W. W., Kilburn, D. G., Miller, R. C., Warren, R. A. and Withers, S. G. (1992). "Stereoselective hydrolysis catalyzed by related beta-1,4-glucanases and beta-1,4-xylanases." J Biol Chem **267**(18): 12559-12561.

Ghose, T. K. (1987). "Measurement of cellulase activities." Pure and Applied Chemistry **59**(2): 257-268.

Ghosh, P. and Singh, A. (1993). Physicochemical and biological treatments for enzymatic/microbial conversion of lignocellulosic biomass. Advances in applied microbiology. N. Saul and I. L. Allen, Academic Press. **Volume 39:** 295-333.

Ghosh, V. K., Ghose, T. K. and Gopalkrishnan, K. S. (1982). "Improvement of *T. reesei* strain through mutation and selected screening techniques." Biotechnol. Bioeng. **24**(1): 241-243.

Gilbert, H. J. (2010). "The biochemistry and structural biology of plant cell wall deconstruction." Plant Physiol. **153**(2): 444-455.

Gilkes, N. R., Jervis, E., Henrissat, B., Tekant, B., Miller, R. C. J., Warren, R. A. and Kilburn, D. G. (1992). "The adsorption of a bacterial cellulase and its two isolated domains to crystalline cellulose." Journal of Biological Chemistry **267**(10): 6743-6749.

Gilkes, N. R., Warren, R. A., Miller, R. C. and Kilburn, D. G. (1988). "Precise excision of the cellulose binding domains from two *Cellulomonas fimi* cellulases by a homologous protease and the effect on catalysis." Journal of Biological Chemistry **263**(21): 10401-10407.

Gusakov, A. V., Sinitsyn, A. P. and Klyosov, A. A. (1985). "Kinetics of the enzymatic hydrolysis of cellulose: 1. A mathematical model for a batch reactor process." Enzyme and Microbial Technology **7**(7): 346-352.

Gusakov, A. V., Sinitsyn, A. P., Salanovich, T. N., Bukhtojarov, F. E., Markov, A. V., Ustinov, B. B., Zeijl, C. V., Punt, P. and Burlingame, R. (2005). "Purification, cloning and characterisation of two forms of thermostable and highly active cellobiohydrolase I (Cel7A) produced by the industrial strain of *Chrysosporium lucknowense*." Enzyme and Microbial Technology **36**(1): 57-69.

Hall, M., Bansal, P., Lee, J. H., Realff, M. J. and Bommarius, A. S. (2010). "Cellulose crystallinity - a key predictor of the enzymatic hydrolysis rate." FEBS Journal **277**(6): 1571-1582.

Hegedus, D. D. and Rimmer, S. R. (2005). "*Sclerotinia sclerotiorum*: When "to be or not to be" a pathogen?" FEMS Microbiology Letters **251**(2): 177-184.

Henrissat, B. (1991). "A classification of glycosyl hydrolases based on amino acid sequence similarities." Biochem J **280 (Pt 2)**: 309-316.

Henrissat, B., Callebaut, I., Fabrega, S., Lehn, P., Mornon, J. P. and Davies, G. (1995). "Conserved catalytic machinery and the prediction of a common fold for several families of glycosyl hydrolases." Proc Natl Acad Sci U S A **92**(15): 7090-7094.

Henrissat, B. and Davies, G. (1997). "Structural and sequenced based classification of glycosyl hydrolases." Current Opinion in Structural Biology **7**: 637-644.

Henrissat, B., Driguez, H., Viet, C. and Schulein, M. (2002). "Synergism of cellulases from *Trichoderma reesei* in the degradation of cellulose." Bio/Technology **3**(8): 722-726.

Himmel, M. E., Ding, S.-Y., Johnson, D. K., Adney, W. S., Nimlos, M. R., Brady, J. W. and Foust, T. D. (2007). "Biomass recalcitrance: Engineering plants and enzymes for biofuels production." Science **315**(5813): 804-807.

Hong, J., Ye, X. and Zhang, Y. H. P. (2007). "Quantitative determination of cellulose accessibility to cellulase based on adsorption of a nonhydrolytic fusion protein containing CBM and GFP with its applications." Langmuir **23**(25): 12535-12540.

Horn, S., Vaaje-Kolstad, G., Westereng, B. and Eijsink, V. G. (2012). "Novel enzymes for the degradation of cellulose." Biotechnology for Biofuels **5**(1): 45.

Hu, R., Lin, L., Liu, T., Ouyang, P., He, B. and Liu, S. (2008). "Reducing sugar content in hemicellulose hydrolysate by DNS method: A revisit." Journal of Biobased Materials and Bioenergy **2**: 156-161.

Igarashi, K., Koivula, A., Wada, M., Kimura, S., Penttilã¤, M. and Samejima, M. (2009). "High speed atomic force microscopy visualizes processive movement of *Trichoderma reesei* cellobiohydrolase I on crystalline cellulose." Journal of Biological Chemistry **284**(52): 36186-36190.

Igarashi, K., Uchihashi, T., Koivula, A., Wada, M., Kimura, S., Okamoto, T., Penttilä, M., Ando, T. and Samejima, M. (2011). "Traffic jams reduce hydrolytic efficiency of cellulase on cellulose surface." Science **333**(6047): 1279-1282.

Igarashi, K., Wada, M., Hori, R. and Samejima, M. (2006). "Surface density of cellobiohydrolase on crystalline celluloses." FEBS Journal **273**(13): 2869-2878.

Irwin, D., Shin, D.-H., Zhang, S., Barr, B. K., Sakon, J., Karplus, P. A. and Wilson, D. B. (1998). "Roles of the catalytic domain and two cellulose binding domains of *Thermomonospora fusca* E4 in cellulose hydrolysis." J. Bacteriol. **180**(7): 1709-1714.

Irwin, D. C., Spezio, M., Walker, L. P. and Wilson, D. B. (1993). "Activity studies of eight purified cellulases: Specificity, synergism, and binding domain effects." Biotechnology and Bioengineering **42**(8): 1002-1013.

Jarvis, M. (2003). "Chemistry: Cellulose stacks up." Nature **426**(6967): 611-612.

Jeoh, T., Ishizawa, C. I., Davis, M. F., Himmel, M. E., Adney, W. S. and Johnson, D. K. (2007). "Cellulase digestibility of pretreated biomass is lmited by cellulose accessibility." Biotechnology and Bioengineering **98**(1): 112-122.

Jeoh, T., Wilson, D. B. and Walker, L. P. (2002). "Cooperative and competitive binding in synergistic mixtures of *Thermobifida fusca* Cel5A, Cel6B and Cel9A." Biotechnology Progress **18**(4): 760-769.

Jeoh, T., Wilson, D. B. and Walker, L. P. (2006). "Effect of cellulase mole fraction and cellulose recalcitrance on synergism in cellulose hydrolysis and binding." Biotechnology Progress **22**: 270-277.

Jørgensen, H., Kristensen, J. B. and Felby, C. (2007). "Enzymatic conversion of lignocellulose into fermentable sugars: Challenges and opportunities." Biofuels, Bioproducts and Biorefining **1**(2): 119-134.

Jung, H., Wilson, D. B. and Walker, L. P. (2002). "Binding of *Thermobifida fusca* CDCel5A, CDCel6B and CDCel48A to easily hydrolysable and recalcitrant cellulose fractions on BMCC." Enzyme and Microbial Technology **31**(7): 941-948.

Jung, H., Wilson, D. B. and Walker, L. P. (2003). "Binding and reversibility of *Thermobifida fusca* Cel5A, Cel6B, and Cel48A and their respective catalytic domains to bacterial microcrystalline cellulose." Biotechnology and Bioengineering **84**(2): 151-159.

Kabel, M. A., Van Der Maarel, M. J. E. C., Klip, G., Voragen, A. G. J. and Schols, H. A. (2006). "Standard assays do not predict the efficiency of commercial cellulase preparations towards plant materials." Biotechnology and Bioengineering **93**(1): 56-63.

King, B. C., Donnelly, M. K., Bergstrom, G. C., Walker, L. P. and Gibson, D. M. (2009). "An optimized microplate assay system for quantitative evaluation of plant cell wall-degrading enzyme activity of fungal culture extracts." Biotechnology and Bioengineering **102**(4): 1033-1044.

King, B. C., Waxman, K. D., Nenni, N. V., Walker, L. P., Bergstrom, G. C. and Gibson, D. M. (2011). "Arsenal of plant cell wall degrading enzymes reflects host preference among plant pathogenic fungi." Biotechnol Biofuels **4**: 4.

Klein-Marcuschamer, D., Oleskowicz-Popiel, P., Simmons, B. and Blanch, H. (2012). "The challenge of enzyme cost in the production of lignocellulosic biofuels." Biotechnology and Bioengineering **109**: 1083 - 1087.

Koshland, D. E. J. (1953). "Stereochemistry and the mechanism of enzymatic reactions." Biological Reviews **28**(4): 416-436.

Ladisch, M. R., Lin, K. W., Voloch, M. and Tsao, G. T. (1983). "Process considerations in the enzymatic hydrolysis of biomass." Enzyme and Microbial Technology **5**: 82-102.

Lee, I., Evans, B. R., Lane, L. M. and Woodward, J. (1996). "Substrate-enzyme interactions in cellulase systems." Bioresource Technology **58**(2): 163-169.

Lennholm, H., Larsson, T. and Iversen, T. (1994). "Determination of cellulose Iα and Iβ in lignocellulosic materials." Carbohydrate Research **261**(1): 119-131.

Liu, Y.-S., Luo, Y., Baker, J. O., Zeng, Y., Himmel, M. E., Smith, S. and Ding, S.-Y. (2010). A single molecule study of cellulase hydrolysis of crystalline cellulose. Single Molecule Spectroscopy and Imaging III, San Francisco, California, USA, SPIE.

Lucena, S. A., Moraes, C. S., Costa, S. G., De Souza, W., Azambuja, P., Garcia, E. S. and Genta, F. A. (2013). "Miniaturization of hydrolase assays in thermocyclers." Analytical Biochemistry **434**(1): 39-43.

Luterbacher, J. S., Parlange, J.-Y. and Walker, L. P. (2013). "A pore-hindered diffusion and reaction model can help explain the importance of pore size distribution in enzymatic hydrolysis of biomass." Biotechnology and Bioengineering **110**(1): 127-136.

Luterbacher, J. S., Walker, L. P. and Moran-Mirabal, J. M. (2013). "Observing and modeling BMCC degradation by commercial cellulase cocktails with fluorescently labeled *Trichoderma reesei* Cel7A through confocal microscopy." Biotechnology and Bioengineering **110**(1): 108-117.

Lynd, L. R., Weimer, P. J., Van Zyl, W. H. and Pretorius, I. S. (2002). "Microbial cellulose utilization: Fundamentals and biotechnology." Microbiol. Mol. Biol. Rev. **66**(3): 506-577.

Macdonald, J., Doering, M., Canam, T., Gong, Y., Guttman, D., Campbell, M. and Master, E. (2011). "Transcriptomic responses of the softwood-degrading white-rot fungus *Phanerochaete carnosa* during growth on coniferous and deciduous wood." Applied and Environmental Microbiology **77**: 3211 - 3218.

Mandels, M., Kostick, J. and Parizek, R. (1971). "The use of adsorbed cellulase in the continuous conversion of cellulose to glucose." Journal of Polymer Science **C36**: 445-459.

Martinez, D., Berka, R. M., Henrissat, B., Saloheimo, M., Arvas, M., Baker, S. E., Chapman, J., Chertkov, O., Coutinho, P. M., Cullen, D., Danchin, E. G. J., Grigoriev, I. V., Harris, P., Jackson, M., Kubicek, C. P., Han, C. S., Ho, I., Larrondo, L. F., De Leon, A. L., Magnuson, J. K., Merino, S., Misra, M., Nelson, B., Putnam, N., Robbertse, B., Salamov, A. A., Schmoll, M., Terry, A., Thayer, N., Westerholm-Parvinen, A., Schoch, C. L., Yao, J., Barbote, R., Nelson, M. A., Detter, C., Bruce, D., Kuske, C. R., Xie, G., Richardson, P., Rokhsar, D. S., Lucas, S. M., Rubin, E. M., Dunn-Coleman, N., Ward, M. and Brettin, T. S. (2008). "Genome sequencing and analysis of the biomass-degrading fungus *Trichoderma reesei* (syn. *Hypocrea jecorina*)." Nature Biotechnology **26**(5): 553-560.

Mccarter, J. D. and Withers, S. G. (1994). "Mechanisms of enzymatic glycoside hydrolysis." Curr Opin Struct Biol **4**(6): 885-892.

Mendgen, K., Hahn, M. and Deising, H. (1996). "Morphogenesis and mechanisms of penetration by plant pathogenic fungi." Annual Review of Phytopathology **34**: 367-386.

Merino, S. and Cherry, J. (2007). "Progress and challenges in enzyme development for biomass utilization." Advances in Biochemical Engineering Biotechnology **108**: 95 - 120.

Meyer, A. S., Rosgaard, L. and Sørensen, H. R. (2009). "The minimal enzyme cocktail concept for biomass processing." Journal of Cereal Science **50**(3): 337-344.

Miller, G. L. (1959). "Use of dinitrosalicylic acid reagent for determination of reducing sugar." Analytical Chemistry **31**(3): 426-428.

Moran-Mirabal, J. M., Bolewski, J. C. and Walker, L. P. (2011). "Reversibility and binding kinetics of *Thermobifida fusca* cellulases studied through fluorescence recovery after photobleaching microscopy." Biophysical Chemistry **155**(1): 20-28.

Moran-Mirabal, J. M., Bolewski, J. C. and Walker, L. P. (2013). "*Thermobifida fusca* cellulases exhibit limited surface diffusion on bacterial micro-crystalline cellulose." Biotechnology and Bioengineering **110**(1): 47-56.

Moran-Mirabal, J. M., Corgie, S. C., Bolewski, J. C., Smith, H. M., Cipriany, B. R., Craighead, H. G. and Walker, L. P. (2009). "Labeling and purification of cellulose-binding proteins for high resolution fluorescence applications." Analytical Chemistry **81**(19): 7981-7987.

Moran-Mirabal, J. M., Corgie, S. C., Bolewski, J. C., Smith, H. M. and Walker, L. P. (2009). "Fluorescence labeling and purification of cellulases for single molecule spectroscopy." Biophysical Journal **96**(3, Supplement 1): 45a-45a.

Moran-Mirabal, J. M., Edel, J. B., Meyer, G. D., Throckmorton, D., Singh, A. K. and Craighead, H. G. (2005). "Micrometer-sized supported lipid bilayer arrays for bacterial toxin binding studies through total internal reflection fluorescence microscopy." Biophysical Journal **89**(1): 296-305.

Moran-Mirabal, J. M., Santhanam, N., Corgie, S. C., Craighead, H. G. and Walker, L. P. (2008). "Immobilization of cellulose fibrils on solid substrates for cellulase-binding studies through quantitative fluorescence microscopy." Biotechnology and Bioengineering **101**(6): 1129-1141.

Moreno, N., Bougourd, S., Haseloff, J. and Feijó, J. A. (2006). Imaging plant cells. Handbook of biological confocal microscopy. J. B. Pawley. New York, SpringerScience+Business Media.

Morrall, R. a. A. and Dueck, J. (1982). "Epidemiology of *Sclerotinia* stem rot of rapeseed in saskatchewan." Canadian Journal of Plant Pathology **4**(2): 161-168.

Nidetzky, B., Steiner, W., Hayn, M. and Claeyssens, M. (1994). "Cellulose hydrolysis by the cellulases from *Trichderma reesei*: A new model for synergistic interaction." Biochemical Journal **298**(3): 705-710.

Niggli, E. and Lederer, W. J. (1990). "Real-time confocal microscopy and calcium measurements in heart muscle cells: Towards the development of a fluorescence microscope with high temporal and spatial resolution." Cell Calcium **11**(2-3): 121-130.

O'sullivan, A. C. (1997). "Cellulose: The structure slowly unravels." Cellulose **4**(3): 173-207.

Okazaki, M. and Moo-Young, M. (1978). "Kinetics of enzymatic hydrolysis of cellulose: Analytical description of a mechanistic model." Biotechnology and Bioengineering **20**(5): 637-663.

Olfa, E., Mondher, M., Issam, S., Ferid, L. and Nejib, M. M. (2007). "Induction, properties and application of xylanase activity from *Sclerotinia sclerotiorum* S2 fungus." Journal of Food Biochemistry **31**: 96-107.

Paper, J. M., Scott-Craig, J. S., Adhikari, N. D., Cuomo, C. A. and Walton, J. D. (2007). "Comparative proteomics of extracellular proteins *in vitro* and *in planta* from the pathogenic fungus *Fusarium graminearum*." Proteomics **7**: 3171-3183.

Paul, P. A., Lipps, P. E., De Wolf, E., Shaner, G., Buechley, G., Adhikari, T., Ali, S., Stein, J., Osborne, L. and Madden, L. V. (2007). "A distributed lag analysis of the relationship between *Gibberella zeae* inoculum density on wheat spikes and weather variables." Phytopathology **97**(12): 1608-1624.

Phalip, V., Delalande, F., Carapito, C., Goubet, F., Hatsch, D., Leize-Wagner, E., Dupree, P., Dorsselaer, A. and Jeltsch, J.-M. (2005). "Diversity of the exoproteome of *Fusarium graminearum* grown on plant cell wall." Current Genetics **48**: 366-379.

Quirk, A., Lipkowski, J., Vandenende, C., Cockburn, D., Clarke, A. J., Dutcher, J. R. and Roscoe, S. G. (2010). "Direct visualization of the enzymatic digestion of a single fiber of native cellulose in an aqueous environment by atomic force microscopy." Langmuir **26**(7): 5007-5013.

Rappé, M. S. and Giovannoni, S. J. (2003). "The uncultured microbial majority." Annual Review of Microbiology **57**(1): 369-394.

Rauscher, R., Wurleitner, E., Wacenovsky, C., Aro, N., Stricker, A. R., Zeilinger, S., Kubicek, C. P., Penttila, M. and Mach, R. L. (2006). "Transcriptional regulation of xyn1, encoding xylanase I, in *Hypocrea jecorina*." Eukaryotic Cell **5**(3): 447-456.

Rivers, D., Gracheck, S., Woodford, L. and Emert, G. (1984). "Limitations of the DNS assay for reducing sugars from saccharified lignocellulosics." Biotechnology and Bioengineering **26**(7): 800-802.

Roman, H., Madikane, M., Pletschke, B. I. and Rose, P. D. (2008). "The degradation of lignocellulose in a chemically and biologically generated sulphidic environment." Bioresource Technology **99**(7): 2333-2339.

Romano, N., Gioffré, A., Sede, S., Campos, E., Cataldi, A. and Talia, P. (2013). "Characterization of cellulolytic activities of environmental bacterial consortia from an Argentinian native forest." Current Microbiology: 1-10.

Rose, J. K. C., Ed. (2003). The plant cell wall. Sheffield annual plant reviews, CRC Press.

Rosgaard, L., Pedersen, S., Cherry, J. R., Harris, P. and Meyer, A. S. (2006). "Efficiency of new fungal cellulase systems in boosting enzymatic degradation of barley straw lignocellulose." Biotechnology Progress **22**(2): 493-498.

Rosgaard, L., Pedersen, S., Langston, J., Akerhielm, D., Cherry, J. R. and Meyer, A. S. (2007). "Evaluation of minimal *Trichoderma reesei* cellulase mixtures on differently pretreated barley straw substrates." Biotechnology Progress **23**(6): 1270-1276.

Saddler, J. N. and Gregg, D. J. (1998). Ethanol production from forest wastes. Forest products biotechnology. A. Bruce and J. W. Palfreyman. London; Bristol, PA, Taylor & Francis**:** 326.

Santa-Maria, M. and Jeoh, T. (2010). "Molecular-scale investigations of cellulose microstructure during enzymatic hydrolysis." Biomacromolecules **11**(8): 2000-2007.

Santhanam, N. and Walker, L. P. (2008). "A high-throughput assay to measure cellulose binding and synergism in ternary mixtures." Biological Engineering Journal **1**(1): 5-23.

Saxena, I. M. and Brown, R. M. J. (2005). "Cellulose biosynthesis: Current views and evolving concepts." Ann Bot **96**(1): 9-21.

Schmer, M. R., Vogel, K. P., Mitchell, R. B. and Perrin, R. K. (2008). "Net energy of cellulosic ethanol from switchgrass." Proceedings of the National Academy of Sciences USA **105**(2): 464-469.

Schwald, W., Chan, M., Breuil, C. and Saddler, J. N. (1988). "Comparison of HPLC and colorimetric methods for measuring cellulolytic activity." Applied Microbiology and Biotechnology **28**(4): 398-403.

Selig, M. J., Knoshaug, E. P., Adney, W. S., Himmel, M. E. and Decker, S. R. (2008). "Synergistic enhancement of cellobiohydrolase performance on pretreated corn stover by addition of xylanase and esterase activities." Bioresource Technology **99**(11): 4997-5005.

Sheir-Neiss, G. and Montenecourt, B. S. (1984). "Characterization of the secreted cellulases of *Trichoderma reesei* wild type and mutants during controlled fermentations." Applied Microbiology and Biotechnology **20**(1): 46-53.

Shoseyov, O., Shani, Z. and Levy, I. (2006). "Carbohydrate binding modules: Biochemical properties and novel applications." Microbiol. Mol. Biol. Rev. **70**(2): 283-295.

Singh, S., Simmons, B. A. and Vogel, K. P. (2009). "Visualization of biomass solubilization and cellulose regeneration during ionic liquid pretreatment of switchgrass." Biotechnology and Bioengineering **104**(1): 68-75.

Somerville, C., Bauer, S., Brininstool, G., Facette, M., Hamann, T., Milne, J., Osborne, E., Paredez, A., Persson, S., Raab, T., Vorwerk, S. and Youngs, H. (2004). "Toward a systems approach to understanding plant cell walls." Science **306**(5705): 2206-2211.

Sprague, B. L., Pego, R. L., Stavreva, D. A. and Mcnally, J. G. (2004). "Analysis of binding reactions by fluorescence recovery after photobleaching." Biophysical Journal **86**(6): 3473-3495.

Stricker, A. R., Grosstessner-Hain, K., Wurleitner, E. and Mach, R. L. (2006). "Xyr1 (xylanase regulator 1) regulates both the hydrolytic enzyme system and d-xylose metabolism in *Hypocrea jecorina*." Eukaryotic Cell **5**(12): 2128-2137.

Suga, K., Dedem, G. V. and Moo-Young, M. (1975). "Degradation of polysaccharides by endo and exo enzymes: A theoretical analysis." Biotechnology and Bioengineering **17**(3): 433-439.

Sutton, J. C. (1982). "Epidemiology of wheat head blight and maize ear rot caused by *Fusarium graminearum*." Canadian Journal of Plant Pathology **4**: 195.

Szczodrak, J. and Fiedurek, J. (1996). "Technology for conversion of lignocellulosic biomass to ethanol." Biomass and Bioenergy **10**(5-6): 367-375.

Tengborg, C., Galbe, M. and Zacchi, G. (2001). "Influence of enzyme loading and physical parameters on the enzymatic hydrolysis of steam-pretreated softwood." Biotechnology Progress **17**(1): 110-117.

Tomme, P., Tilbeurgh, H., Pettersson, G., Damme, J., Vandekerckhove, J., Knowles, J., Teeri, T. and Claeyssens, M. (1988). "Studies of the cellulolytic system of *Trichoderma reesei* QM 9414." European Journal of Biochemistry **170**(3): 575-581.

Tomme, P., Warren, R. A. and Gilkes, N. R. (1995). "Cellulose hydrolysis by bacteria and fungi." Advances in Microbial Physiology **37**: 2-81.

Tonukari, N. J. (2003). "Enzymes and fungal virulence." Journal of Applied Sciences & Environmental Management **7**(1): 5-8.

Toth, I. K. and Birch, P. R. J. (2005). "Rotting softly and stealthily." Current Opinion in Plant Biology **8**: 424-429.

USDOE (2003). Biomass feedstock composition and property database, U.S. Department of Energy, Office of Energy Efficiency and Renewable Energy.

USDOE (2006). Biofuels joint roadmap. Breaking the biological barriers to cellulosic ethanol: A joint research agenda. U. S. D. o. E. Office of Science and Office of Energy Efficiency and Renewable Energy.

Vaaje-Kolstad, G., Westereng, B., Horn, S., Liu, Z., Zhai, H., Sorlie, M. and Eijsink, V. (2010). "An oxidative enzyme boosting the enzymatic conversion of recalcitrant polysaccharides." Science **330**: 219 - 222.

Voutilainen, S. P., Boer, H., Linder, M. B., Puranen, T., Rouvinen, J., Vehmaanperä, J. and Koivula, A. (2007). "Heterologous expression of *Melanocarpus albomyces* cellobiohydrolase Cel7B, and random mutagenesis to improve its thermostability." Enzyme and Microbial Technology **41**(3): 234-243.

Walker, L. P., Belair, C. D., Wilson, D. B. and Irwin, D. C. (1993). "Engineering cellulase mixtures by varying the mole fraction of *Thermomonospora fusca* E5 and E3, *Trichoderma reesei* CBHI, and *Caldocellum saccharolyticum* beta-glucosidase." Biotechnology and Bioengineering **42**: 1019-1028.

Walker, L. P. and Wilson, D. B. (1991). "Enzymatic hydrolysis of cellulose: An overview." Bioresource Technology **36**(1): 3-14.

Walton, J. D. (1994). "Deconstructing the plant cell wall." Plant Physiology **104**: 1113-1118.

Wang, J., Quirk, A., Lipkowski, J., Dutcher, J. R., Hill, C., Mark, A. and Clarke, A. J. (2012). "Real-time observation of the swelling and hydrolysis of a single crystalline cellulose fiber catalyzed by cellulase 7B from *Trichoderma reesei*." Langmuir **28**(25): 9664-9672.

Warren, R. A. (1996). "Microbial hydrolysis of polysaccharides." Annual Review of Microbiology **50**: 183-212.

Watson, D. L., Wilson, D. B. and Walker, L. P. (2002). "Synergism in binary mixtures of *Thermobifida fusca* cellulases Cel6B, Cel9A and Cel5A on BMCC and avicel." Applied Biochemistry and Biotechnology **101**: 97-111.

Webb, E. C. (1992). Enzyme nomenclature : 1992 : Recommendations of the nomenclature commitee of the international union of biochemistry and molecular biology on the nomenclature and classification of enzymes. London [etc.], Academic Press.

Wen, Z., Liao, W. and Chen, S. (2004). "Hydrolysis of animal manure lignocellulosics for reducing sugar production." Bioresource Technology **91**(1): 31-39.

Wickholm, K., Hult, E.-L., Larsson, P. T., Iversen, T. and Lennholm, H. (2001). "Quantification of cellulose forms in complex cellulose materials: A chemometric model." Cellulose **8**(2): 139-148.

Wilson, D. B. (2008). "Three microbial strategies for plant cell wall degradation." Ann NY Acad Sci **1125**(1): 289-297.

Wilson, D. B. (2009). "Cellulases and biofuels." Current Opinion in Biotechnology **20**(3): 295-299.

Wilson, D. B. and Irwin, D. C. (1999). "Genetics and properties of cellulases." Advances in Biochemical Engineering Biotechnology: Recent Progress in Bioconversion **65**: 1-21S.

Withers, S. and Williams, S. (2010). Glycoside hydrolases. Cazypedia http://www.cazypedia.org/.

Wood, T. M. and Bhat, K. M. (1988). Methods for measuring cellulase activities. Methods in enzymology, Academic Press. **Volume 160:** 87-112.

Woodward, J., Lima, M. and Lee, N. E. (1988). "The role of cellulase concentration in determining the degree of synergism in the hydrolysis of microcrystalline cellulose." Biochemical Journal **255**: 895-899.

Xiao, Z., Storms, R. and Tsang, A. (2004). "Microplate-based filter paper assay to measure total cellulase activity." Biotechnology and Bioengineering **88**(7): 832-837.

Xiao, Z., Storms, R. and Tsang, A. (2005). "Microplate-based carboxymethylcellulose assay for endoglucanase activity." Analytical Biochemistry **342**(1): 176-178.

Xu, F. and Ding, H. (2007). "A new kinetic model for heterogeneous (or spatially confined) enzymatic catalysis: Contributions from the fractal and jamming (overcrowding) effects." Applied Catalysis A: General **317**(1): 70-81.

Yajima, W. and Kav, N. N. V. (2006). "The proteome of the phytopathogenic fungus *Sclerotinia sclerotiorum*." Proteomics **6**(22): 5995-6007.

Yang, D., Moran-Mirabal, J. M., Parlange, J.-Y. and Walker, L. P. (2013). "Investigation of the porous structure of cellulosic substrates through confocal laser scanning microscopy." Biotechnology and Bioengineering.

Zhang, Y.-H. P. and Lynd, L. R. (2004). "Toward an aggregate understanding of enzymatic hydrolysis of cellulose: Noncomplexed cellulase systems." Biotechnology and Bioengineering **88**: 797-824.

Zhang, Y.-H. P. and Lynd, L. R. (2006). "A functionally based model for hydrolysis of cellulose by fungal cellulase." Biotechnology and Bioengineering **94**(5): 888-898.

Zhang, Y. H. P., Himmel, M. E. and Mielenz, J. R. (2006). "Outlook for cellulase improvement: Screening and selection strategies." Biotechnology Advances **24**(5): 452-481.

Zhu, P., Moran-Mirabal, J., Luterbacher, J., Walker, L. and Craighead, H. (2011). "Observing *Thermobifida fusca* cellulase binding to pretreated wood particles using time-lapse confocal laser scanning microscopy." Cellulose **18**(3): 749-758.